Dielectric heating of carbon precursors

Michał Adam Stróżyk

Publication date

01-01-2021

Dielectric heating of carbon precursors

Michał Adam Stróżyk

Supervised by

Dr Maurice N. Collins

Dr Mario Culebras Rubio

A thesis submitted for the degree of

Doctor of Philosophy

Submitted to the University of Limerick, Oct 2021

Abstract

Carbon fibre (CF) composites are becoming more widespread in many applications such as automotive, aerospace, defence, wind turbines and pressure vessels. CF is produced from precursor fibre via a series of energy-intensive heat treatments. During conventional heating processes, the energy is transferred from the source through heat transfer. Microwave (MW) heating has been identified as a more energy-efficient alternative due to direct transfer of energy into the material via a susceptor structure.

An alternative carbonisation method has been developed to reduce energy consumption and environmental impact during manufacture of CF utilising a susceptor assisted MW heating technique, which is achieved by a layer by layer approach at the nanoscale. The project goes beyond the state-of-the-art through the carbonisation of PAN and sustainable precursors via MW heating.

Initially, the technology is applied for conversion of the most commonly used, petroleum-based precursor – polyacrylonitrile (PAN). The effects of susceptor coating procedure and MW power level are studied. It is found that addition of even a single layer of susceptor allows for a successful MW carbonisation. Addition of extra layers can increase temperatures. Application of susceptor before stabilisation leads to fusion of the layer and more stable heating. Susceptor layers applied after stabilisation allow higher temperatures and CF conversion rates, but tend to be more prone to damage during the process. MW carbonisation at high power enables carbonisation temperatures within seconds, but promotes development of defects via gas emission. MW carbonisation at progressive power levels limits overheating, leads to noticeable improvement of morphology and mechanical properties, especially for lignin-based CF. The latter approach is used to produce lignin-based CF with properties matching those of control samples prepared via conventional techniques.

Finally, results of MW heating modelling and life cycle assessment are presented.

Declaration

The substance of this thesis is the original work of the author and due reference and acknowledgement has been made, where necessary, to the work of others. No part of this thesis has been submitted by the candidate for any other degree.

Candidate:

Michał A. Stróżyk

_____

Supervisors:

Dr Maurice N. Collins

_____

Dr Mario Culebras Rubio

_____

Acknowledgement

Foremost, I am grateful to God, the Almighty for the creation of this world where we can study and marvel at its beauty.

I would like to express sincere gratitude to my supervisors, Dr Maurice Collins and Dr Mario Culebras Rubio for this PhD opportunity. Their mentorship has been invaluable and helped to create the researcher I am today.

I acknowledge the financial support of Biobased Industries Joint Undertaking (Horizon 2020 Grant No 720707). I would like to thank all partners from the "LIBRE" consortium for their help in this project.

I would like to thank the amazing research, technical, academic and administration staff at UL, especially Fionnuala, Wynette, Paula, Catherine, Con, Jeff, Eric, Serguei, Nigel, Clive and Tom, who have supported me in so many ways during my research.

Special thanks to all of my colleagues from Stokes: Anne, Aleksandra, Fernanda, Caroline, Valeria, Guang, Tim, as well as the intern students. I will never forget your help and the wonderful time we shared.

I am grateful to my parents Monika and Michał, my sister Maria, my brothers Mikołaj and Maciej, for their love, encouragement and formation throughout the years. I am indebted to the country of Ireland, which shares credit in my education.

Finally, I would like to thank my wife Barbara for her love and patience. Thank you for enduring the partings we had to go through in order to see this work to the end.

Table of Contents

List of Figures

List of Tables

List of Acronyms

AA	Acrylic Acid
AFM	Atomic Force Microscopy
ANN	Artificial Neural Network
CF	Carbon Fibre
CFRP	Carbon Fibre Reinforced Polymer
CNF	Carbon Nanofiber
Co-PAN	Polyacrylonitrile Copolymer
CVD	Chemical Vapour Deposition
DI	Deionised
EB	Electron Beam
EDS	Energy Dispersive X-Ray Spectroscopy
G	Guaiacyl
GF	Glass Fibre
H	p-Hydroxyphenol
IR	Infrared Radiation
ITA	Itaconic Acid
LBL	Layer by layer
LCA	Life Cycle Assessment
MA	Methyl Acrylate
MAA	Methacrylic Acid
MAP	Microwave Assisted Plasma
MMA	Methyl Methacrylate
MW	Microwave
MWCNT	Multi-Walled Carbon Nanotube

NF	Nanofiber
PAN	Polyacrylonitrile
PDADMAC	Polydiallyldimethylammonium chloride
PDI	Polydispersity Index
PEEK	Polyetheretherketone
PEGDGE	Polyethylene glycol diglycidyl ether
PEO	Polyethylene Oxide
PLA	Polylactic Acid
PP	Polypropylene
PTFE	Polytetrafluoroethylene
RF	Radio Frequency
S	Syringyl
SDOC	Sodium Deoxycholate
SEM	Scanning Electron Microscope
TDI	Tolylene Diisocyanate
TGA	Thermogravimetric Analysis
TPU	Thermoplastic Polyurethane
TS	Tensile Strength
UV	Ultraviolet
YM	Young's Modulus

Publications

Stróżyk, M.A., Culebras, M., Collins, M.N. (2019) 'Susceptor induced dielectric heating of PAN for energy-efficient carbon fibre production', Presented at the The IEEE 17th International Symposium on Electrets (ISE17).

In preparation (tentative title):

Stróżyk, M.A., Culebras, M., Conroy, T.J., Frank, E., Hermansson, F., Janssen, M., Svanström, M., Collins, M.N. (2021) 'Decreasing the environmental impact of carbon fibre production via microwave carbonisation assisted by self-assembled nanostructured coatings'.

The author of this thesis also contributed to the following publications:

Collins, M.N., Nechifor, M., Tanasă, F., Zănoagă, M., McLoughlin, A., Stróżyk, M.A., Culebras, M., Teacă, C.-A. (2019) 'Valorization of lignin in polymer and composite systems for advanced engineering applications – A review', *International Journal of Biological Macromolecules*, 131, 828–849.

Culebras, M., Beaucamp, A., Stróżyk, M.A., Collins, M.N. (2019) 'Valorization of lignin through carbon fibres for advanced biomedical applications', Presented at the Bioengineering in Ireland.

Culebras, M., Beaucamp, A., Stróżyk, M.A., Collins, M.N. (2020) 'Carbon based nanomaterials derived from biopolymers for biomedical wearable devices', Presented at the 11th World Biomaterials Congress (WBC 2020).

Zamboni, F., Okoroafor, C., Ryan, M.P., Pembroke, J.T., Strozyk, M., Culebras, M., Collins, M.N. (2021) 'On the bacteriostatic activity of hyaluronic acid composite films', *Carbohydrate Polymers*, 260, 117803.

Culebras, M., Stróżyk, M.A., Collins, M.N. (2021) 'CARBON FIBRE PRODUCTION VIA SUSCEPTOR INDUCED MICROWAVE ABSORPTION', 23rd International Conference on Composite Materials (Abstract submitted).

Chapter 1

Introduction

1.1 Carbon fibre composites

A composite is a material consisting of two or more constituents which remain separate after assembly and possess distinct properties [1,2]. Resulting materials feature superior mechanical performance or chemical resistance. Common examples of composites are: concrete – aggregate of stones in a matrix of cement; fibre reinforced polymers - containing glass fibre (GF) or carbon fibre (CF) as reinforcement embedded in thermoset or thermoplastic polymer matrix; and wood – naturally occurring composite of cellulose fibres embedded in a matrix of lignin and hemicellulose. One of the most important advantages of composite materials is higher strength-to-weight ratio compared to isotropic materials like ceramics or metals, as shown in Figure 1.1. As a result, composites find applications whenever a lightweight structure is required in a design of a product or part.

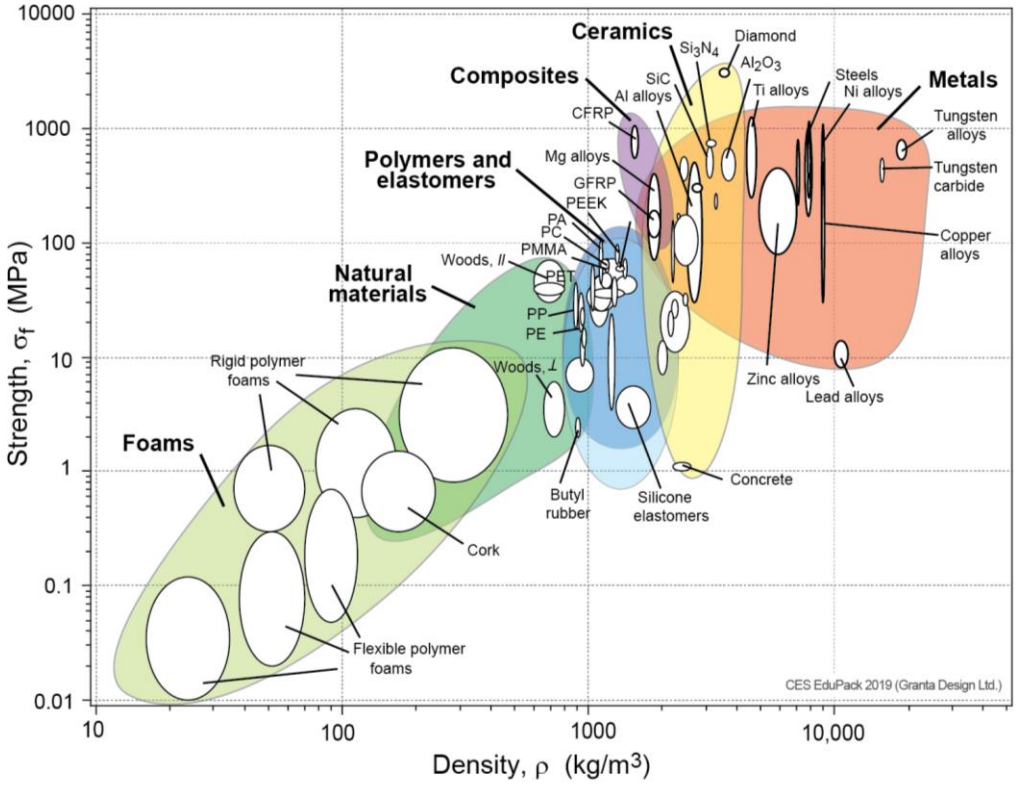

Figure 1.1 Strength vs Density chart of materials. Chart created using CES EduPack 2019, ANSYS Granta © 2020 Granta Design.

Carbon fibre (CF) composites or carbon fibre reinforced polymers (CFRPs) can be classified by the type of polymer matrix, often called a resin [3,4]. Thermoset resins include phenolic, polyester, epoxy vinyl ester, epoxide (the most widely used for CFRPs), cyanate, polyimide and others. Thermoplastic resins include polyamide, polycarbonate, polyetheretherketone (PEEK), polyetherimide, polyethersulfone, polyphenylene sulphide and others. They can be used for injection molding or the prepreg route of CFRP preparation. Some advantages of thermoplastic over thermoset matrix include relatively quick processing with no curing involved, unrestricted shelf life, ability to be reprocessed, thermoformed and welded. Thermoplastic resin improves toughness of the composite through polymer chain slippage which is impossible in a cross-linked structure of a thermoset. A schematic of a unidirectional CFRP is shown in Figure 1.2.

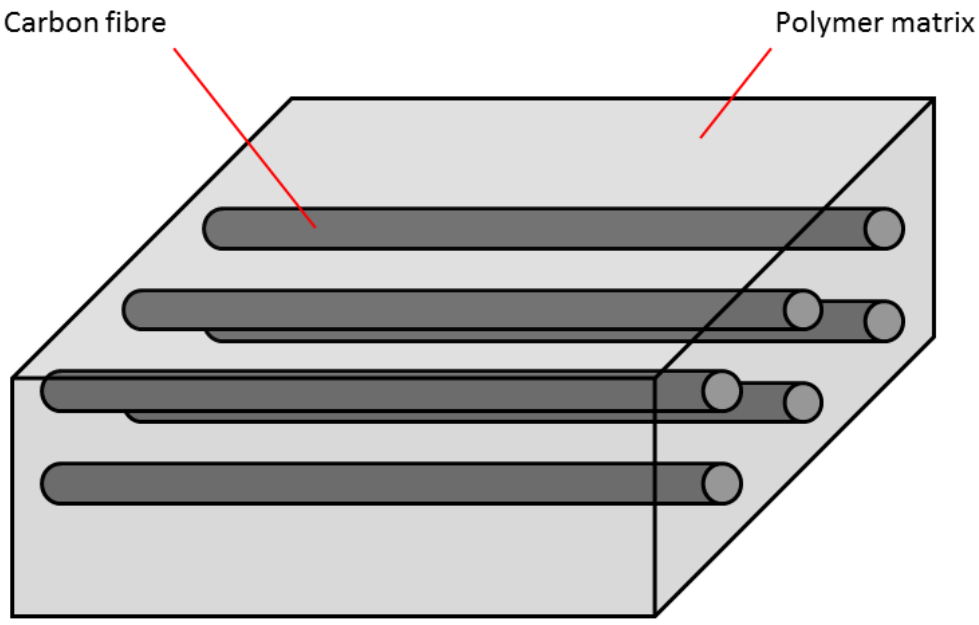

Figure 1.2 Schematic representation of a unidirectional CFRP.

CFRPs are becoming more widespread in many applications such as military, aerospace, automotive, marine, construction, corrosion resistant equipment, wind turbines, pressure vessels and sporting goods. As a result, carbon fibre market is predicted to grow from USD 3.7 billion in 2020 to USD 8.9 billion by 2031 [5]. However, non-aerospace applications of CFRPs are still restricted by relatively low degree of automation and low-volume processing which translate to higher production costs compared to metals. The cost is greatly affected by the high cost of CF production

[6], which involves energy-intensive processes and long cycle times [7]. These can be addressed via developments in alternative raw materials and production technologies.

1.2 Carbon fibre production

By definition, CF consists of at least 92% carbon atoms by weight, mostly in the turbostratic state. CFs are often classified by their properties: (i) high stiffness – Young's modulus (YM) values of about 150 – 300 GPa, with tensile strengths (TS) up to 7 GPa, which is flaw dependent and improves as the diameter of the fibre decreases; (ii) low modulus – YM values of 100 GPa and low strength; (iii) intermediate modulus – with values of 275 – 350 GPa and relatively high strength achievable by reduction of radius down to about 5 μm; (iv) high modulus – YM higher than 300 GPa; (v) ultra-high modulus – YM values larger than 600 GPa.

Cost breakdown of the CF production from polyacrylonitrile (PAN) – the most common CF precursor, is shown in Figure 1.3. Cost of a precursor fibre and its conversion to CF are contributing to nearly 90% of the total.

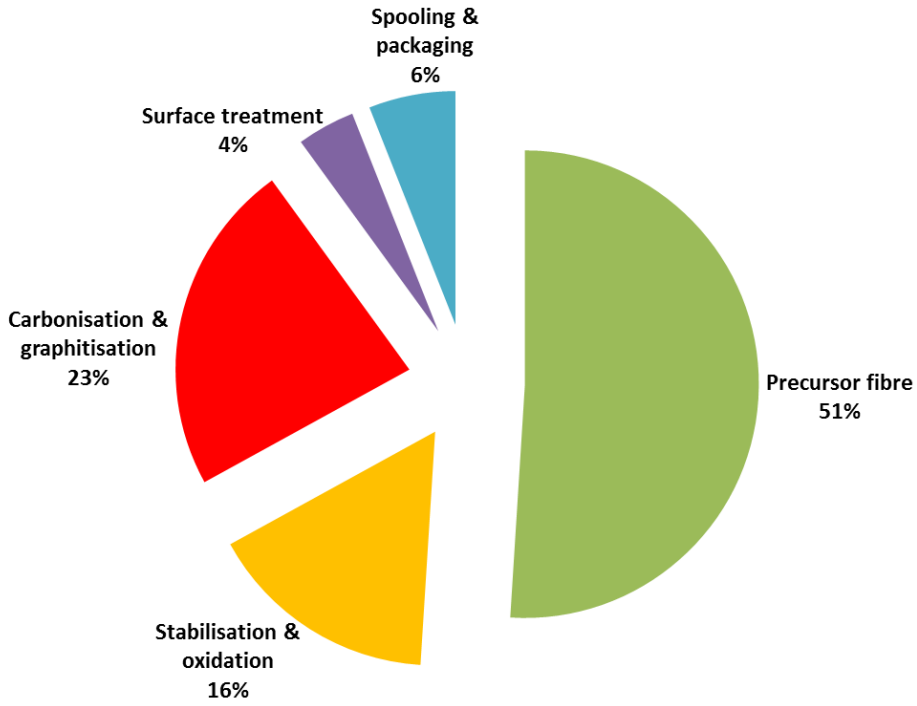

Figure 1.3 Cost distribution of CF production from polyacrylonitrile (PAN) [8,9].

In general, conversion of any precursor into carbon fibre involves three heat treatments: stabilisation (often called oxidation), carbonisation and graphitisation [3]. These are followed by surface and sizing treatments prior to spooling. The process of CF production from PAN is shown in Figure 1.4.

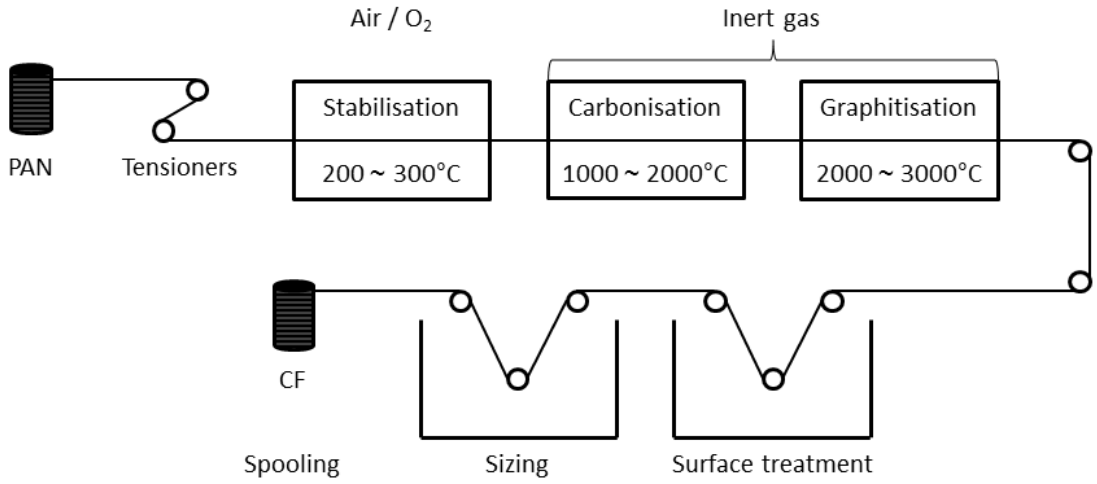

Figure 1.4 Schematic of CF manufacturing process.

During stabilisation fibres are passed through an oven with a series of heating zones of increasing temperatures, typically between 200 and 300°C [10–12]. In this step, filaments are heated in an oxidising atmosphere, which allows further processing, improves carbon yield and mechanical properties of the final product, by changing a character of a precursor from thermoplastic to thermoset. Tension or drawing is applied to prevent shrinkage.

Stabilised fibre is then subjected to thermal pyrolysis in an inert atmosphere called carbonisation. Reactions such as dehydrogenation, denitrogenation, condensation, hydrogen transfer and isomerisation take place in this complex process [13]. Initial heating rates are often low to prevent damage of the fibre by escaping volatile products. Most of them are evolved in the range of 200-1000°C. At this stage carbon content of the fibre exceeds 90%. Fibres are often heated up to 2000°C to allow for additional reactions and increase C content to over 99%.

In the final stage called graphitisation, CF is heated in an inert atmosphere to temperatures of up to 3000°C. This leads to orientation of the graphite crystallites along the fibre axis, which increases Young's modulus (YM), but decreases tensile strength (TS) of the fibre.

After that fibre is subjected to surface treatment in electrolytic bath and application of sizing which preferably matches the matrix used in the composite.

During conventional heating processes, the energy is transferred from the source via radiation, convection or conduction. This decreases efficiency of the heating and increases the cost of production. On the contrary, microwave heating occurs via

conversion of energy in the material which significantly reduces heat transfer limitations of conventional heating. Furthermore it results in different heat gradient compared to conventional processing where heat propagates from the surface of the sample. Thus, the MW processing offers some important advantages: (i) high heating rates; (ii) selective heating; (iii) volumetric heating; (iv) cost reduction; (v) high potential for automation [14]. MW assisted processing has attracted significant attention of researchers as a more energy-efficient alternative for material processing, synthesis and waste treatments [15]. However, it has not yet been successfully applied to CF production. Schematic comparison between conventional and microwave heating mechanisms is shown in Figure 1.5.

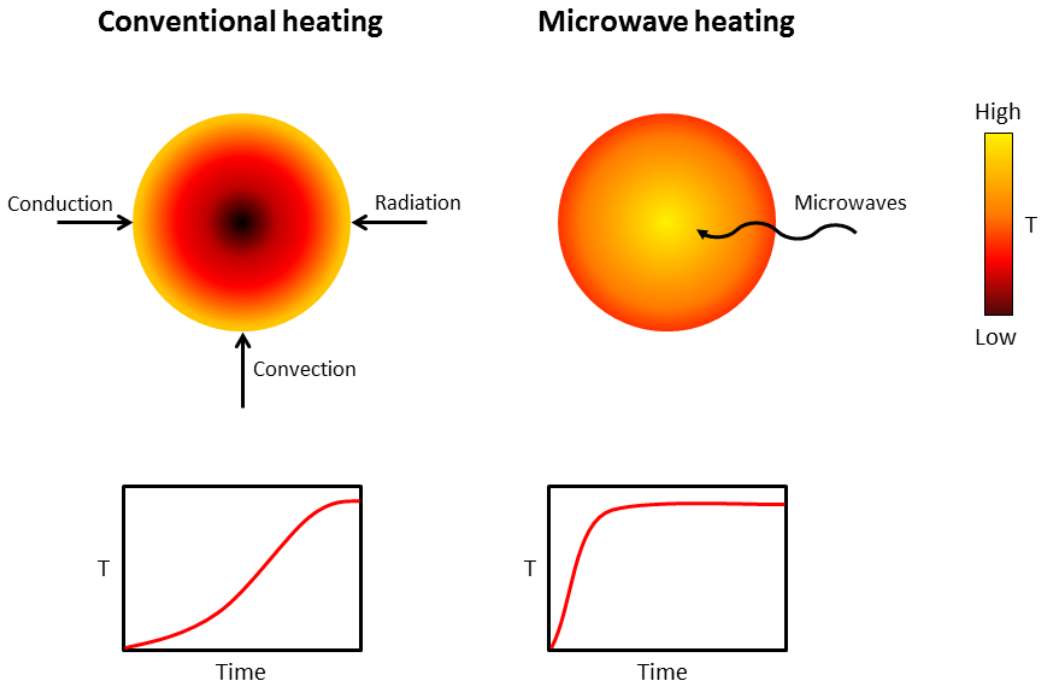

Figure 1.5 Conventional vs Microwave heating mechanism.

1.3 Theory of microwave heating

Microwaves (MW) are electromagnetic waves with frequencies between 300 MHz and 300 GHz [16]. MW heating of a material depends on its response to the alternating electric and magnetic fields [17]. Heating under the electric field, proceeds through either relaxation of polarised molecules (polarisation loss) or conduction of free electrons (conduction loss). Energy conversion under magnetic field involves mechanisms such as the hysteresis loss, eddy current loss and domain wall/electron spin resonance loss. The response to an electric field is determined by the ability to store

electric energy – represented by permittivity or dielectric constant (ε'), and the ability to convert that energy to heat – represented by dielectric loss (ε"). Similarly, storage and conversion of the magnetic energy are measured by the permeability (μ') and magnetic loss (μ"), respectively. These properties are usually presented relative to the free space permittivity and permeability (ε_0 = 8.854 x 10^{-12} Farad/m and $\mu_0 = 4\pi$ x 10^{-7} Henry/m):

$$\varepsilon'_r = \frac{\varepsilon'}{\varepsilon_0}, \qquad \varepsilon''_r = \frac{\varepsilon''}{\varepsilon_0}, \qquad \mu'_r = \frac{\mu'}{\mu_0} \qquad \text{and} \qquad \mu''_r = \frac{\mu''}{\mu_0}. \qquad (1 - 4).$$

Dielectric loss due to conduction is given by:

$$\varepsilon'' = \frac{\sigma}{2\pi f} \qquad (5),$$

where σ is the conductivity of the material and f is the frequency of the radiation.

Penetration depth of electromagnetic field into a given material is the depth at which the intensity of the electromagnetic field decreases to 1/e (=0.368) of the initial amplitude, and is given by

$$d_p = \frac{c}{\sqrt{2}\pi f\sqrt{\mu'_r\varepsilon'_r}}\left[\sqrt{1+\left(\frac{\varepsilon''_r}{\varepsilon'_r}\right)^2\left(\frac{\mu''_r}{\mu'_r}\right)^2+\left(\frac{\mu''_r}{\mu'_r}\right)^2+\left(\frac{\varepsilon''_r}{\varepsilon'_r}\right)^2}-\left(1-\frac{\varepsilon''_r}{\varepsilon'_r}\frac{\mu''_r}{\mu'_r}\right)\right]^{-1/2} \qquad (6),$$

where $c = 1/\sqrt{\varepsilon_0\mu_0} = 3 \times 10^8 m/s$. In the above, the important parameters are the frequency, permittivity, permeability and loss tangents $\tan\delta_e$ and $\tan\delta_m$ given by

$$\tan\delta_e = \frac{\varepsilon''_r}{\varepsilon'_r} \text{ and } \tan\delta_m = \frac{\mu''_r}{\mu'_r} \qquad (7 – 8).$$

For most materials processed by MWs such as ceramics, glasses and polymers, $\tan\delta_m \rightarrow 0$ and therefore loss tangent values of $\tan\delta_e$ or penetration depth are used for MW absorption comparison. Materials can be classified as reflectors, transparent and microwave absorbing, depending on the magnitude of the penetration. Reflectors are materials with MW penetration depths of the order μm. Microwaves cannot penetrate further and are reflected back from the material. MW absorbing are highly lossy materials with penetration depth of the order of cm and loss tangent >0.1. These materials readily convert MW radiation into heat. Transparent are low lossy materials with penetration depth of the order of meters and loss tangent <0.01. MW radiation can travel though such materials without significant absorption. Most ceramic and polymer materials fall into this cathegory, including CF precursors. Energy efficiency of the

microwave heating is significantly reduced when it is applied to microwave transparent materials. Furthermore, successful utilisation of microwave heating and its benefits requires dealing with phenomenon of temperature-dependent properties. The dielectric properties of the material may change with temperature and therefore some materials which are microwave transparent may become absorbing materials at elevated temperatures. For example, alumina couples with 2.45 GHz microwaves at temperatures greater than 1000°C. This phenomenon could lead to thermal runaway and uncontrollable heating of the material. In order to overcome the above challenges, microwave susceptors are used.

1.4 Microwave susceptors

Susceptors are highly microwave absorbing materials, which readily heat in the electromagnetic field even at room temperature. Some applications of MW susceptors for material processing include: (i) sintering of ceramics such as alumina, zirconia, silicon nitride yttria-stabilised zirconia and others using silicon carbide (SiC) as susceptor [18–21]; (ii) silica and pyrex glass processing using SiC as susceptor [22,23]; (iii) polymer joining using carbon powders as susceptors [24,25]; (iv) SiC-assisted sintering of metals and alloys [26,27]; (v) ore processing [28]; (vi) semiconductor processing using SiC or carbon based susceptors [29,30]. In most cases susceptor-assisted MW processing reduced energy consumption and/or time of processing [15], as illustrated in Figure 1.6.

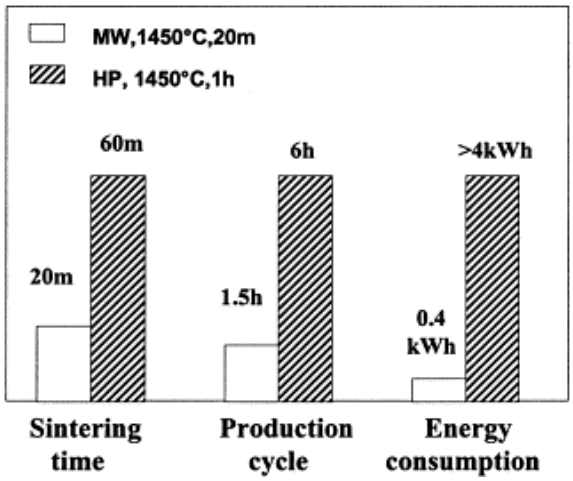

Figure 1.6 Comparison between microwave hybrid sintering (MW) and conventional sintering (HP) of yttria-stabilised zirconia. Reproduced with permission from Elsevier [21].

Susceptors can be applied on the surface so that the composition and the structure of the material remains unaltered. The heat is transferred to the sample via conventional modes of heat transfer, which mimics conditions of the conventional furnace until it couples with the microwaves at higher temperatures or (in case of CF production) enough carbon phase is developed. At that point the sample is heated by microwaves from the centre and by the susceptor from the surface. This results in a more uniform heating compared to conventional or direct microwave heating of the material. Furthermore, application of the susceptor on the surface will significantly reduce cost of such modification. It is therefore the most favourable approach for CF production. Carbon materials such as carbon black, graphite, carbon fibres and carbon nanotubes are all classified into the group of MW absorbing materials [31]. They offer very good MW absorption and limit chemical contamination which could diminish mechanical performance of the CF. Therefore they are very good candidates for MW carbonisation susceptors for production of CF.

1.5 Carbon fibre precursors

1.5.1 PAN

The most common precursor for CF production is poly(acrylonitrile) (PAN). It was firstly used for making of CF by Shindo [32] and an improved process was later patented by Johnson *et al.* [33]. Currently, PAN is a starting material for about 90% of CF production. Structure of an acrylonitrile unit is shown in Figure 1.7.

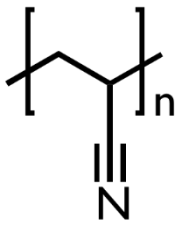

Figure 1.7 Molecular structure of acrylonitrile unit [34].

A typical PAN-based precursor should possess the following properties:

1. Acrylonitrile content between 85 – 95% of a copolymer. Co-monomers such as methyl acrylate (MA), methyl methacrylate (MMA) act as plasticisers and improve quality of precursor spinning whereas monomers such as acrylic acid (AA), methacrylic acid (MAA), itaconic acid (ITA) are used to reduce

stabilisation time and improve carbon yield in addition to their plasticising effect. Homopolymers are not used commercialy.

2. The number average molecular weight (M_n) in the range of 40,000 – 70,000 g/mol.
3. The weight average molecular weight (M_w) of 90,000 – 140,000 – too high could make spinning difficult.
4. A polydispersity index of 1.5 – 3 (M_w/M_n).

PAN is produced via wet-spinning from highly polar organic solvents to avoid ion contamination from inorganic solvents. Polymer concentration in the solvent is typically about 15 wt. %. Precursor fibre is then converted to CF through the process described previously in this chapter and shown in Figure 1.4. During stabilisation, the fibre increases in density from 1.18 g cm^{-3} to about 1.36 – 1.4 g cm^{-3}. Gases such as HCN, H_2O, CO_2, CO, NH_3 are produced in the process and are continuously removed using an inlet of fresh air. Temperature and tension are closely monitored to control exothermicity, accommodate for the phases of fibre shrinkage, prevent breakage and ensure good quality. Stabilised fibre is then subjected to low temperature carbonisation in a multizone electrical furnace where temperature of different zones is gradually increased to about 1000°C or lower (heating above 950°C leads to decomposition of tars and fibre stickiness). The furnace is purged with N_2 to provide inert atmosphere and remove gases evolved in the process. Fibre may be subjected to high temperature carbonisation to increase its YM. However, the strength of the fibre is reduced if temperatures are increased above 1500°C, as the structure becomes graphitic and more oriented. Typical carbonisation of PAN is generally assumed to occur via the following:

1. evolution of HCN, CO_2, CO, H_2O from about 300°C onwards
2. evolution of NH_3, cross-linking via H_2O emission at about 400°C
3. cross-linking via dehydrogenation – suggested by increased H_2 evolution in the range of about 500 – 700°C
4. cross-linking via denitrogenation – suggested by increased N_2 evolution from about 800°C onwards.

Carbonisation leads to development of a characteristic turbostratic carbon phase in which graphite-like layers (sp^2 carbon) are connected via tetrahedral bonds of sp^3-hybridised C atoms. Even fibre carbonised at 1400°C can have a residual nitrogen content of up to 4%. Figure 1.8 summarises structural changes involved in carbonisation

of PAN-based PF. Additional heat treatment called graphitisation results in CF with high YM through an alignment of graphite crystallites. CF with highest values of YM is usually produced from mesophase pitch precursor.

Currently, PAN is a starting material for about 90% of CF, the remaining 10% being petroleum pitch or rayon. There are significant disadvantages associated with petroleum-based precursors such as PAN. The majority of the precursor fibre is produced via wet-spinning which requires the use of highly polar solvents. Significant costs of production and environmental problems encourage researchers to look for alternative CF precursors [9,35,36]. To address dependency on petroleum extraction and its price variation, bio-based precursor systems are being developed from bio resources such as cellulose [37] or lignin [35,38].

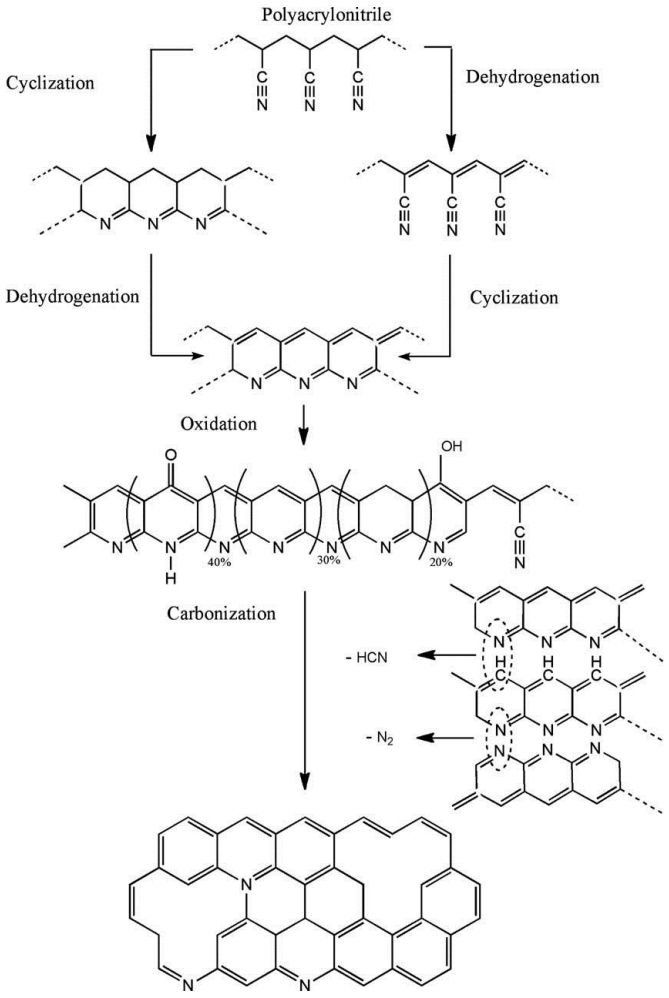

Figure 1.8 Schematic representation of structural changes in PAN during CF production. Reproduced with permission from John Wiley and Sons [39].

1.5.2 Lignin

Lignin is one of the most abundant biopolymers on the planet. It is a highly cross-linked alkyl-aromatic heteropolymer synthesised in the cell wall of plants from three monolignol units: sinapyl alcohol (S), coniferyl alcohol (G), and p-coumaryl alcohol (H) [40]. The synthesis occurs via enzymatic dehydrogenation and creation of phenoxyl radicals which polymerise randomly to create 3D network of corresponding phenylpropanoid moieties: syringyl (S), guaiacyl (G) and *p*-hydroxyphenol (H) [41]. This leads to creation of linkage units such as: aryl ether (β-O-4), resinol (β -β), phenylcoumaran (β -5), biphenyl (5-5'), spirodienone, β -1, 4-O-5, α-O-4 [40,42]. Schematic representation of lignin structure, showing S/G/H units and linkages is shown in Figure 1.9.

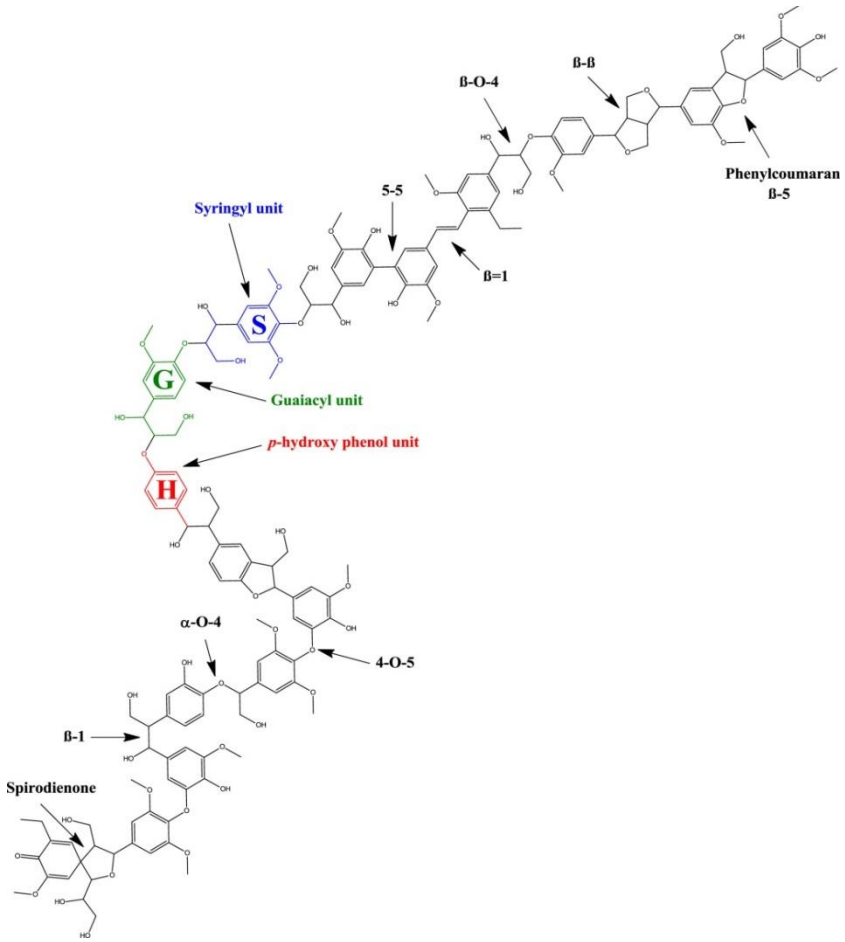

Figure 1.9 Schematic representation of lignin including syringyl (S, blue), guaiacyl (G, green), and p-hydroxyphenol (H, red) phenylpropanoid moieties, and lignin–lignin linkages. Reproduced from [43].

Respective amounts of building units and linkages vary with lignin source and separation method used. Lignin content is typically in the range of 25 – 35% in

softwood (gymnosperm trees e.g. pine, spruce), 20 – 25% in hardwood (angiosperm trees e.g. beech, oak) and 15 – 25% in herbaceous plants [44], and is usually determined by the Klason acid hydrolysis method [44,45].

Summary of different lab-scale and industrial methods used for lignin separation is shown in Figure 1.10 The most common methods of extraction involve the following processes [46–49]:

1. Alkaline pulping: otherwise known as the Kraft process which involves treatment of wood fibers in a 1 M NaOH and 0.25–0.70 M Na_2S aqueous solution at 165–175°C. Depolymerisation proceeds through the cleavage of non-phenolic β–ethers and then through entrapment of quinone methide intermediates. The latter mechanism is an important improvement over the soda pulping process (NaOH only), which prevents additional condensation by formation of styryl ethers and diphenylmethane structures. However, sulphide introduces significant sulfur content into the Kraft lignin, and this impedes the subsequent valorisation of lignin. The Kraft process leads to replacement of C-O bonds of native lignins with C-C bonds inducing higher bond dissociation energies. Black liquor, contains highly complex and cross-linked lignin, is incinerated to recover Na_2S and to produce steam for power generation [49].
2. Organosolv treatment which involves pulping of wood chips (1 part solid for 4 to 10 parts liquid) at 180–195°C in a solvent/water solution at 35–70% wt/vol with or without acidic catalyst. The lignin, recovered by precipitation, has a high degree of purity: it is sulphur-free with low carbohydrates and ash content. Organosolv lignins are readily soluble in organic solvents however, this leads to lignin with a high level of α-O-4 and β-O-4 cleavages while the biphenyl (5-5') content is increased, affecting the reactivity of the lignin. One of the best known organsolv lignins is Alcell lignin (from the ethanol based process) and it is expected that once these lignins are valorised to high end applications such as for example carbon fibres, the level of investment required for the implementation of the organosolv process at scale will be justified [49].
3. Sulphite process called acidic pulping which involves treatment with aqueous (bi)sulphite with Na-, Mg-, Ca- or NH_4-hydroxide. Lignin is extracted from black liquor as water-soluble lignosulphonate.

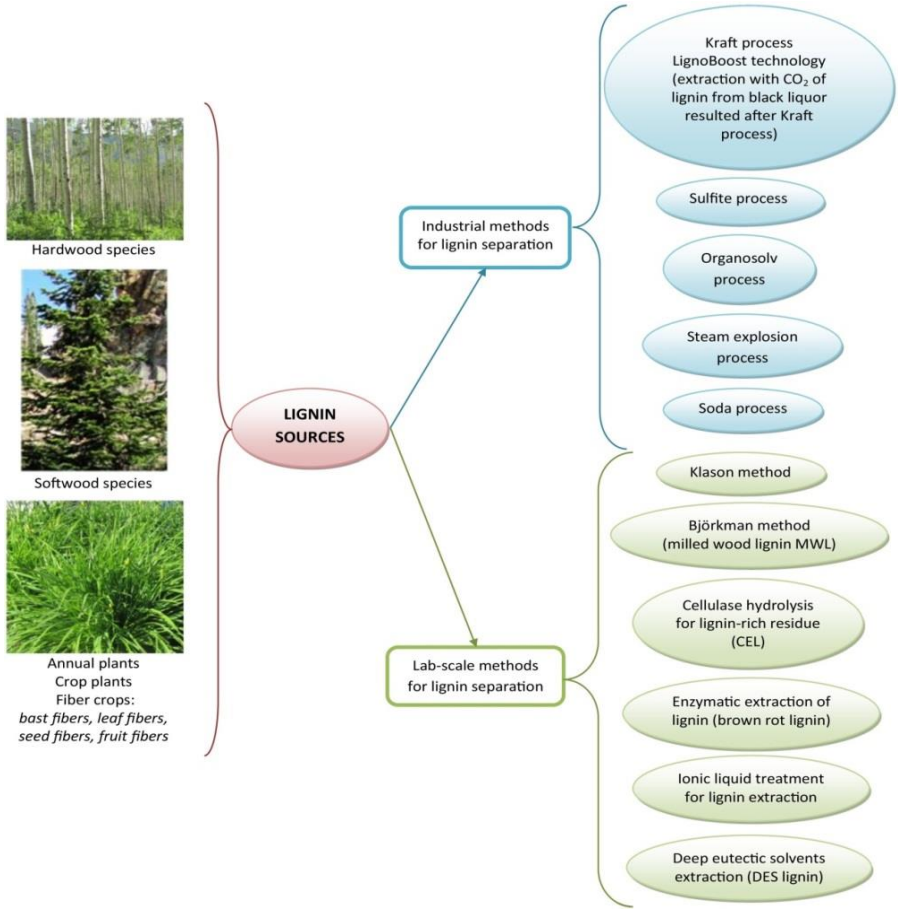

Figure 1.10 Schematic representation of the industrial and lab-scale methods used for lignin separation [49].

4. Steam explosion process which involves short-period steam pre-treatments at temperatures ≥200°C and subsequent fast decompression. This is followed by lignin extraction with organic or aqueous alkali solvents from the exploded lignocellulosic material.

Successful lignin valorisation of highly cross-linked lignin structure often requires preceding chemical modification or fractionation step. In the latter process, fractions of lignin with different M_w are separated by organic solvents, selective precipitation, ultrafiltration or enzymatic treatments. Individual fractions with different chemical and physical properties can be separated from each other sequentially, as illustrated in Figure 1.11. Fractionation has been found beneficial for mechanical performance of CF derived from Kraft lignin [50].

As a low value by-product of the pulp and paper industry, most of lignin is burned for onsite electricity generation. Hence, lignin is a perfect renewable feedstock candidate for wide range of engineering applications [49] such as energy storage devices [51],

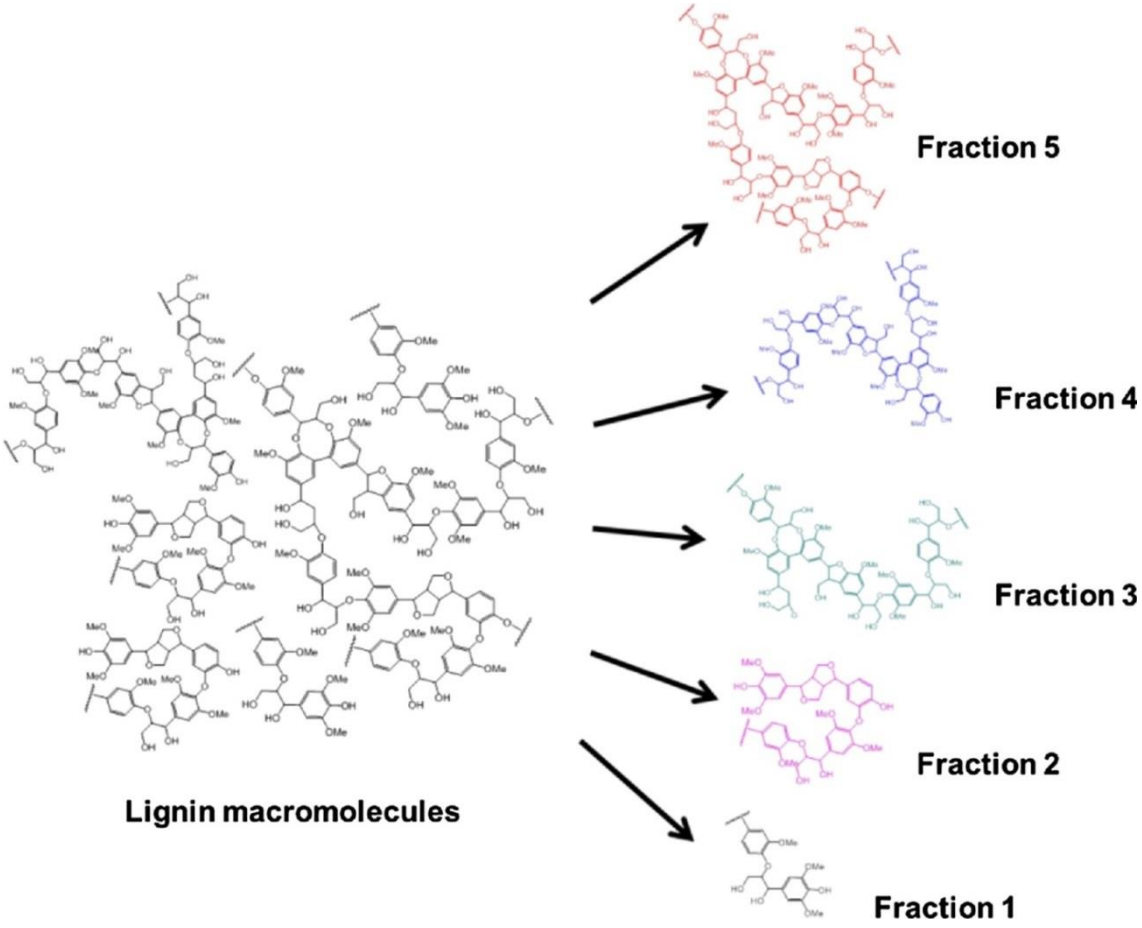

Figure 1.11 Schematic representation of sequential fractionation of lignin. Reproduced with permission from Elsevier [52].

hydrogels [53], resins [54], adhesives [55], antioxidants [56] and most importantly as cost-effective precursor for carbon fibre production due to its aromatic structure [9,35,57,58]. Lignin can be formulated to enable processing via melt spinning of precursor fibre. An important advantage of melt spinning over wet spinning process used for PAN precursor production is that no solvent is required. Instead, melt spinning involves melting of the polymer which eliminates the need for subsequent solvent recovery. Comparison of the three main types of spinning is shown in Figure 1.12.

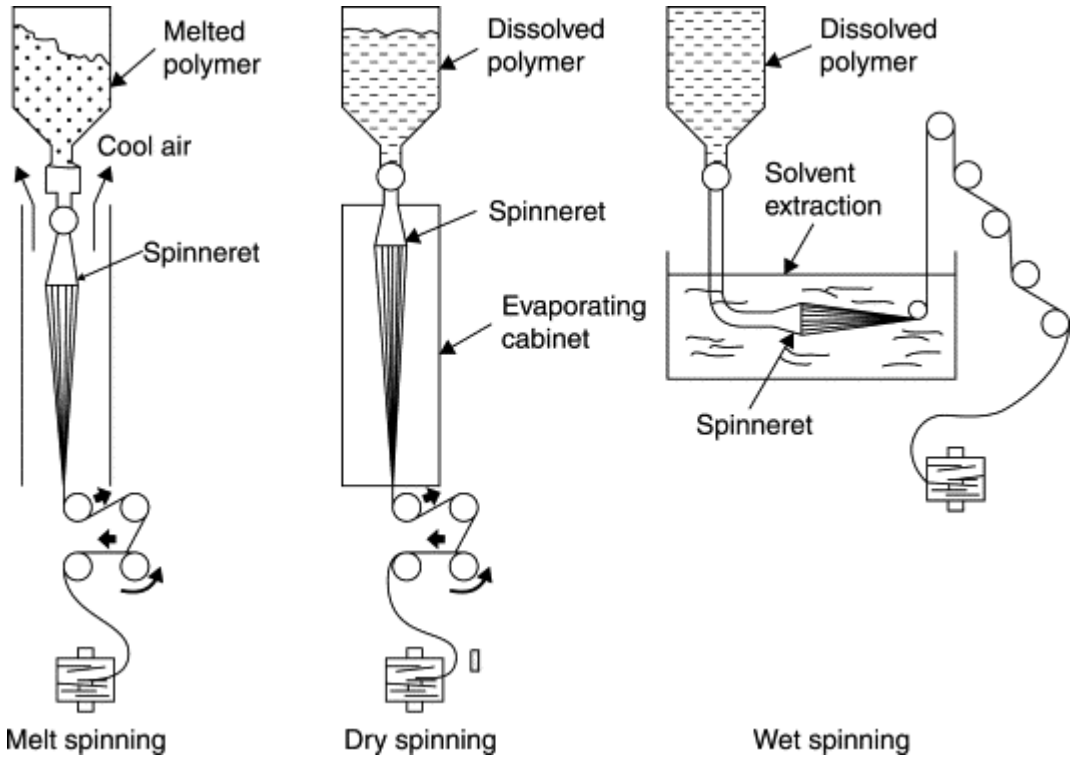

Figure 1.12 Schematic representation of Reproduced with permission from Elsevier [59].

1.6 Objectives

This project aims to reduce energy consumption during manufacturing of CF through a microwave carbonisation, utilising a microwave susceptor technology at the nanoscale. The project goes beyond the state-of-the-art through the incorporation of this technology in sustainable lignin-based precursor materials as well as PAN-based precursor materials for energy-efficient and cheaper carbon fibre production. The objectives can be summarised as follows:

1) Application of susceptor assisted MW heating for carbonisation of PAN and lignin-blend precursor.
2) Investigate the effects of susceptor coating thickness, sample preparation sequence and MW power level on maximum achievable conversion rate to CF, morphology and mechanical properties (modulus and tensile strength).
3) Life cycle analysis and modelling of temperature distribution during MW carbonisation.
4) Low energy, low carbon emission process utilising a modified domestic microwave system.

Summary of Chapters

A chapter map is illustrated in Figure 1.13, which outlines the methodology behind this thesis.

In Chapter 2, recent advances in lignin precursor systems and alternative conversion methods are summarised.

In Chapter 3, starting materials, sample preparation, characterisation and experimental methods are detailed.

Chapter 4 deals with susceptor technology used for MW heating and their characterisation.

In Chapter 5, susceptor assisted MW carbonisation of PAN is studied. The effects of susceptor coating thickness, route of preparation and microwave power are investigated in order to find optimal carbonisation conditions for enhanced mechanical properties of produced CF.

In Chapter 6, susceptor assisted MW carbonisation of bio-based and sustainable lignin/TPU blend has been investigated. Similarly, the effects of susceptor coating thickness, sample preparation sequence and MW power level on maximum achievable temperatures, conversion to CF and mechanical properties have been investigated.

In Chapter 7, results of a model of microwave heating and LCA analysis are presented, where data from previous chapters was utilised to model the heating mechanism. Furthermore, microwave carbonisation is applied to carbonise other lignin-based materials: foams and carbon nanofiber (CNF) mats, to show the transferability of this technology.

Finally in Chapter 8, conclusions have been drawn and future work has been proposed.

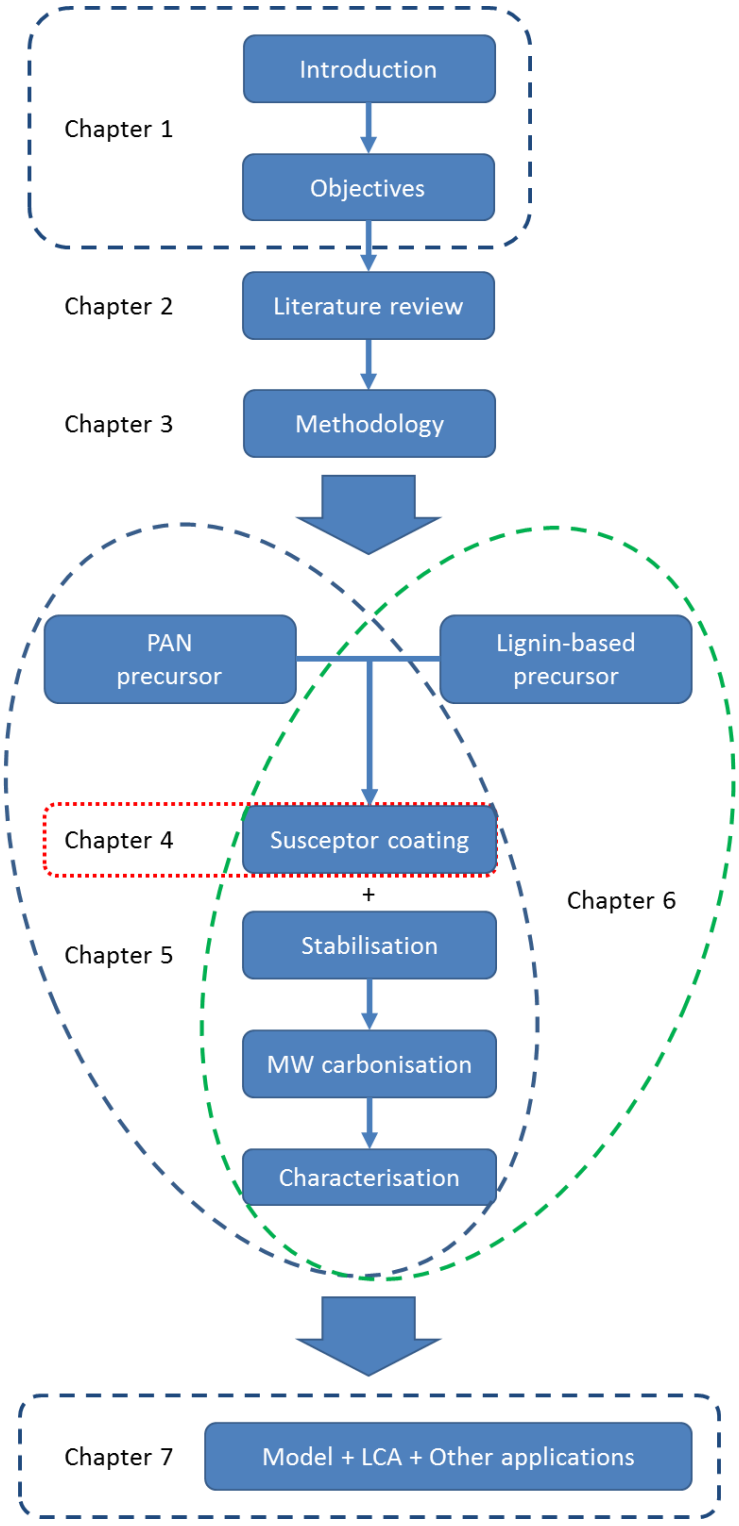

Figure 1.13 Chapter map illustrating the line of thought.

Chapter 2

Literature review of alternative CF conversion methods

2.1 Optimisation of conventional process

To reduce cost and time of CF production, the conventional conversion process has been optimised and modelled over the years [7,60–63]. Stochastic modelling of carbonisation [64] and heuristic modelling of stabilisation [65] were demonstrated. While Artificial Neural Network (ANN) and Support Vector Regression techniques were compared in a study to optimise the stabilisation process [66]. It was reported that ANN offered better accuracy and achieved up to 48.6% energy savings at a density constraint of 1.27 g/cm^3 ≤ ρ ≤ 1.29 g/cm^3. In another study [67], it was concluded that the Recurrent Neural Network outperformed other models in predicting CF tensile strength (TS) and modulus (YM) from precursor information and process parameters.

2.2 Alternative stabilisation methods

Alternative stabilisation treatments or pre-treatments have been investigated in the past. Effects of electron beam (EB) pre-oxidation/cyclisation are reported in several studies. Dietrich *et al.* reported reduction in stabilisation time to one-third for EB-irradiated PAN precursor fibre, but at the expense of up to 50% of relative tensile strength [68]. Miao *et al.* noticed that pre-irradiation of PAN decreases the onset temperature of stabilisation and increases char yields [69]. (Yuan, Wang, Liu, *et al.* reported EB-induced cyclisation at room temperature, which similarly led to lower onset temperature of stabilisation, but resulted in formation of skin-core structure of the fibre [70]. Interestingly, Seo *et al.* demonstrated EB-crosslinking of electrospun PAN/lignin nanofiber (NF) mats in nitrogen atmosphere, which resulted in an increase of relative tensile strength even up to 480% [71]. Yu *et al.* studied the effect of EB irradiation, which could reduce stabilisation time and increase fibre density, but provided no data of its mechanical performance [72]. Park *et al.* reported shortening of stabilisation of PAN even at low doses (200kGy) of EB-irradiation [73]. Derived CF had TS and YM of 2.3 and 216 GPa, respectively. Yoo *et al.* showed that EB irradiation could prevent fusion of fibres and reduce thermal stabilisation by up to 64% [74]. Zhang *et al.* monitored degree of pre-oxidation by measuring polyene radical concentration in the samples [75]. EB-irradiation of 400kGy reduced the original stabilisation time to a quarter. Gohs *et al.*

investigated reactions induced by EB in PAN copolymer (Co-PAN) powder [76]. The effects of air and nitrogen atmosphere on properties such as gel content, radical content, extent of cyclisation and the residual mass at 800°C were studied.

The effect of γ–irradiation is described by several authors. Tarakanov reported that γ–rays decrease duration of PAN oxidation until fibre with a given density is obtained [77]. Zhao *et al.* concluded that γ–irradiation of PAN reduces the onset and heat evolution of thermal reactions [78]. Liu *et al.* studied γ–rays irradiation of Co-PAN fibres in vacuum, which led to similar conclusions: low dose of radiation induces crosslinking, reduces the onset temperature of cyclisation, alleviates the exothermic behaviour and hence accelerates the stabilisation process [79]. In another publication, Liu *et al.* compared the effects of vacuum, air and oxygen atmosphere on γ–irradiation of PAN and its thermal curing [80]. More recently, Zhao, Lu, Wang, *et al.* investigated radiation-induced crosslinking of PAN/Co-PAN in their publications [81–83]. They reported that apart from previously mentioned effects, the use γ–rays give rise to fewer defects, increased crystallite size/orientation and hence improve tensile strength and modulus by 13.2 and 2.6 %, respectively. Naskar *et al.* described UV-irradiation and thus accelerated stabilisation of melt-processible Co-PAN [84]. Yuan, Wang, Yu, *et al.* studied the effect of UV on stabilisation of PAN [85]. They indicated that the treatment increases fibre density, crystallite size/orientation and reduces skin-core effect.

There are few reports of plasma processing and pre-treatments as an alternative to conventional stabilisation. Xu *et al.* demonstrated that radio frequency (RF) plasma pre-oxidation improved morphology and oxidation uniformity of fibres [86]. Lee *et al.* reported that RF plasma stabilisation occurs at faster rate and can enhance tensile strength and modulus of CF by up to 30% and 4%, respectively [87]. Kim, Lee, *et al.* described continuous RF plasma-assisted stabilisation of PAN [88]. CF with TS and YM of up to 2.6 GPa and 148 GPa, respectively, was reported for the sample stabilised in 45 min. Finally, the same group demonstrated combined plasma-assisted stabilisation of EB-irradiated PAN, managed to reduce total stabilisation time to 13.3 min and produce CF with TS of 2.4 GPa and YM of 196 GPa [89]. CF properties were improved to 2.9 GPa and 224 GPa by increasing stabilisation time to 33.3 min. Elagib *et al.* described microwave stabilisation of PAN incorporated with CNTs and titania nanoparticles [90]. The proposed approach reduced onset and exothermic rate of cyclisation, but involved addition of MW susceptors into the spinning solution. Recently, Zhao *et al.* showed that MW heating can shorten time and reduce temperature

of stabilisation by about 20°C [91]. Wang *et al.* demonstrated molecular dynamics simulations of MW heating of PAN in the frequency range of 20-100 GHz [92]. They suggested that predicted selective heating of -C≡N groups could be exploited for MW stabilisation of PAN.

2.3 Alternative carbonisation methods

There are fewer reports of alternative carbonisation methods. White *et al.* patented a continuous system for Microwave Assisted Plasma (MAP) conversion to CF [93]. Kim, Kim, Choi, *et al.* described MAP carbonisation and showed that addition of short low power carbonisation treatment improved tensile strength of the CF [94,95]. Schematic representation of the MAP system is shown in Figure 2.1. Norris, Jr *et al.* evaluated feasibility of carbonisation via MAP, atmospheric pressure plasma torch, induction heating, capacitively-coupled RF plasma [96]. The team (Oak Ridge National Laboratory) managed to scale-up the MAP carbonisation for up to five tows at about 48in/min. However evolution of volatile products during the initial stages of carbonisation is a challenge for the MAP system which operates in the low-to-medium vacuum regime in order to maintain stable plasma. Jin *et al.* compared conventional and MW carbonisation of PAN samples heated at the same rate of 5°C min^{-1}, which resulted in heating times of over 3h to get to 1000°C [97]. Furthermore, control rings used in the study could act as MW susceptors. Cho *et al.* patented MW carbonisation using carbon-based heating element on the surface of a polymer fibre [98]. Lam *et al.* reported MW

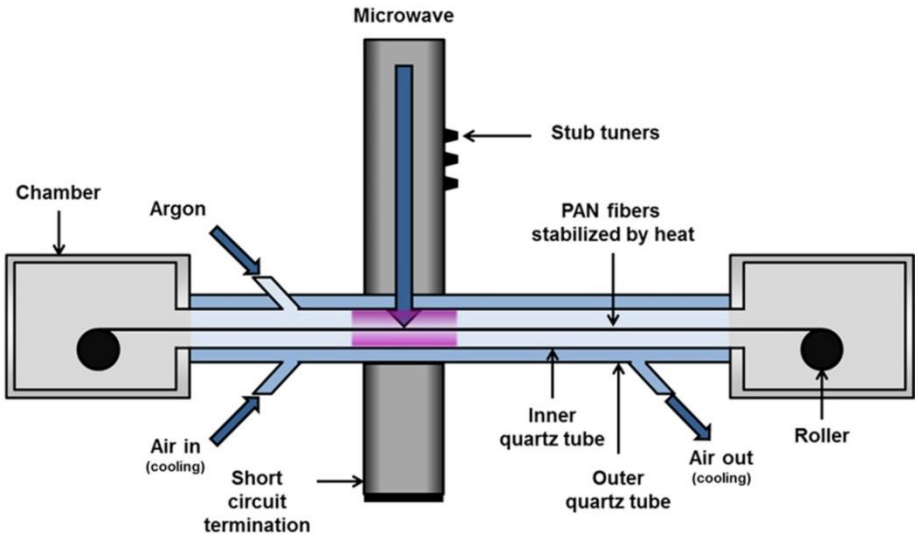

Figure 2.1 Schematic representation of the MAP system. Reproduced with permission from Elsevier [95].

pyrolysis of cellulose-rich bamboo fibre with coconut-based activated carbon as MW susceptor [99]. Unfortunately, the susceptor application method would be difficult to apply for continuous production of CF.

Alternative pre-treatments, stabilisation and carbonisation methods are summarised in Table 2.1. It is evident that most of the research up to date focused on alternative

Table 2.1 Summary of alternative conversion methods and pre-treatments found in the literature. Conv: conventional stabilisation/carbonisation reported; "-": no treatment/conversion step reported.

Pre-treatment	Stabilisation Technique	Carbonisation Technique	Precursor Material	Reference
EB	Conv	-	PAN	[68]
EB	-	-	PAN	[69]
EB	Conv	-	PAN	[70]
EB	-	Conv	PAN/lignin	[71]
EB	Conv	-	PAN	[72]
EB	Conv	Conv	PAN	[73]
EB	Conv	Conv	PAN	[74]
EB	Conv	-	PAN	[75]
EB	-	-	Co-PAN	[76]
γ	Conv	-	PAN	[77]
γ	-	-	PAN	[78]
γ	Conv	-	Co-PAN	[79]
γ	-	-	PAN	[80]
γ	Conv	-	Co-PAN	[83]
γ	Conv	Conv	Co-PAN	[82]
γ	Conv	Conv	PAN	[81]
UV	Conv	-	Co-PAN	[84]
UV	Conv	-	PAN	[85]
-	RF plasma	-	PAN	[86]
-	RF plasma	Conv	PAN	[87]
-	Atmospheric plasma assisted	Conv	PAN	[88]
EB	Atmospheric plasma assisted	Conv	PAN	[89]
-	MW	-	PAN	[90]
-	MW	-	PAN	[91]
-	MW simulation	-	PAN	[92]
-	Microwave Assisted Plasma (MAP)	Microwave Assisted Plasma (MAP)	-	[93]
-	Conv	MAP	PAN	[94,95]
-	-	MAP, atmospheric plasma torch, induction heating, RF plasma	PAN	[96]
-	-	MW	PAN	[97]
-	-	MW	-	[98]
-	-	MW (activated carbon)	Cellulose-rich bamboo fibre	[99]

stabilisation techniques and treatments that could shorten stabilisation time. Alternative carbonisation methods are scarce and not easily transferable to continuous CF production. MW was already reported as a viable alternative for PAN stabilisation [90–92], whereas application of MW susceptor technology enables achievement of higher temperatures required for successful carbonisation [15].

2.4 MW heating in CFRP processing

It is worth noting that MW heating has already been considered as an alternative method for composite curing, offering volumetric heating at reduced time and cost of processing. Although reports of microwave curing date back quite a long time [100–102], it still receives much attention in the context of CF reinforced composites [103–108]. Most of these studies compared conventional autoclave and microwave curing of CF/epoxy systems, reported reduction of curing time and temperature gradients. Homogeneity of MW curing was further improved by development of the "Hephaistos" MW curing system [14]. Selective heating of CF during MW can lead to improvement of mechanical properties via enhanced adhesion between the fibre and the matrix [104,108,109]. On the other hand, this prevents penetration of MW radiation and could result in uneven heat distribution in thicker sections of the composite [110]. Recent reviews discuss these issues in detail and emphasize the need for production of real-world components for full potential realisation of MW curing [111,112].

Recently, MW assisted recycling of CF reinforced composites has been reported [113], which is an important aspect in view of growing composite market [114,115]. This also indicates a potential for MW heating as a versatile heating method to be employed at various processing stages, including recycling of waste CF.

2.5 Choice of MW susceptor and application method

Carbon nanotubes are known for their excellent conductivity and absorption of microwave energy [116–119]. Conventional conducting fillers require the filler content to be as high as 10-50%. Due to the high aspect ratio of carbon nanotubes, the percolation threshold required for transition from an insulator to a conductor is achieved at a lower concentration of the conducting filler [117]. Thus the susceptor cost fraction of the microwave heating is reduced and introduction of defect-inducing impurities into the carbon fibre is limited. The amount of the susceptor used can be reduced further by application only at the surface of the material, which reduces the problem of uniform

dispersion of CNTs in the precursor fibre. CNTs grown on CFs by chemical vapour deposition (CVD) were reported to improve mechanical performance of the fibres and their composites [120–123]. This approach involves growth on already carbonised material, usually above 700°C and in the presence of reactive atmospheres which can lead to fibre degradation. The problem of uniform distribution of CNTs at the surface of the precursor fibre can be solved by a layer-by-layer method proposed by other researchers [124–127]. Culebras *et al.* reported layer-by-layer deposition of thin films of nanocomposite with multiwalled carbon nanotubes (MWCNT) [127]. This technique involves electrostatic self-assembly of highly conductive nanolayers from aqueous suspensions and at room temperatures, which is very important from an energy usage perspective.

Although MW absorption of carbonaceous materials was studied over wide range of MW frequencies [31,128], the frequency of 2.45 GHz was chosen for this study as it is most commonly used for heating in industrial, scientific and medical applications.

2.6 Choice of precursor

As described in the previous chapter, PAN is currently the most common precursor for CF production. Due to drawbacks associated with PAN and petroleum-derived chemicals in general, renewable precursors have attracted increasing attention, in particular lignin [58,129]. Properties of lignin are strongly dependent on the source (plant species) and extraction methods used. Latest developments in lignin utilisation have been summarised in a review by Collins *et al.* [49]. Processing of lignin for CF production is challenging due to its brittleness and lack of melting. Lignin fractionation [130], modification or blending with other polymers [38] have been proposed to overcome these issues. Lignin blends with thermoplastic polyethylene oxide (PEO), polypropylene (PP) and polylactic acid (PLA) have been investigated in the past [58], but proved to be difficult to carbonise or not compatible with lignin. Recently, melt-processible blend of Alcell organosolv hardwood lignin (lignin) and thermoplastic polyurethane (TPU) has been identified as a promising precursor for sustainable carbon fibre [38]. The work reported promising results for the 50:50 lignin:TPU blend, with TS and YM values of 1.1 and 80 GPa, respectively. The work presented here was a part of the same H2020 “LIBRE” consortium and therefore the material was readily available for investigation of MW susceptor technology for CF production from sustainable lignin-based precursor.

Chapter 3

Materials and experimental methods

3.1 Materials

Wet spun PAN fibres were obtained from Dralon GmbH, Germany. A blend of Alcell organosolv hardwood lignin (lignin) with a M_w = 3950 g/mol, PDI = 4.7 (supplied by Tecnaro, Ilsfeld, Germany) and thermoplastic polyurethane (TPU; Pearlthane ECO 12T95, obtained from Veltox, France, manufactured by Lubriozol) was developed at UL and prepared via melt-spinning into precursor fibre in a ratio of 50:50. Fibres were extruded using an xplore MC15 microcompounder. Materials were compounded during the first run, and precursor fibres were produced in the second run of extrusion. The spinneret diameter was 1.5 and 0.5 mm for compounding and spinning, respectively. The screw speed was 100 and 50 rpm for compounding and fibre spinning, respectively. The processing temperature profile used was 155/180/190/180°C. Elicarb™ Multi-Walled Carbon Nanotubes (MWCNTs) with an average diameter of 10 - 12 nm were obtained from Thomas Swan and Co. LTD. The following were purchased from Sigma Aldrich (St. Louis, MI, United States): Poly(diallyldimethylammonium chloride) (PDADMAC), with a molecular weight of 100,000 - 200,000 g/mol; sodium deoxycholate (SDOC) ($C_{24}H_{39}NaO_4$); Tolylene-2,4-diisocyanate; n-hexane; Poly(ethylene glycol) diglycidyl ether (PEGDGE) with M_w = 500 g/mol.

3.2 Susceptor coating

Prior to the coating, surface activation by corona treatment of the precursor fibre was performed using BD-20AC Laboratory Corona Treater (Electro-Technic Products) in order to improve wettability and hence the quality of the subsequent susceptor coating. This was done by placing prepared lengths of precursor fibres on the desk and treatment of the fibre bundle a few times on each side before coating. Precursor fibres were then coated with a microwave susceptor coating containing multi-walled carbon nanotubes (MWCNTs) following similar procedure to previously described in the literature [127]. Cationic solution of 0.5 wt% of PDADMAC in DI water was prepared. Anionic suspension of MWCNTs was prepared via manual grinding of 0.05 wt % MWCNTs with an agate mortar and pestle and dispersing in an aqueous solution of 2 wt% SDOC. It was then sonicated for 20 min, followed by 15 min sonication with a 15 W tip in an

ice water bath, and another 10 min of bath sonication for homogenisation. The suspension was then centrifuged at 4000 rpm for 5 min and the supernatant was decanted. Fibres were immersed into a cationic solution for 5 min, followed by rinsing and drying using a gentle stream of compressed air, and then dipped into an anionic suspension for another 5 min. This process results in one deposition cycle of a susceptor coating, as illustrated in Figure 3.1. Immersion in PDADMAC solution deposits a layer of positively charged polymer on the precursor fibre surface. This is followed by immersion of the fibre in MWCNT aqueous suspension in SDOC. Electrostatic interaction between negatively charged SDOC and positively charged polymer leads to deposition of MWCNTs. By repeating this procedure, a MWCNT-based thin film is grown incrementally with each cycle.

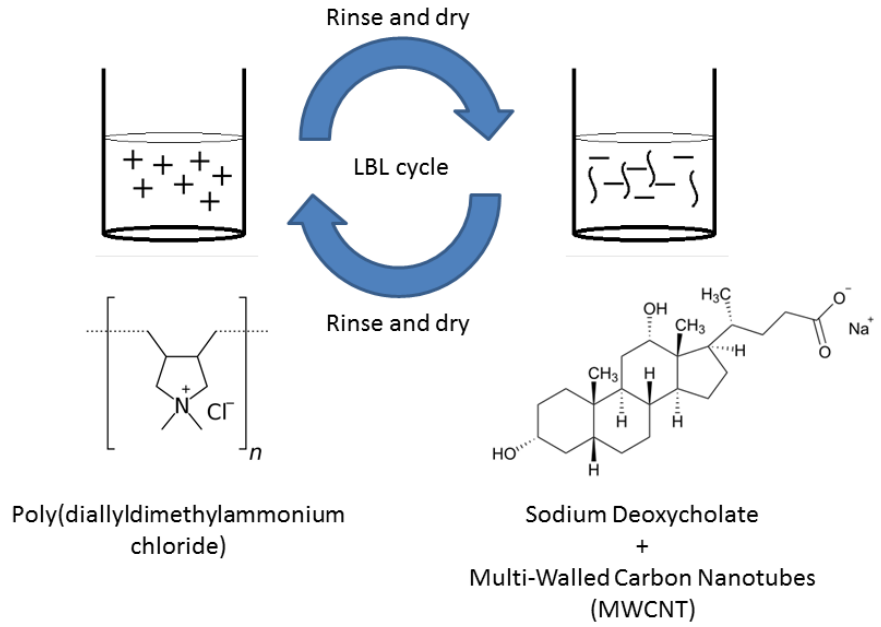

Figure 3.1 Layer-by-layer cycle of susceptor coating deposition.

After the initial cycle, all subsequent cycles were completed with 2 min dip times. This was repeated to deposit desired number of susceptor layer cycles. Subsequent samples are referred to as Xc, where X signifies the number of cycles. Fibre samples with deposited multilayer films were air-dried overnight and then stored in a desiccator prior to further processing and characterisation. Two routes of sample preparation were investigated: (i) susceptor coated before stabilisation, (ii) susceptor coated after stabilisation. The experimental process and two routes of sample preparation are illustrated in Figure 3.2.

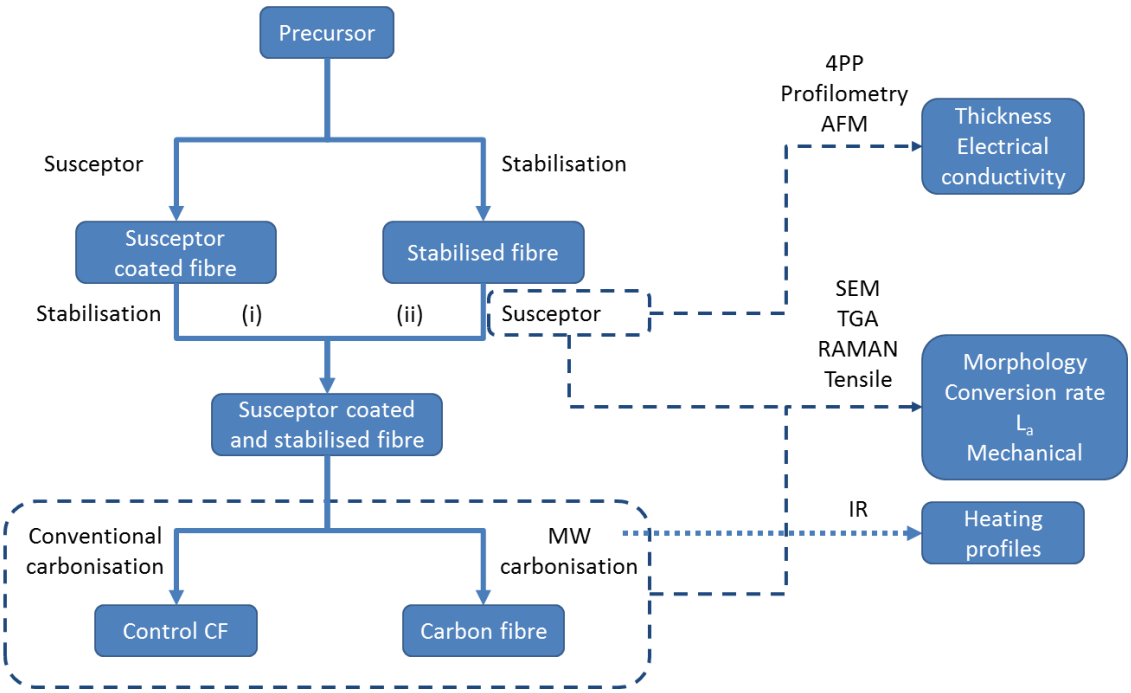

Figure 3.2 Summary of the experimental process, including two routes of sample preparation (i) and (ii).

3.3 Thermo-oxidative stabilisation

PAN samples were stabilised by heating in air at a ramp of 1°C min^{-1} until 250°C, followed by 1h isothermal at 250°C. All stabilisation was performed in a BINDER convection heating oven, where fibre samples were stretched using paper clips, as shown in Figure 3.3.

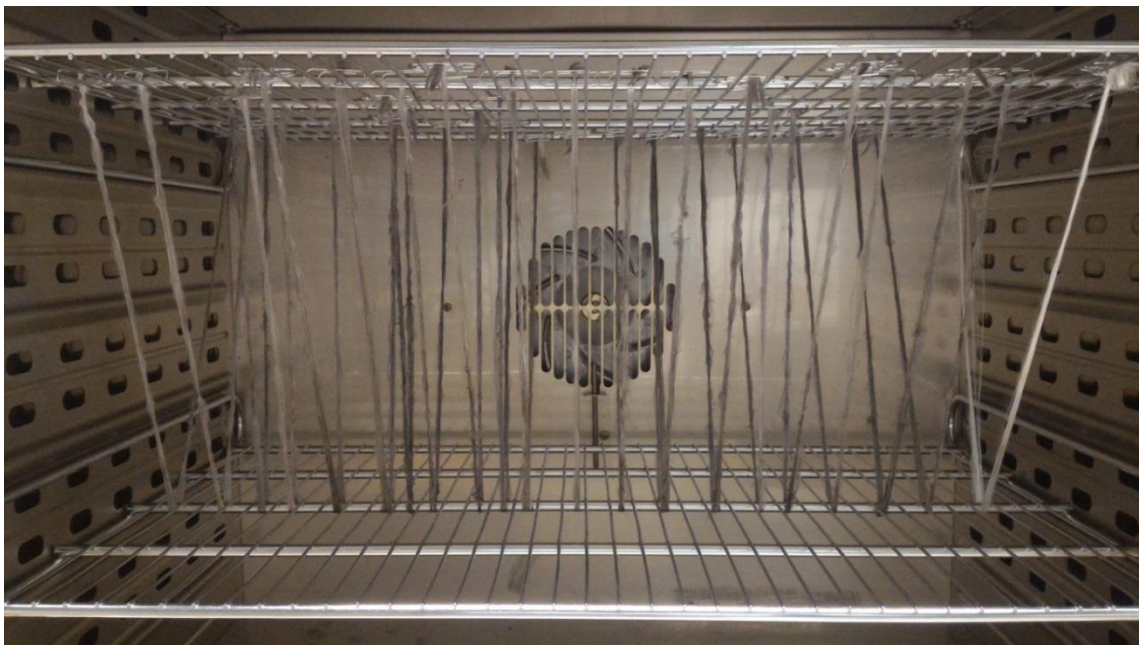

Figure 3.3 PAN precursor fibres prepared for stabilisation in a convection oven.

Lignin/TPU blend samples were dipped for 5 min in a cross-linker solution of 10 wt. % of Tolylene-2,4-diisocyanate (2,4-TDI) in n-hexane prior to stabilisation. Cross-linking of lignins using diisocyanates such as TDI was reported in the past [131] and is known to proceed by reaction of the isocyanate group (-N=C=O) with the hydroxyl (-OH) group of lignin with the formation of a urethane bond [132]. Schematic representation of 2,4-TDI and the cross-linking of lignin via the –OH group is shown in Figure 3.4.

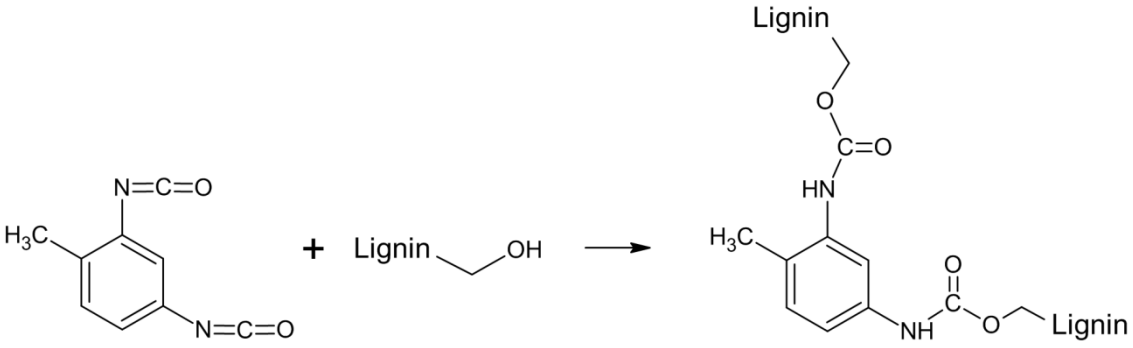

Figure 3.4 Simplified representation of cross-linking of lignin with TDI.

Stabilisation of lignin/TPU samples was performed in air at a ramp of 1°C min^{-1} until 250°C, with 2h isothermals at 100, 150, 170, 200 and 250°C. The samples were hanging more loosely compared to PAN samples shown in the image above, to prevent breakage and fusion of fibres during shrinkage. Individual fibres of each lignin/TPU sample were separated manually before dipping in a cross-linker solution and after each isothermal to prevent build-up of fused fibres during stabilisation (Figure 3.5). If too many of individual fibres in the strand were fused, the sample lost its flexibility and it was very difficult to mount it for MW carbonisation, which is explained in the following parts.

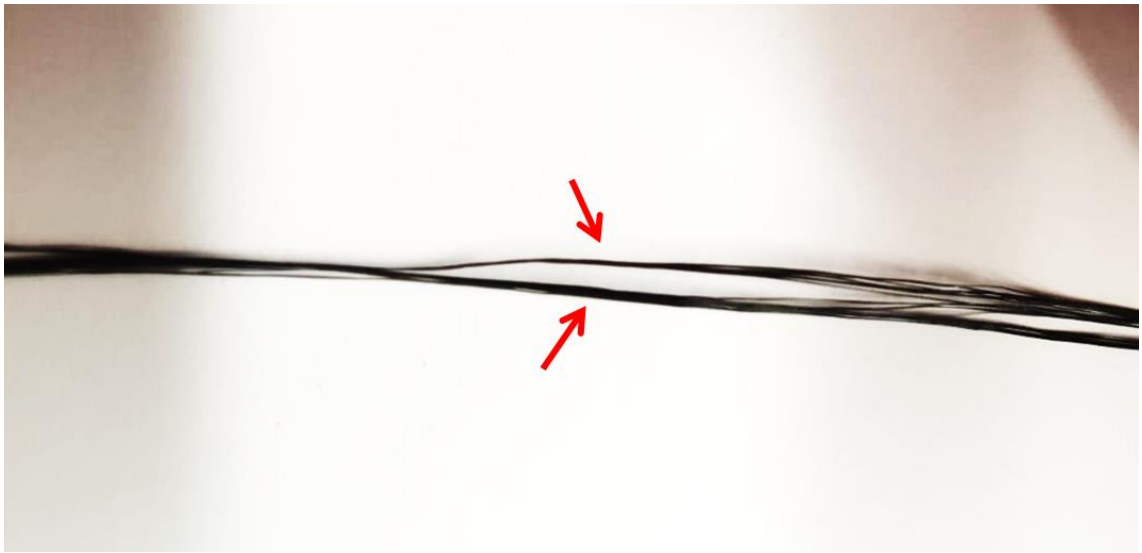

Figure 3.5 Image showing fused lignin/TPU fibres.

3.4 Conventional carbonisation

Stabilised PAN and lignin/TPU fibres were placed on a stainless steel holder inside a quartz tube reactor of an electrical LENTON tube furnace. Reactor was then closed and vented with N_2 for 30 min. After that samples were carbonised by heating to 1000°C at 10°C min^{-1} with a 30 min isothermal at 1000°C. Schematic of a tube furnace used for conventional carbonisation is shown in Figure 3.6.

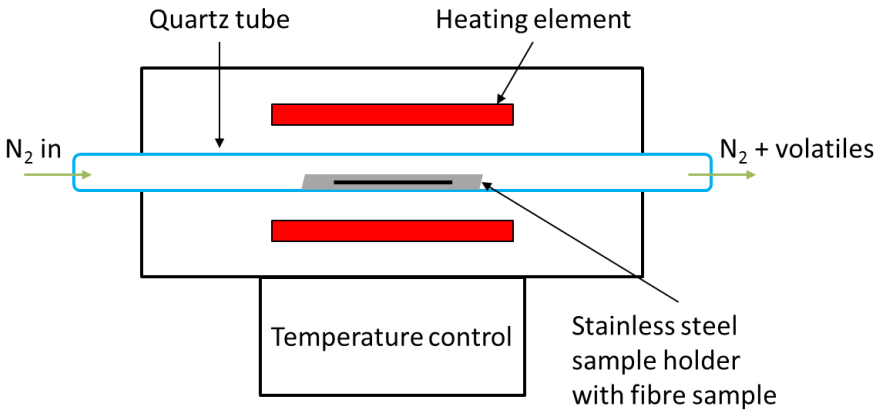

Figure 3.6 Schematic of a tube furnace and a stainless steel sample holder used for conventional carbonisation.

3.5 Microwave carbonisation

Prepared fibre samples were carbonised in a custom-made setup designed by the author of this thesis based on a domestic microwave oven, as illustrated in Figure 3.7. Firstly, locations of hot spots in the oven were estimated using food products. Accordingly, a hole was drilled in the top cover of the MW oven, above the hot spot location, to allow for temperature reading and ventilation of the flask.

A holder for an Erlenmeyer flask was designed by the author to ensure the following:

1) The precursor fibre sample could be positioned about 10 cm below the infra-red (IR) temperature sensor to enable focusing of the IR radiation through its lens.

2) The inside of the flask could be sealed off and vented with N_2 gas.

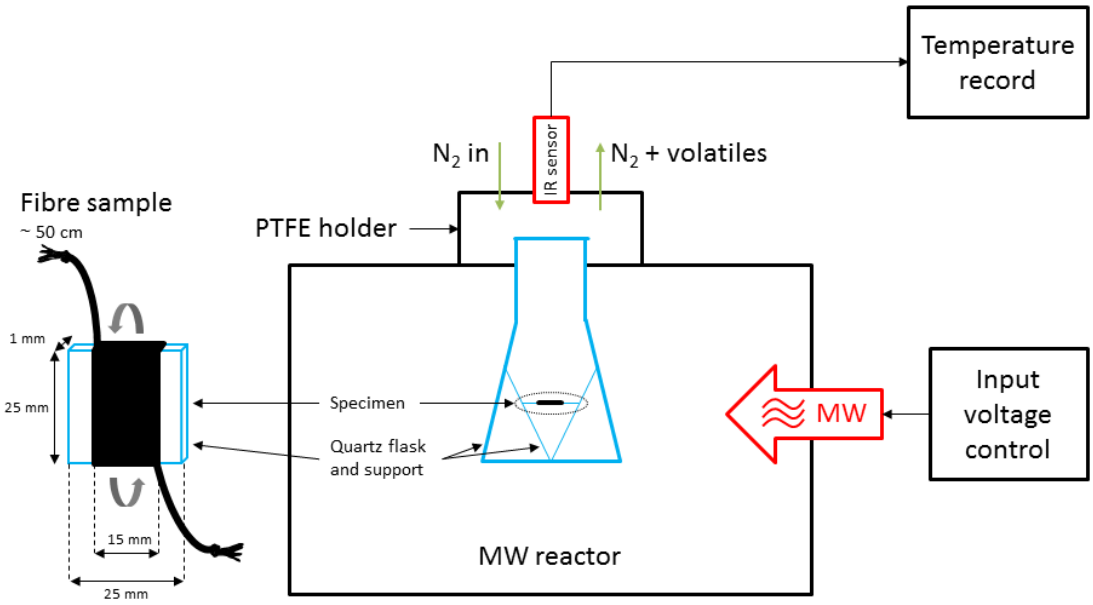

Figure 3.7 Schematic representation of the microwave heating setup used in this study.

Figure 3.8 shows three designs of the flask holder prepared for this study. First design (Figure 3.8 A) was adapted to IR sensor with a lower temperature range (0-1000°C) and machined from Polytetrafluoroethylene (PTFE). Figure 3.8 B shows the second holder adapted to IR sensor with broader temperature range (250-1800°C). The holder was machined from Al-alloy, but this resulted in no heating of the fibre, possibly due to absorption of MWs by the holder and hence this design was abandoned. Therefore, the third holder (Figure 3.8 C) was made from PTFE and allowed recording of MW carbonisation heating profiles presented in this work.

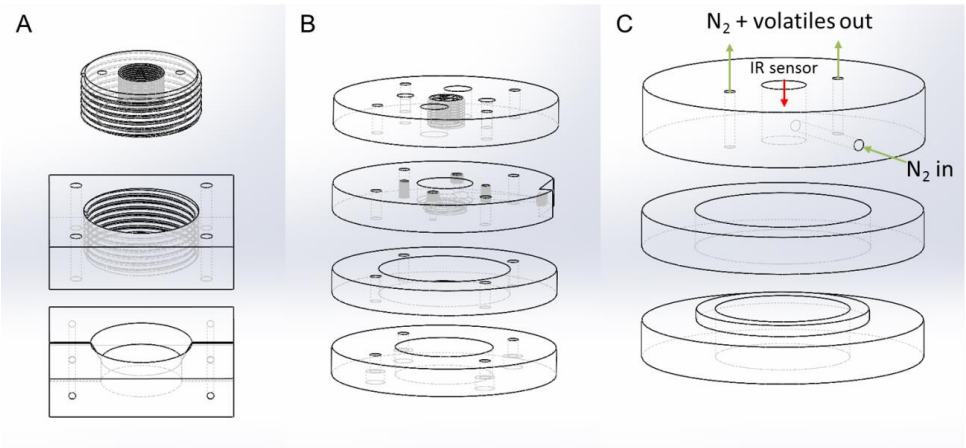

Figure 3.8 Solidworks designs of the flask holders prepared in this study. A – design used during the first tests (PTFE), B – unsuccessful design made for high temperature sensor (Al-alloy), C – the most successful design for high temperature sensor (PTFE).

Images of MW carbonisation setup are shown in Figure 3.9. The choice of materials for the sample support, the flask (Figure 3.9 A) and the holder (Figure 3.9 B) was dictated by experimental conditions and properties of microwaves at 2.45 GHz. Initially, samples supports made from alumina plates and flasks from borosilicate glass were used, but the former shattered during heating and the latter were prone to overheating and even melting, especially during carbonisation of lignin/TPU precursor. Consequently, microscope slides and flasks from fused quartz were used due to their excellent thermal shock resistance, MW transparency (loss tangent of 0.0003 - [133,134]) and high operating temperatures >1000°C. Microscope slides were cut to appropriate lengths to support the fibre sample at the correct position below the IR sensor. Polytetrafluoroethylene (PTFE) was used for making the flask-sealing holders, due to the low loss tangent value of 0.00048 [133,134]. The holder was covered with layers of aluminium foil and electromagnetic shielding box which prevented leakage of MWs during operation.

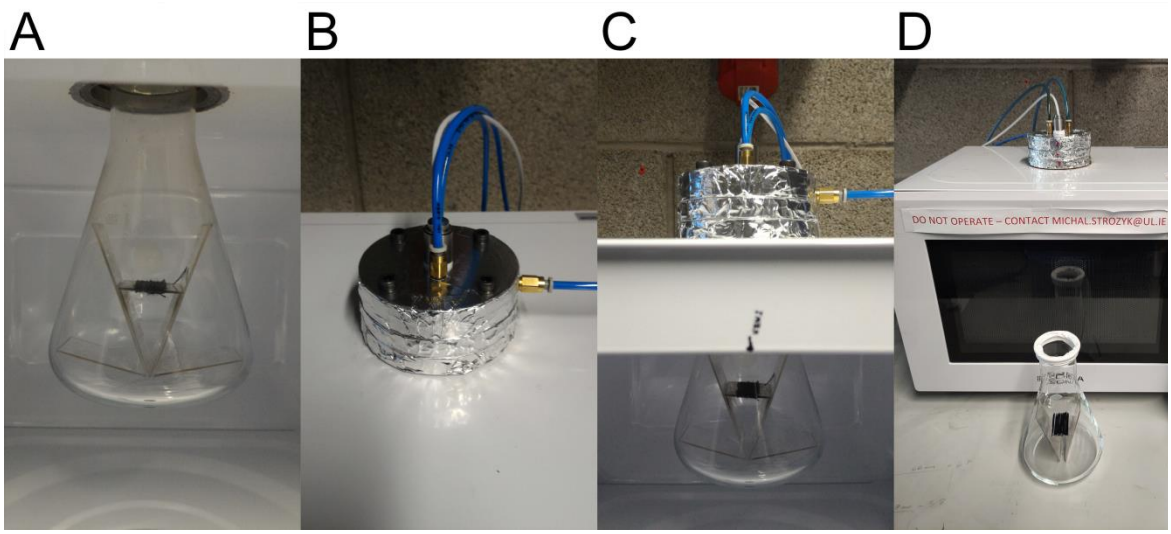

Figure 3.9 Images of MW carbonisation setup used in this study. A – Quartz flask and sample support, B – flask holder (PTFE wrapped with aluminium foil) with IR sensor and gas inlet/outlet tubing, C – fibre sample prepared for MW carbonisation, D – image of the domestic microwave.

Fibre samples were wrapped around a piece of microscope slide, placed in an Erlenmeyer flask and sealed with the top part of the flask holder. N_2 gas was allowed to flow through the flask for 30 min after insertion of the sample (Figure 3.9 C) and during the heating. Microwave heating was performed in a modified domestic microwave (Figure 3.9 D) with a maximum output power of 700W. The microwave was operated in two modes: (a) high power level - at full power; (b) progressive power levels – where

input voltage was increased progressively from 165V to 230V. The voltage was increased incrementally from 160-165V to provide five progressive levels of MW power, with the final one at 230V (700W). The power was not changed until the sample temperature was stable, which resulted in differences in carbonisation times of progressive carbonisation. Total heating time was up to 20 min for mode (a) and 30 - 40 min for mode (b). MW carbonisation heating profiles were recorded using an IR pyrometer Calex PyroUSB PUA8 with a temperature range of 0-1000°C or Optris CT 3M with a temperature range of 250-1800°C. Experimental estimation of the emissivity was performed using a setup shown in Figure 3.10. Stabilised fibre was heated from below and the surface temperature was measured using Type K thermocouple. IR sensor recorded the surface temperature and the emissivity was adjusted to match the reading of the thermocouple. It was in reasonable agreement with values found in literature [135,136], and the emissivity was assumed to be constant at 0.9.

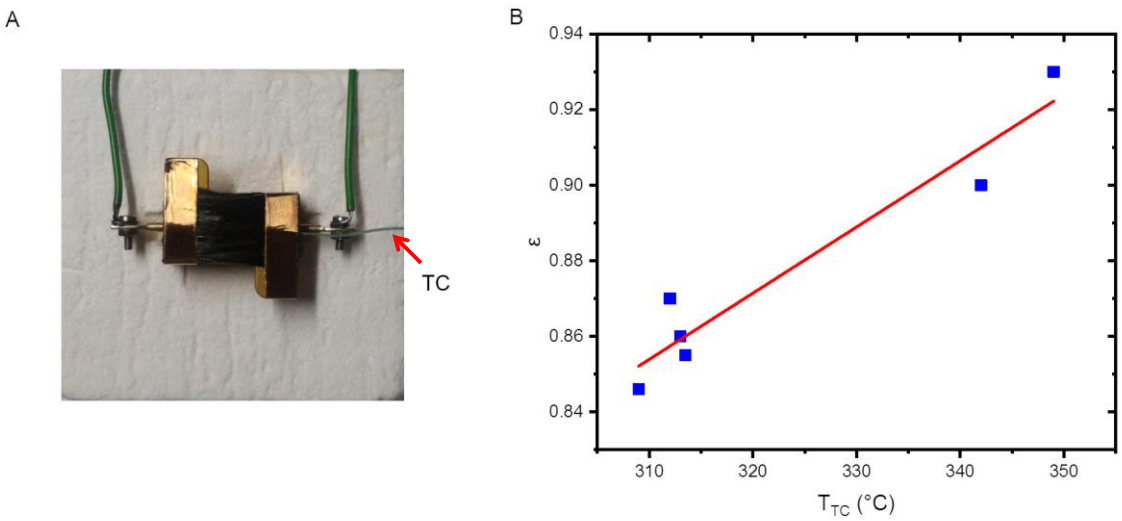

Figure 3.10 A - Setup used for emissivity estimation, B - Emissivity (ε) adjusted as a function of thermocouple temperature (T_{TC}).

After heating, the fibre was allowed to cool down to at least 250°C in an N_2 atmosphere prior to storage and characterisation. Periodic signal noise/vibration was present in some of the recorded heating profiles, which is due to periodical change of the electromagnetic field of the microwave [92]. These profiles were smoothed for clarity in Origin software.

3.6 Material characterisation

SEM was performed utilising a Hitachi TM1000 at 15 kV for general imaging of the produced CF and a Hitachi SU70 microscope at 10 kV for higher magnification

imaging. Samples were mounted on 15 mm aluminium stubs using carbon and copper conductive tapes prior to analysis. Fibre diameter was calculated from SEM images, as an average of at least 12 separate measurements.

RAMAN spectra were recorded by utilising a Horiba LabRAM 1A spectrometer in a backscattering configuration, equipped with a 514.5 nm laser source, calibrated with the spectra of a silicon sample before each session. It was focused onto the sample surface using a 50x objective through a 200 μm confocal hole, which results in magnification of 70x and collection of signal from an area of 2.9 μm. The 10% density filter was used to avoid damage of the sample. The spectra were accumulated over 40-50 s and averaged over five scans to improve signal-to-noise ratio. Fits of the spectra were obtained using a Pseudo-Voigt function in Origin software. The graphite particle size (L_a) was calculated using a Tuinstra and Koenig proportionality improved by Cançado *et al.* for any laser in the visible range [137,138], given by:

$$L_a(nm) = \frac{560}{E_l^4}\left(\frac{I_D}{I_G}\right)^{-1} \quad (9),$$

Where excitation energy of the laser used in the experiments is E_l = 2.41 eV and I_D, I_G are the integrated intensities (areas) of the D and G bands observed at 1350 and 1580 cm^{-1}, respectively. Raman was performed on samples prepared for SEM imaging.

Thermo-gravimetric analysis (TGA) was performed using a Seteram Labsys DSC-TGA. TGA samples were heated in an N_2 atmosphere at a rate of 10-20°/min to 1000°C and then held for a 5 min isothermal. Fibre samples were ground manually using an agate mortar and pestle prior to analysis. Al_2O_3 crucibles (100μL) were used and background runs were subtracted from all spectra before data interpretation. CF conversion rate has been evaluated as the percentage remaining mass at 1000°C.

Tensile testing of fibre samples was performed on the FAVIMAT single-fibre tester, using a clamping length of 12 mm and a speed of 0.5 and 1 mm/min for PAN and lignin/TPU samples, respectively. Measurements were carried out at DITF in Denkendorf, Germany.

Atomic force microscopy (AFM) images were recorded in contact mode, in air, using Thorlabs EDU-AFM1/M microscope. The measurements were performed using monolithic silicon AFM probe with aluminum reflective coating (ContAl-G, Budgetsensors), at room temperature and ambient pressure. The experiments were

conducted on square areas of 20 μm x 20 μm, in 250 x 250 pixels resolution, at a scan speed of 75 pixels s^{-1}. Height calibration was performed using a silicon dioxide calibration standard (HS-100MG, Budgetsensors) with a step height of 100 nm. AFM images were analysed with Gwyddion 2.56 software.

Thickness measurements were performed using profilometer (P6 Stylus Profiler, KLA-Tencor Corporation, Milpitas, CA) and represent an average of 5 separate measurements. Measurements were carried out at the University of Valencia, Spain.

The electrical conductivity has been determined using the Van Der Pauw method (4-point probe) with custom-made equipment, where four contacts are used to eliminate the effect of the contact resistance, as shown in Figure 3.11. For the first resistance measurement, a current I_{AB} was driven between two contacts, A and B, and the potential difference V_{CD} between the other two contacts, C and D was measured, giving the first resistance $R_1 = V_{CD}/I_{AB}$. The second resistance, $R_2 = V_{BD}/I_{AC}$, was obtained by driving the current between A and C and measuring the voltage between B and D. The voltage and current values were then plotted giving a lineal trend according to Ohms law. The conductivity of the sample was obtained by solving the Van Der Pauw equation [139]:

$$e^{-\pi R_1 \sigma} + e^{-\pi R_2 \sigma} = 1 \qquad (10),$$

where d is the sample thickness. A Keithley 2400 current source was used and measurements were carried out at the University of Valencia, Spain.

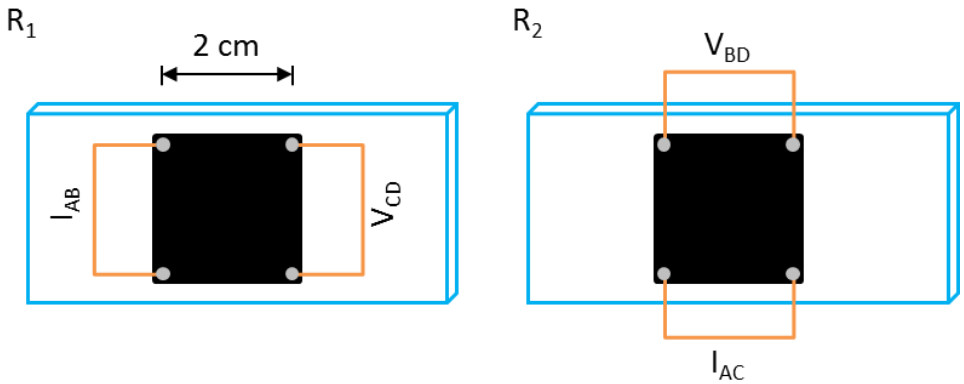

Figure 3.11 Contact configurations to measure R_1 and R_2.

3.7 Alternative applications of MW carbonisation

Susceptor assisted MW carbonisation was used for carbonisation of other materials to obtain preliminary data on potential applications of the technique presented in this

study. MW heating was applied for preparation of lignin-based porous carbon materials: foams derived from hydrogel and electrospun carbon nanofiber mats.

3.7.1 Lignin-based hydrogel

8g of lignin was dissolved in 20 mL of 3.3M NaOH solution. The solution was magnetically stirred for 24 h at 60°C. After that, the solution was loaded with PEGDGE cross-linker (in 1:1 lignin to cross-linker ratio) and magnetically stirred for another 15 min. The solution was then poured into 4 cm Petri dish. After completion of the cross-linking reaction (24 h), the cross-linked hydrogel was moulded in 1 cm cylinders and rinsed several times with DI water until neutral pH. The hydrogel was coated with MW susceptor according to 3.2 and carbonised using MW in nitrogen atmosphere, as per 3.5.

3.7.2 CNF mat preparation

A custom-built electrospinner, composed of a syringe driver (Harvard PHD 2000) and a power source (SIMCO Eurocharger Master), was used for producing the nanofibres. The samples were produced at an infusion rate of 30 $\mu L\,min^{-1}$. The substrate distance between the needle and the aluminium collector foil was set to 10 cm, and the electrospinning was performed at 7.7 kV. The needle was connected to the power supply, and the aluminium foil was ground to the power supply. The electrospun lignin/PLA were collected over a carbon coated quartz electrode attached to the aluminium foil. Schematic representation of the electrospinning process is shown in Figure 3.12. After 1h of electrospinning, the electrodes were removed from the aluminium foil for the subsequent steps. The CNFs were stabilised in air as follows: the temperature was ramped from 25 to 150°C at $1°C\,min^{-1}$ and kept at 150°C for 14h. Then, the temperature was raised from 150 - 200°C at $1°C\,min^{-1}$, kept at 200°C for 1h, ramped again from 200 - 250°C at $1\ °C\,min^{-1}$ and kept at 250°C for 1h. The stabilised lignin/PLA nanofibres were coated with MW susceptor, according to 3.2 and carbonised using MW in nitrogen atmosphere, as per 3.5.

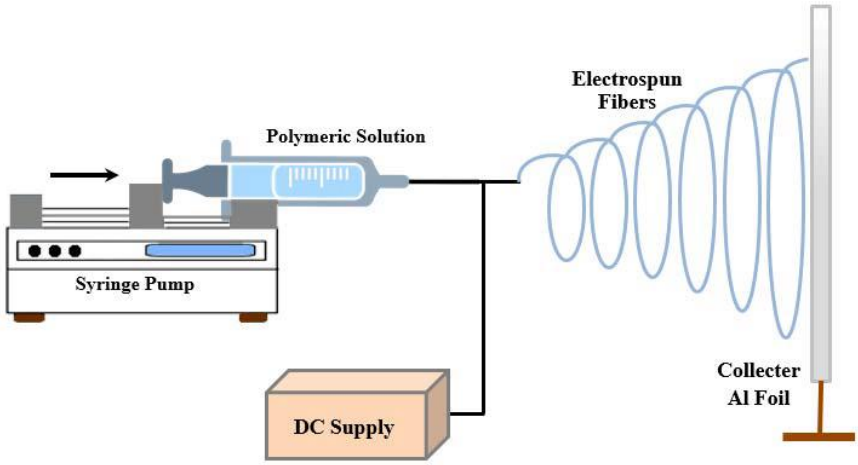

Figure 3.12 Schematic of the electrospinning process [140].

Chapter 4

Susceptor coating

4.1 Introduction

Due to MW transparency of precursor fibres, a conductive nanocomposite susceptor coating containing MWCNTs is applied on the surface according to procedure described in 3.2, utilising layer by layer (LBL) deposition. This approach improves homogeneity of dispersion of nanoparticles, which is a common problem in fabrication of conductive polymers containing CNTs [117,141].

Immersion in PDADMAC solution deposits a layer of positively charged polymer on the precursor fibre surface. This is followed by immersion of the fibre in MWCNT aqueous suspension in SDOC. Electrostatic interaction between negatively charged SDOC and positively charged polymer leads to deposition of MWCNTs. Similar layer-by-layer approaches were previously used to prepare multilayer assemblies containing CNTs for preparation of thin films with improved electrical properties and high thermoelectric power factors [124–127,142,143].

In this chapter the effects of the increasing number of coating cycles and the sequence of sample preparation on the visual appearance, morphology and properties of the susceptor layer are presented. In order to find the thickness and electrical conductivity at each interval, glass microscope slides were coated with 1 – 5 cycles, then analysed by AFM, profilometry and 4-point probe measurements, as described in 3.6.

4.2 Results

First tests showed that stabilised PAN and lignin/TPU fibres, without susceptor coating, reach maximum temperatures of about 250°C in the first 20 min of MW heating. Although higher numbers of cycles were tested, preliminary data showed that 5 cycles of susceptor coating are sufficient for rapid heating of PAN precursor to desired temperatures ≥1000°C and therefore it is used as a maximum in other sections.

PAN and lignin/TPU precursor samples are shown in Figure 4.1. The coating resulted in discoloration of the PAN fibre (Figure 4.1 A). The higher the number of LBL cycles, the darker the sample, which is attributed to the colour of MWCNTs. After the

stabilisation step all samples appeared black in colour and the difference in shade was no longer observable with the naked eye. After drying individual fibres do not stick and were easily separated. Lignin/TPU precursor fibres are almost black in appearance both before and after stabilisation; therefore no change is observable with naked-eye during sample preparation (Figure 4.1 B).

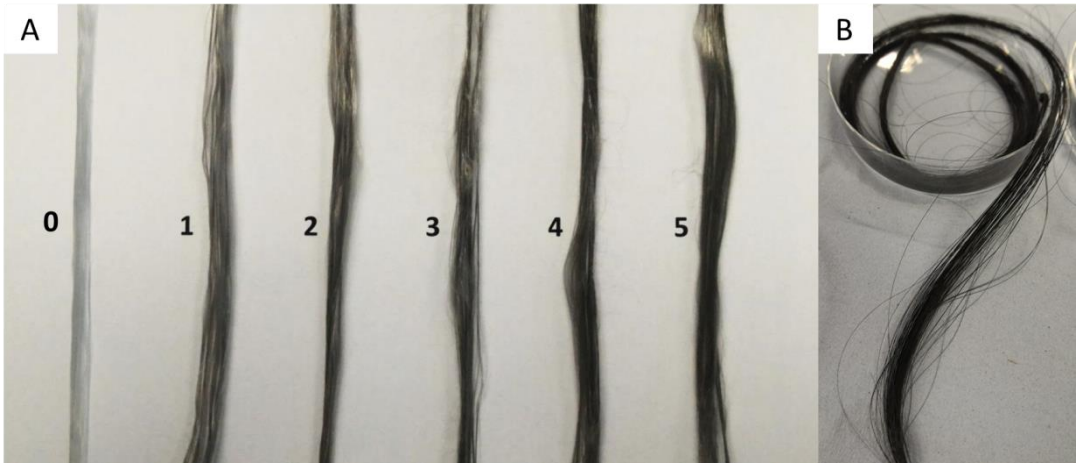

Figure 4.1 PAN precursor fibre coated with 0-5 cycles of LBL susceptor coating (A). Stabilised lignin/TPU precursor (B).

An SEM image of PAN precursor fibre surface coated with 5 cycles of MW susceptor deposition is shown in Figure 4.2**.** A relatively uniform network of MWCNTs can be observed, which is beneficial for even heat distribution during carbonisation. Bright contrast particles are observed, which might indicate presence of dust or some entangled MWCNTs.

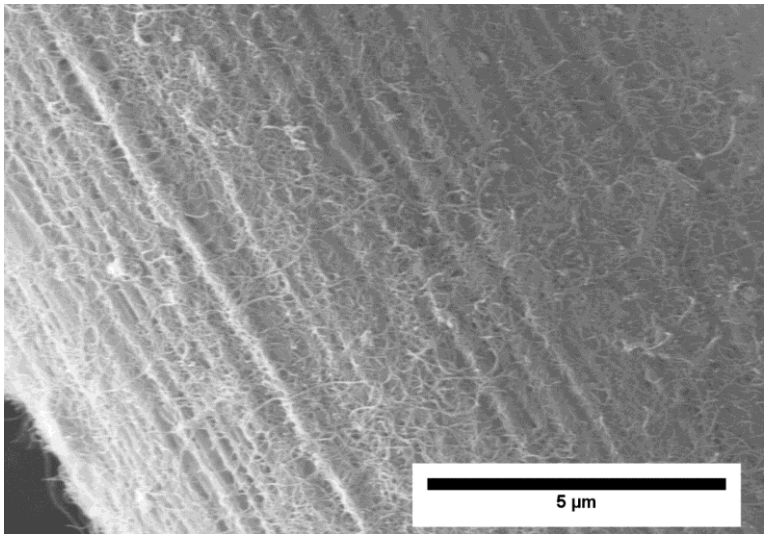

Figure 4.2 PAN precursor fibre surface after 5 cycles of LBL susceptor coating.

Comparison of susceptor coating on CF prepared via two different coating sequences is illustrated in Figure 4.3. It is observed that coating before stabilisation (A) results in

incorporation of the susceptor layer on the surface of the fibre, most likely due to degradation or melting during stabilisation step. Susceptor coating applied after stabilisation (B) tends to be more fragile and peels off from the fibre surface. This is possibly due to it remaining as an individual layer that is not fused or melted during stabilisation.

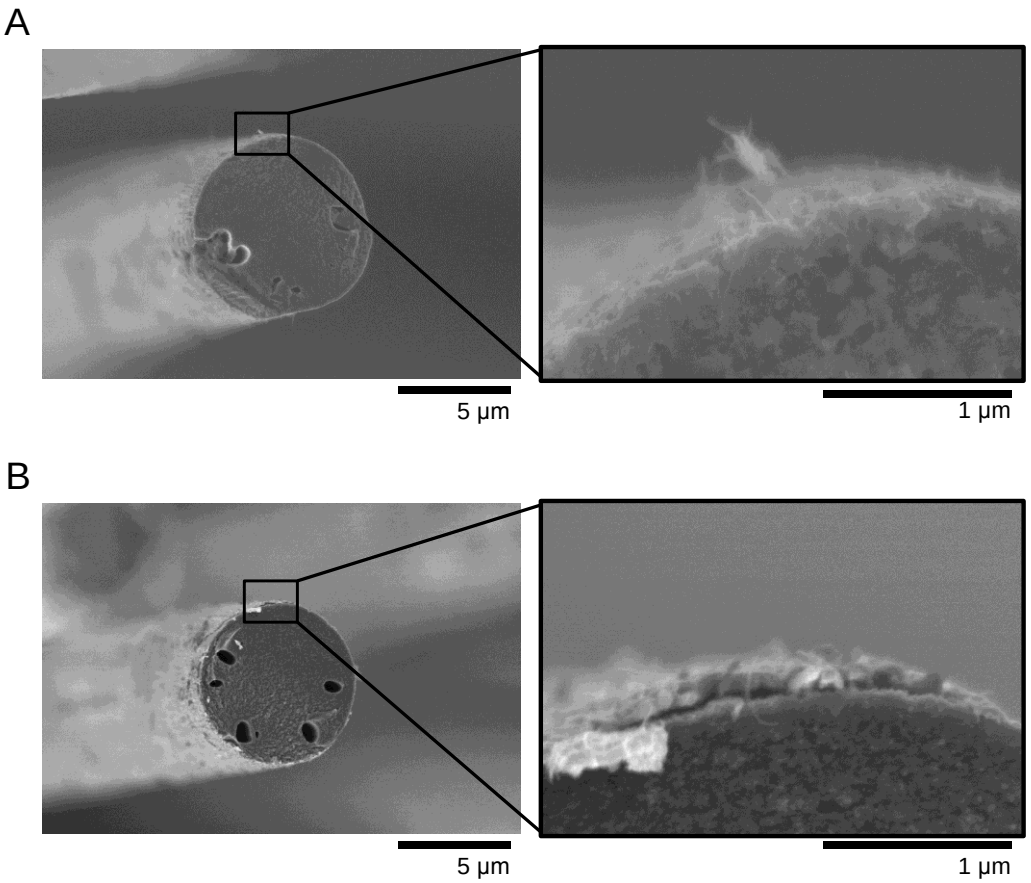

Figure 4.3 Comparison of susceptor coating applied before (A) and after stabilisation (B). A – 5 cycles of susceptor applied before stabilisation with higher magnification view showing the susceptor incorporated into the structure of the fibre. B – 4 cycles of susceptor applied after stabilisation with higher magnification view showing the susceptor remaining as an individual layer.

Glass microscope slides were coated with 1 – 5 cycles of LBL coating and analysed by AFM, profilometry and 4-point probe measurements.

Figure 4.4 shows that conductivity and thickness increase as a function of LBL coating cycles. Each cycle increases the thickness by 20 – 40 nm. This confirms incremental growth of susceptor coating during LBL process. Highest rise in conductivity is observed between 3c and 4c, probably due to some sort of percolation threshold. This might be correlated with higher maximum temperatures observed in the next chapters,

especially for samples coated after stabilisation (5.2.1 and 6.3.1). After 5c of deposition, conductivity and thickness of up to 55.9 S m^{-1} and 223 nm are recorded, respectively.

Figure 4.5 shows AFM image of a boundary between a film created after 5 cycles and clean surface of the glass. A grainy surface is observed with a broad distribution of height, mostly in the range of 10 - 210 nm and the average at 76 nm which is lower than value obtained for the same no. of coating cycles with profilometry measurements. Small grains with thickness of up to 380 nm are recorded in certain locations, which are most likely regions with larger bundles of entangled MWCNTs, similar to the ones observed through SEM (Figure 4.2). Small size and complicated shapes of MWCNTs result in inconsistency of results in terms of thickness of the coating. Uncertainty of AFM measurements is also increased by the presence of the background slope (up to 1 μm in height per 20 μm in length). Similar observations are made for 4c sample, with the average height at 65 nm.

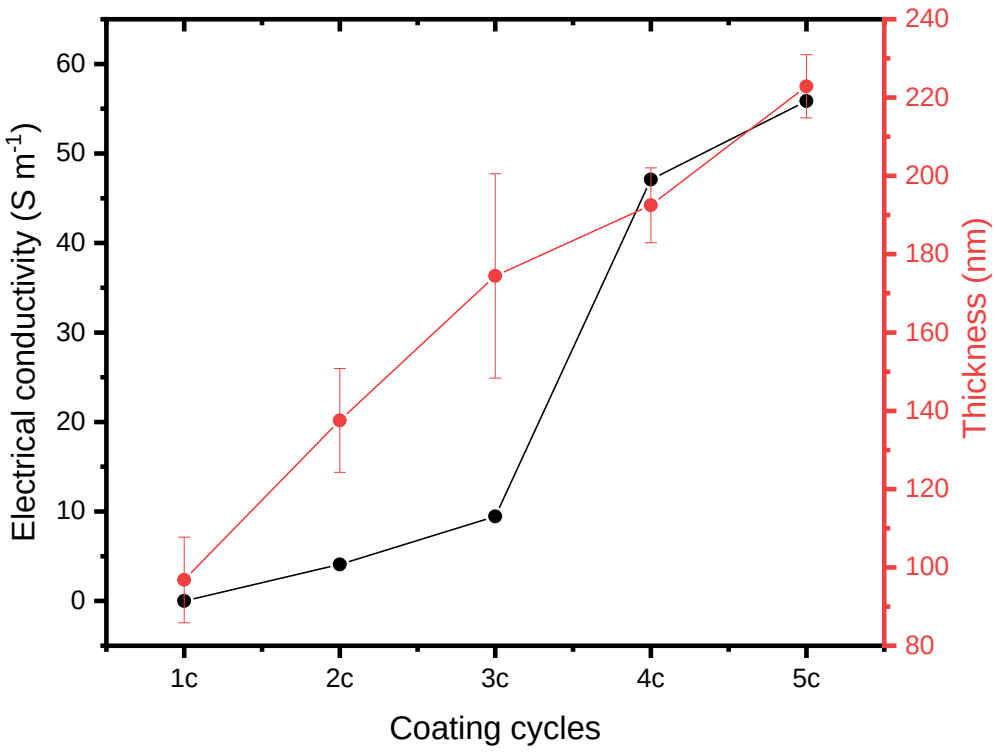

Figure 4.4 Electrical conductivity and thickness of LBL coating as a function of deposition cycles.

Results of conductivity, thickness and roughness measurements are summarised in Table 4.1. LBL coatings developed after 1 – 3 cycles were not measured via AFM, due to difficulty in locating the coating boundary. Average roughness increases with increasing number of layers.

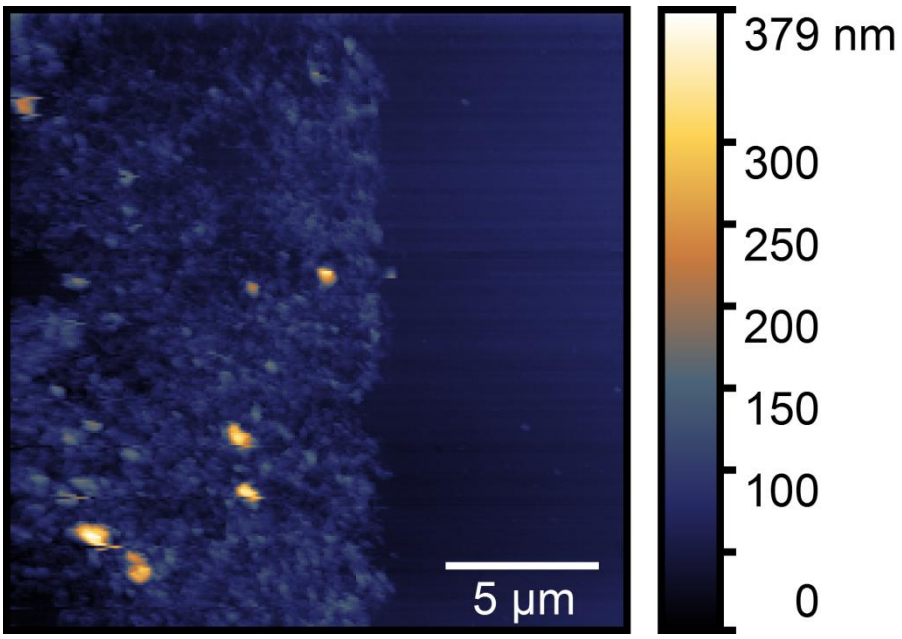

Figure 4.5 AFM image of the 5 cycle coating deposited on glass slide.

Table 4.1 Conductivity, thickness and roughness for LBL nanocomposite film after up to 5 cycles of deposition.

LBL coating cycles	Conductivity, σ (S m^{-1})	Thickness from profilometry (nm)	Thickness from AFM (nm)	Roughness from AFM (nm)
1c	1.73e-03	97 ± 11	-	-
2c	4.1	138 ± 13	-	-
3c	9.4	175 ± 26	-	-
4c	47.1	193 ± 10	65	19
5c	55.9	223 ± 8	76	22

4.3 Conclusions

Susceptor used in this study was characterised and the effects of the sample preparation sequence on its morphology were investigated in order to improve understanding of MW heating mechanism. The following conclusions can be drawn:

1) Thickness and conductivity of the susceptor layer increase with increasing number of coating cycles. Thickness of up to 223 nm and electrical conductivity of up to 56 S m^{-1} are recorded after 5 cycles of LBL coating.
2) Coating before stabilisation results in degradation or melting of the susceptor nanocomposite layer on the surface during stabilisation. Coating of the fibre after stabilisation can result in delamination of the susceptor layer during subsequent handling and processing of the fibre.
3) First experiments showed that 5 cycles of susceptor coating are sufficient for heating to desired temperatures (≥1000°C) and therefore this thickness is used as a maximum in the following section.

Chapter 5

Microwave carbonisation of PAN fibres

5.1 Introduction

As explained in the previous chapters, MW heating is more efficient than conventional heating. Successful application of microwave carbonisation reduces environmental impact and cost of CF production. In this chapter, MW carbonisation was applied for PAN, currently the most common precursor material for CF production. PAN is difficult to heat in MWs, due to its transparency in the wavelength of interest. A susceptor coating containing MWCNTs was applied on the surface of the precursor fibre to absorb MWs to allow carbonisation.

The effect of susceptor coating thickness and coating sequence were evaluated. To achieve this, PAN precursor fibres were coated with 1-5c (cycles) of susceptor, following the procedure outlined in 3.2. Preliminary data showed that 5 cycles of susceptor coating are sufficient for heating of PAN precursor to carbonisation temperatures. The susceptor layer was applied before or after stabilisation (3.3). Firstly, samples were carbonised at high power level to ensure repeatability of the process. After that, an equivalent batch of samples was carbonised at progressive power levels in order to improve mechanical properties of the CFs produced via MW carbonisation.

5.2 Carbonisation at high power level

5.2.1 Heating profiles

Heating profiles for high power MW carbonisation of PAN precursor are shown in Figure 5.1. For clarity purposes, only the first 10 min of heating is presented. Most of the samples experienced extremely fast heating to temperatures above 800°C in the first 30 s of MW heating. Recorded maximum temperatures (T_{max}) are in the range of 847-956°C for fibres coated before stabilisation and 911-1076°C for fibres coated after stabilisation. T_{max} temperatures are summarised in Table 5.1. High efficiency of MW heating can be attributed to a combination of conduction and eddy current loss in an electric and magnetic fields, respectively, which are main contributors in heating of highly conducting materials [15,134].

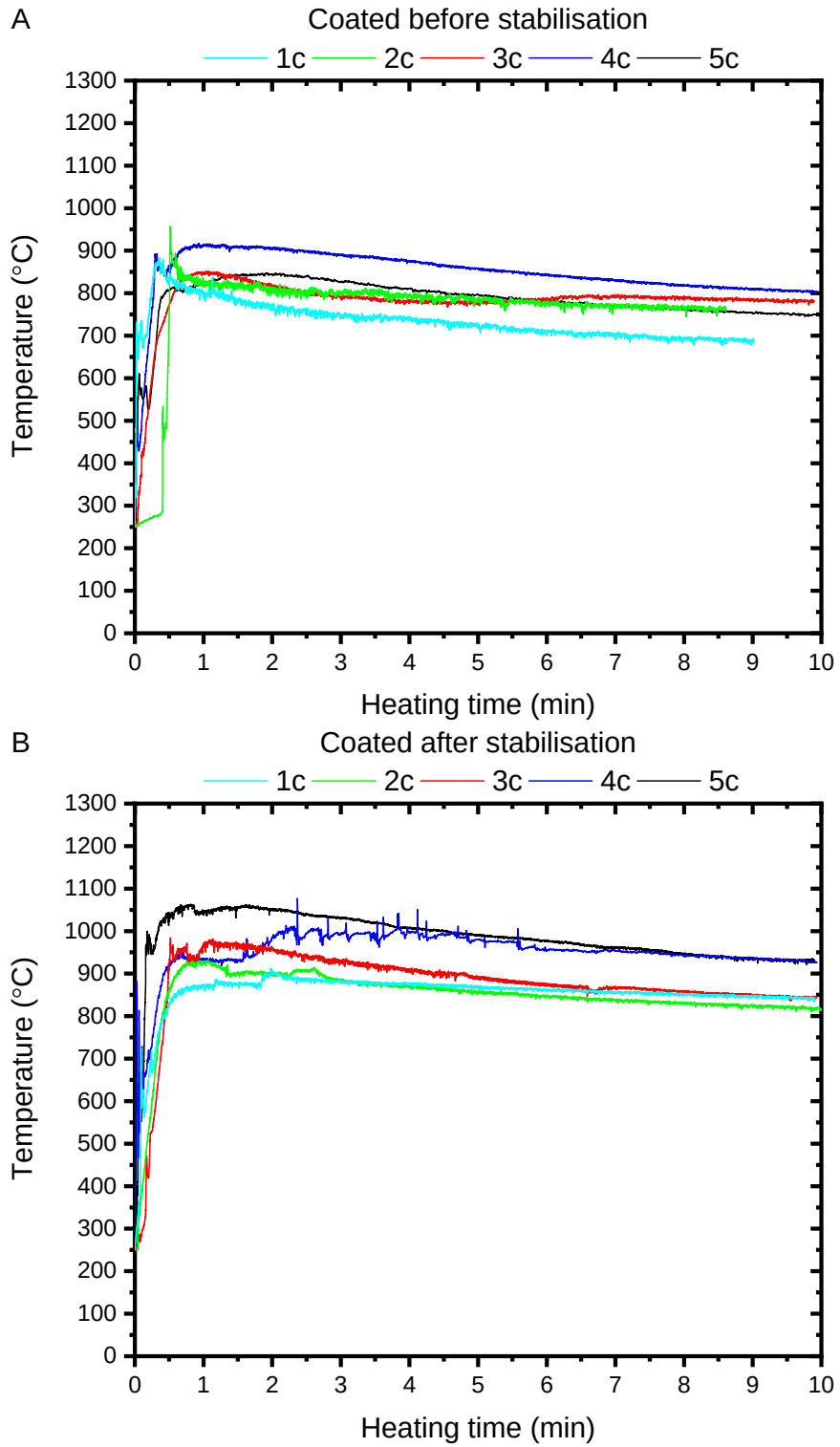

Figure 5.1 Heating profiles of high power MW carbonisation of PAN precursor coated before (A) and after stabilisation (B).

In general the T_{max} increases with the increasing number of coating cycles and is higher for fibres coated after stabilisation. This is attributed to the lack of degradation/melting of the coating explained in the previous section. This is most likely the cause for higher spread of T_{max} and general noisiness of the corresponding heating profiles. This coating responds more efficiently to electromagnetic waves through increased electrical

conductivity. Also it is more fragile, more readily peeled off by the volatile matter during carbonisation which may account for the abrupt changes of recorded temperature during MW heating. Increased difference between 3c and 4c samples coated after stabilisation suggests that there may be a correlation between electrical conductivity data (4.2) and T_{max}. On the contrary, coating applied before stabilisation undergoes aforementioned degradation/melting, which results in the decrease of heating response and in smaller T_{max} differences within the group.

Table 5.1 Maximum temperatures recorded during high power MW carbonisation of PAN precursor.

Sample	Maximum temperature, T_{max} (°C)
Coated before stabilisation	
1c	883
2c	956
3c	852
4c	916
5c	847
Coated after stabilisation	
1c	911
2c	930
3c	984
4c	1076
5c	1063

A significant delay in temperature rise (about 1-1.5 min) was observed for two samples coated before stabilisation (1c and 2c) and can be explained by lower thickness of susceptor coating, which should decrease absorption of MW radiation. Duration of this heating lag was previously reported to be dependent on the MW power used for processing and the moisture content of the granular activated carbon sample [144]. It is conceivable that the moisture absorbed by some samples during storage was sufficient to manifest this effect, especially in samples that should display the lowest rate of MW absorption. Once the moisture is evaporated and samples reach the lower limit of the IR-sensor (250°C), the heating rates are almost equally high.

All samples experience a series of peaks or signal disruptions, especially during initial phase of the heating. These features are observed at temperature ranges of 400-750°C and 300-900°C, for samples coated before and after stabilisation, respectively. In some cases (especially in samples coated after stabilisation, e.g. 4c), these sharp peaks keep occurring until several minutes into the MW carbonisation. They are most likely caused

by volatile products of carbonisation [145], i.e. crosslinking condensation, dehydrogenation and denitrogenation reactions [3,36], which occur at temperatures above 400°C. Alternatively, some of the most abrupt peaks can be a sign of plasma formation [21]. After reaching the maximum temperature at the beginning of the carbonisation, a gradual fall in the temperature is observed through the remaining carbonisation time. One reason for this could be shrinkage of the fibres and reduction of the IR-radiation reaching the sensor. Another plausible explanation is decreased efficiency caused by overheating of the experimental setup. This could be a result of an increased absorption of MWs by parts of the setup heated from the sample, decreased efficiency of overheated magnetron or combination of both. Periodic signal noise/vibration was present in some of the recorded heating profiles, which is due to periodical change of the electromagnetic field of the microwave [92]. These profiles were smoothed for clarity in Origin software.

5.2.2 Morphology

Representative SEM images of CFs produced via high power MW carbonisation from PAN precursor are shown in Figure 6.2. Average diameter of the fibre is in the range of 6.35-8.51 μm for CF coated before stabilisation and 6.59-8.78 μm for CF coated after stabilisation. In both groups, diameter is smaller compared to stabilised fibre (10.62 ± 1.05 μm) and slightly decreases with increasing maximum temperature of MW carbonisation. This change is associated with the loss of matter, increase of density and hence decrease of fibre volume during carbonisation [3,36]. Surprisingly, CF produced via conventional carbonisation at 1000°C (Conv) presents the highest value of diameter (9.8 ± 1.21 μm), but this may be explained by the biggest deviation in measurements of this sample.

Cross-sections of CFs show characteristics of brittle fracture. Oval pores/defects of up to about 1.5 μm in the longest (radial) direction are observed in all samples. Pores are found along the circumference of the fibre's cross-section and sometimes elongated radially. Similar features were reported previously by Barnet and Norr in a structural model of high modulus PAN-based CF [3,36,146]. It was proposed that a radial structure of disordered crystalline webs and large voids is surrounded by highly-ordered crystalline skin/sheath. Formation of such a structure was attributed to radial stresses

and differential shrinkage during carbonisation and cooling of the fibre. These defects/voids visible in fibres are most likely caused by the high heating rates observed during MW carbonisation. Development of skin-core structure could lead to stress between the two zones during shrinkage. It was previously reported that incomplete stabilisation could result in different orientations of inner and outer zones of the cross-section [147]. Also, fast carbonisation leads to evolution of large amounts of decomposition products over short periods of time instead of slow diffusion of volatiles to the outer surface. This could promote creation of relatively large voids. There is no tension to ensure no space is left within the structure of the fibre as the volatile products of carbonisation are released.

In general, voids in cross-sections are slightly smaller in CFs coated before stabilisation. As mentioned before, this coating sequence results in lower T_{max} temperatures (Table 5.1). This limits overheating and ultimately the development of bigger voids. Pores observed in CF produced via conventional carbonisation are much smaller, which suggests that the rates of heating and cooling have a predominant effect on their formation.

Fibres retain their overall shape but there are signs of deformations or scars running in longitudinal direction on the outer surface (red arrows). These may be characteristic Mrozowski cracks [36,146,148], which are formed by anisotropic thermal shrinkage of graphite crystal domains upon cooling of CF. They may also be considered a surface manifestation of voids visible in cross-sections and volume loss during carbonisation. Orientation of these features parallel to the fibre axis is most likely the result of CF structure orientation, whether in crystalline or amorphous form [149], which is induced already on the spinning stage and by stretching. The cracks are smaller in conventional sample, so the magnitude is most likely connected to severity of MW carbonisation and development of voids visible in cross-sections. Bright contrast particles are also visible on the surface of the fibres and can be attributed to loose fragments of susceptor coating. This is somewhat more pronounced in samples coated after stabilisation, where the coating is more prone to damage, and is likely the result of fast evolution of volatiles during MW carbonisation.

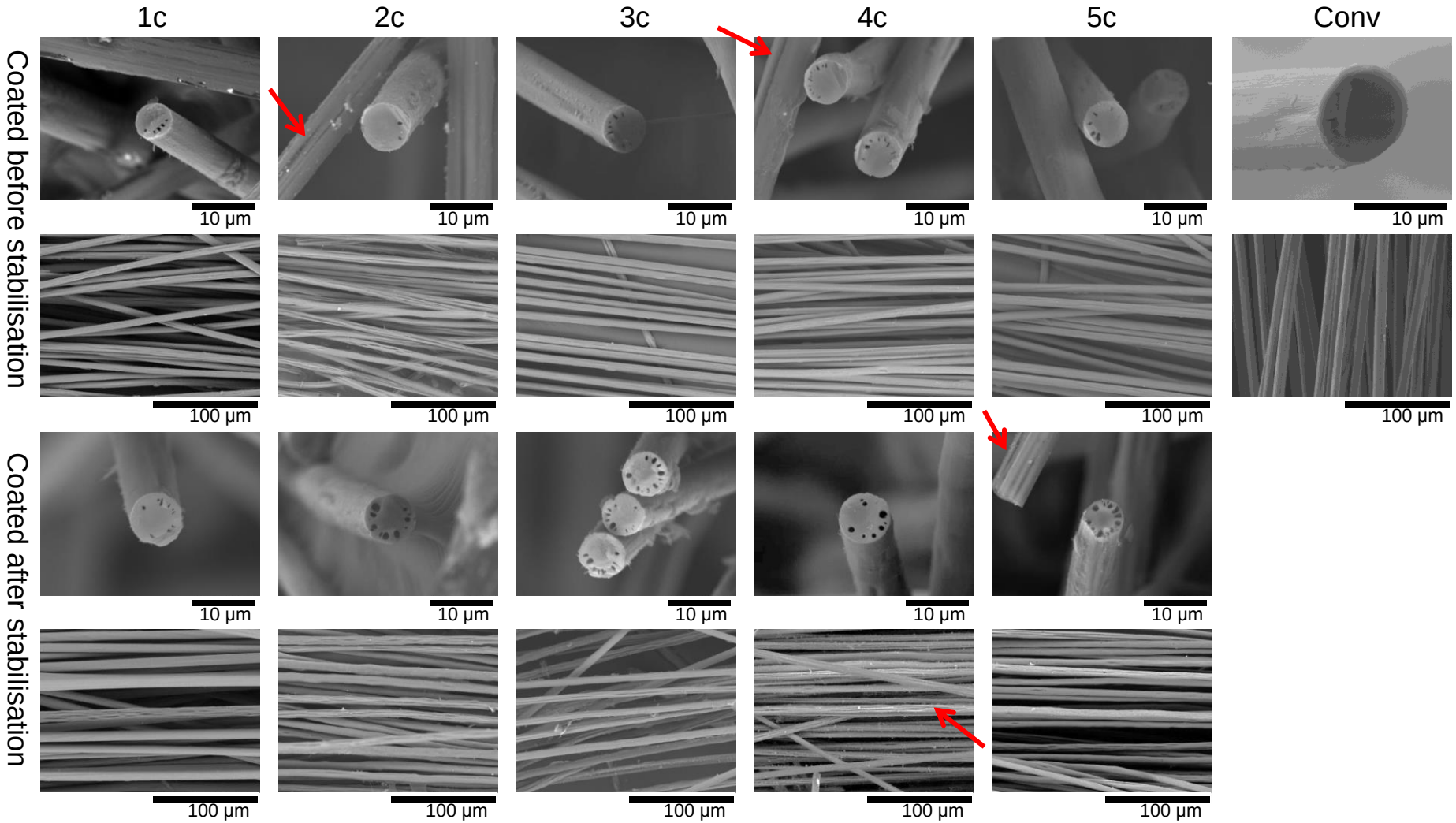

Figure 5.2 SEM images of CFs produced via high power MW carbonisation from PAN precursor. Red arrows – Mrozowski cracks.

5.2.3 TGA

Thermogravimetric analysis of CFs produced via high power MW carbonisation from PAN precursor is presented in Figure 5.3. Conversion rate evaluated from TGA is in the range of 86 – 91% for CFs coated before stabilisation and 95 – 98% for CF coated after stabilisation. This is in agreement with higher T_{max} temperatures recorded for samples coated after stabilisation (Table 5.1), which results in fuller conversion to CF. Conversion rate of CF produced via conventional carbonisation at 1000°C (Conv) is considerably low at 88.2%. The most probable reason is the temperature gradient inside the tube furnace used for conventional carbonisation, which results in uneven carbonisation conditions. It is probable that parts of the fibre never reached 1000°C, and hence the deviation from the expected 100% value. On the other hand, there is about 3-4% of mass lost in the temperature range of 30-100°C which can be assigned to moisture [38,150,151] absorbed from atmosphere due to porosity or grinding prior to TGA, so the conversion rate is >91%.

Trends are not easily identified for samples with increasing numbers of coating cycles, because the differences in thickness are nanoscale (20 – 40 nm). Furthermore, the temperature recorded by IR-sensor may be considered as the average temperature, even if a temperature gradient, caused by non-uniform electromagnetic field, is present. Ideally the area covered by fibres should be at least 2 times larger than the spot size, i.e. the area monitored by IR-sensor. It is therefore not surprising that manual sampling of CFs produced via MW carbonisation poses similar challenges as conventional carbonisation and may contribute to a certain degree of error in TGA measurements.

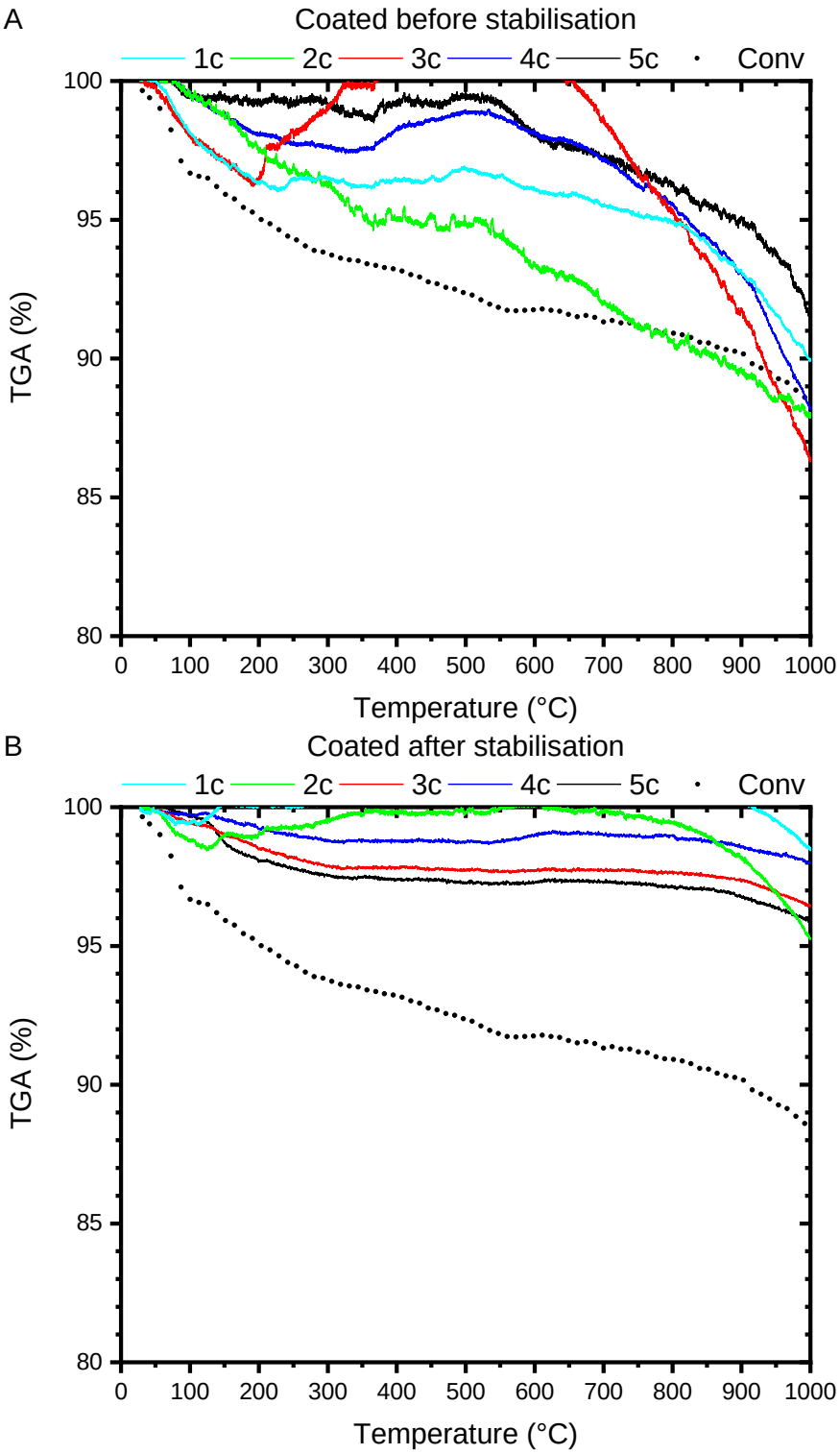

Figure 5.3 TGA of CF produced via high power MW carbonisation from PAN precursor coated before (A) and after stabilisation (B).

Data interpretation is further complicated by the noisiness of the TGA traces (especially for CFs coated before stabilisation). This is caused by smaller sample size due to low availability of material, and was later increased for all other samples.

5.2.4 Raman

Raman spectra of CFs produced via high power MW carbonisation from PAN precursor are shown in Figure 5.4. Characteristic D and G bands are observed in the range of 1344-1360 cm^{-1} and 1580-1590 cm^{-1}, respectively. D and G bands of CF produced via conventional carbonisation at 1000°C (Conv) are in the range of 1349-1350 cm^{-1} and 1584-1588 cm^{-1}, respectively. The G band is present in all carbon fibres and is attributed to the vibration of the graphite crystal cell. The D band is attributed to breaking of the crystal lattice symmetry which is caused by small crystal size and structural disorder. The D band is present in turbostratic CFs and disappears at higher graphitisation temperatures. All samples (including Conv) show overlapping of peaks which is characteristic for CFs with highly disordered graphitic structure after low temperature carbonisation [152–154]. Although researchers argue whether samples can be considered crystalline at this stage of carbonisation and advise caution when CFs from different precursors are compared [154]. Nevertheless, the Raman can still be a useful tool for comparison of theoretical L_a calculated for CFs from the same precursor.

The calculated graphitic crystallite size (L_a) is in the range of 6.42-9.23 nm for CFs coated before stabilisation, 5.12-11.43 nm for CFs coated after stabilisation and 9.61 for sample carbonised conventionally (Conv). It is generally bigger in samples with higher recorded T_{max}. CFs that reached temperatures close to or exceeding 1000°C display the particle size comparable with the conventional carbonisation at 1000°C. This is attributed to the crystallite growth in CFs as the temperature or the duration of the treatment is increased, which leads to higher L_a [154]. The values are somewhat smaller compared to 15-22 nm and 14-19 nm reported previously for PAN carbonised at 1000°C in microwave and via conventional method, respectively [97]. Although the same method was used for calculating L_a [138], authors used much lower heating rates. Final temperatures were maintained for 1h, which resulted in total carbonisation time (incl. ramps) of about 4h 20min [97], which is significantly longer compared to carbonisation times of about 20min (MW) or 2h 10min (Conv) used in this study. Furthermore, the result can be affected by application of PAN with different copolymer composition [154]. For the above reasons, the calculated L_a for conventional sample is regarded as the target (>9.61 nm).

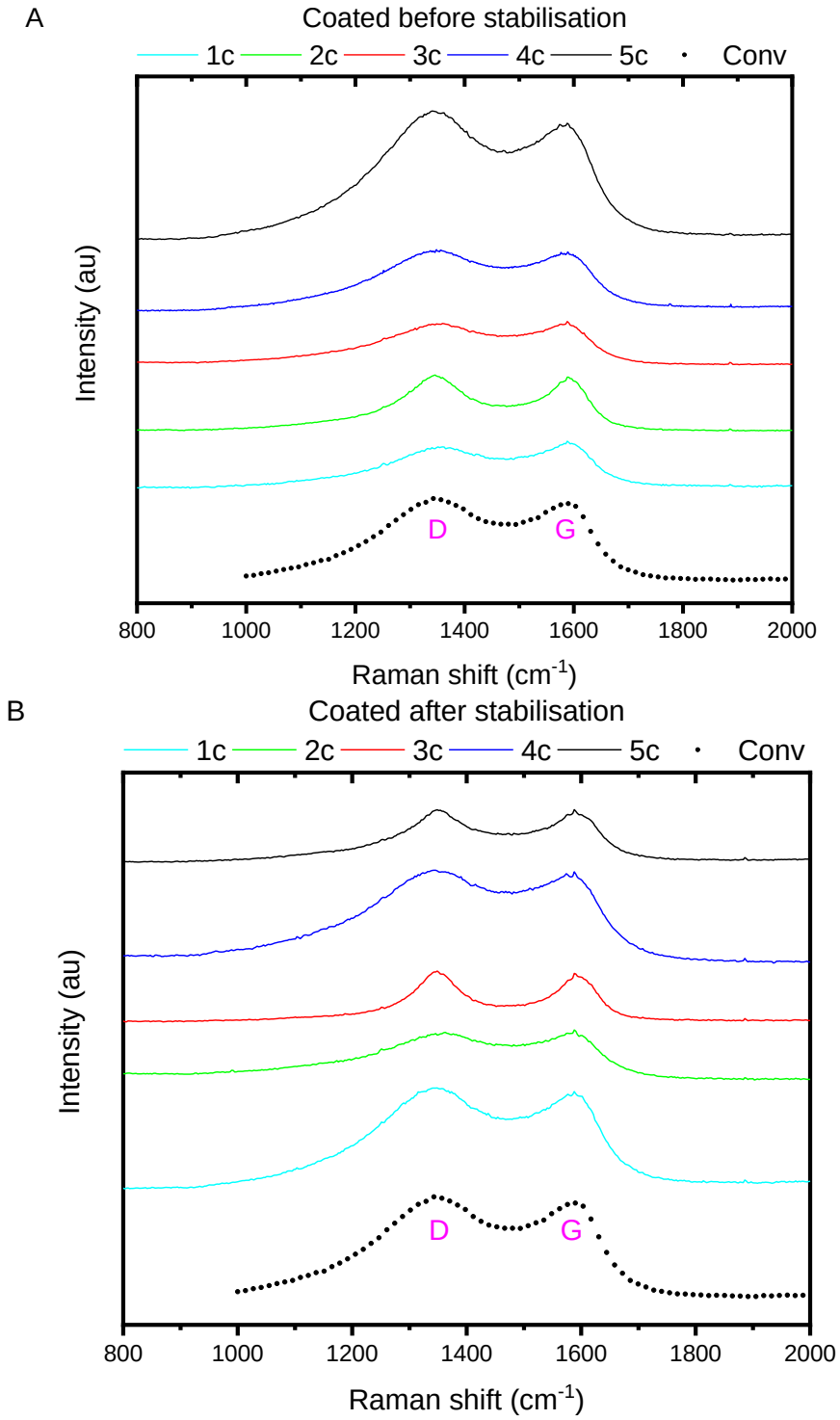

Figure 5.4 RAMAN spectra of CF produced via high power MW carbonisation from PAN precursor coated before (A) and after stabilisation (B).

To prevent information loss, the Raman spectra were not normalised. This results in the visible differences in intensities of individual spectra, but has no adverse effects on subsequent L_a calculations.

5.2.5 Mechanical properties

Mechanical properties of CFs produced via high power MW carbonisation from PAN precursor are shown in Figure 5.5. Average TS, YM and strain of samples coated before stabilisation are in the range of 0.84-0.93 GPa, 75.5-160.7 GPa and 0.6-1.25 %, respectively. Average TS, YM and strain of samples coated after stabilisation are in the range of 0.41-0.83 GPa, 76.5-131.75 GPa and 0.64-0.84 %, respectively.

Average TS, YM and strain were benchmarked off control sample, carbonised in conventional tube furnace (Conv). Measured TS of 1.42 GPa, YM of 114.8 GPa and strain of 1.24 % are close to values previously reported for PAN carbonised with no tension applied [97]. At this stage, comparison to commercial CF data would be of limited use, as the carbonisation temperatures >1100°C and the control of tension are critical to achieve such performance.

TS (Figure 5.5 A) is generally lower than that of the control, which can be attributed to premature fracture due to pores observed through SEM and explained above. Defects are also formed by the thermal decomposition products which are known to have detrimental effect on mechanical properties during carbonisation at high heating rates [36]. Overlapping of the error bars indicates that it was possible to produce CF with properties comparable to control CF (Conv), but they were scarce. This is supported by promising YM values (Figure 5.5 B) of several samples that matched those of the control. Tested fibres ruptured at strain values (Figure 5.5 C) lower than that of the control, but an overlap of the error bars is also visible in this case.

Coating before stabilisation produced CFs with higher TS, YM and strain. This can be explained by milder conditions of carbonisation observed in this group. Also, highest values of TS and YM in both groups correspond to median values of T_{max} (Table 5.1), which indicates improvement of mechanical properties when overheating is limited. On the other hand, heat treatment at higher temperatures should increase L_a and and improve mechanical properties [3,36,97]. Disagreement between L_a and mechanical data (especially TS) presented here suggests that not the microstructure, but the presence of defects is the main factor limiting the performance of CFs presented here.

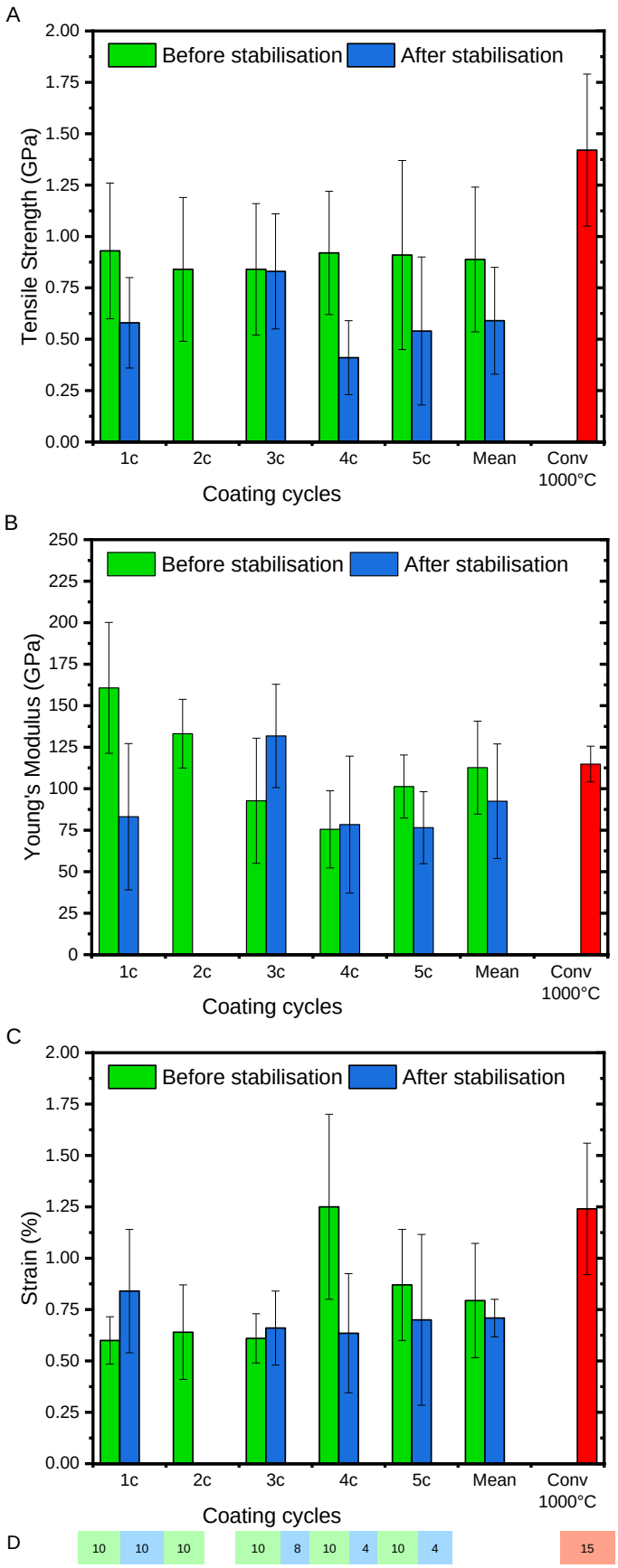

Figure 5.5 Mechanical properties of CFs produced via high power MW carbonisation from PAN precursor and conventional (Conv) at 1000°C. Tensile strength – A, Young's Modulus – B, Strain at break – C, number of fibres successfully tested - D.

5.2.6 Summary

Carbonisation conditions and properties of CFs produced via high power MW carbonisation from PAN precursor are summarised in Table 5.2, where the trends described above may be easily followed and values compared to conventional carbonisation at 1000°C. Standard deviation is reported where possible.

MW carbonisation at high power results in high initial heating rates which result in formation of defects observed through SEM. Coating samples before stabilisation results in lower T_{max} and conversion rate, but produces CFs with superior mechanical properties compared to the second group. Coating samples after stabilisation results in higher T_{max} and conversion rate, but deteriorates mechanical performance, most likely due to higher heating rates. Coating samples before stabilisation appears to be more reliable procedure for MW carbonisation at high power. However, the performance of the other preparation sequence may be also improved if the MW power is reduced. Therefore it is decided to continue experimentation with samples coated before and after stabilisation due to higher T_{max} and conversion rates offered by the latter sequence.

Table 5.2 Carbonisation conditions and properties of PAN-based CFs. Samples carbonized at high power level.

Sample	Maximum temperature, T_{max} (°C)	Carbonisation time (min)	Fibre diameter (μm)	Conversion rate (%)	L_a (nm)	Tensile Strength (GPa)	Modulus (GPa)	Strain (%)
Coated before stabilisation								
1c	883	20	6.35 ± 0.29	89.6	7.34 ± 0.79	0.93 ± 0.33	160.70 ± 39.41	0.60 ± 0.11
2c	956	20	6.69 ± 0.98	87.8	9.23 ± 1.97	0.84 ± 0.35	133.13 ± 20.66	0.64 ± 0.23
3c	852	20	7.36 ± 0.79	85.8	6.76 ± 0.56	0.84 ± 0.32	92.70 ± 37.70	0.61 ± 0.12
4c	916	20	7.30 ± 0.42	87.6	6.86 ± 2.49	0.92 ± 0.30	75.50 ± 23.24	1.25 ± 0.45
5c	847	20	8.51 ± 0.41	90.7	6.42 ± 2.74	0.91 ± 0.46	101.30 ± 18.97	0.87 ± 0.27
Coated after stabilisation								
1c	911	20	8.78 ± 0.73	98.2	5.99 ± 0.37	0.58 ± 0.22	83.10 ± 44.09	0.84 ± 0.30
2c	930	20	8.26 ± 0.77	94.7	5.12 ± 0.04	-	-	-
3c	984	20	6.62 ± 0.58	96.3	11.43 ± 0.69	0.83 ± 0.28	131.75 ± 31.13	0.66 ± 0.18
4c	1076	20	6.66 ± 0.47	97.8	9.91 ± 2.52	0.41 ± 0.18	78.33 ± 41.24	0.64 ± 0.29
5c	1063	20	6.59 ± 0.43	95.7	6.48 ± 0.51	0.54 ± 0.36	76.50 ± 21.67	0.70 ± 0.42
Conventional furnace	1000	130+	9.80 ± 1.21	88.2	9.61 ± 1.05	1.42 ± 0.37	114.80 ± 10.79	1.24 ± 0.32

5.3 Carbonisation at progressive power levels

It was found in the previous experiments that high power MW carbonisation leads to deterioration of mechanical properties due to high heating rates, which lead to formation of voids. It was decided to continue experimentation with samples coated before and after stabilisation, despite lower mechanical performance of the latter. It was expected that reduction of MW power should improve properties of samples coated after stabilisation, while maintaining higher T_{max} and conversion rates offered by this coating sequence. It was also decided not to increase coating cycles to enable easier optimisation of MW heating.

In this part, an input voltage of the MW setup was adjusted in an effort to reduce high initial heating rates during MW carbonisation of an equivalent batch of PAN samples (1-5c coated before and after stabilisation) and improve properties of the produced CFs. The voltage was increased incrementally from 160-165V to provide five progressive levels of MW power, with the final one at 230V (700W). The power was not changed until the sample temperature was stable, which resulted in differences in carbonisation times. Furthermore, heating lags at low power levels were omitted and only temperature changes above 250°C have been compared by graphing them from the 0 min position.

5.3.1 Heating profiles

Heating profiles of an equivalent set of PAN samples carbonised at progressive power levels are shown in Figure 5.6. Noticeably lower heating rates are observed during the initial stage at lowest power (Figure 5.6 A and B), with temperatures not exceeding 600°C in the first minutes of carbonisation. Increasing the MW power increases the rate of heating significantly (Figure 5.6 C and D) and heats the samples to temperatures above 600°C. At a certain point during initial and intermediate stages of heating, sample temperature suddenly increases from about 400°C to about 500-800°C. This is generally associated with sharp peaks (see 2c and 3c in Figure 5.6 C), which are analogous to initial peaks observed in the previous PAN experiments (5.2.1). A significant peak is usually observed once for each sample and therefore a round shoulder is observed instead, in heating profiles at subsequent power levels (Figure 5.6 E). The rise is recorded earlier in the process for samples with thicker susceptor coating and is followed by a gradual fall to a relatively stable temperature, which scales with MW power until the final stage at full power, 230V, 700W (Figure 5.6 E and F).

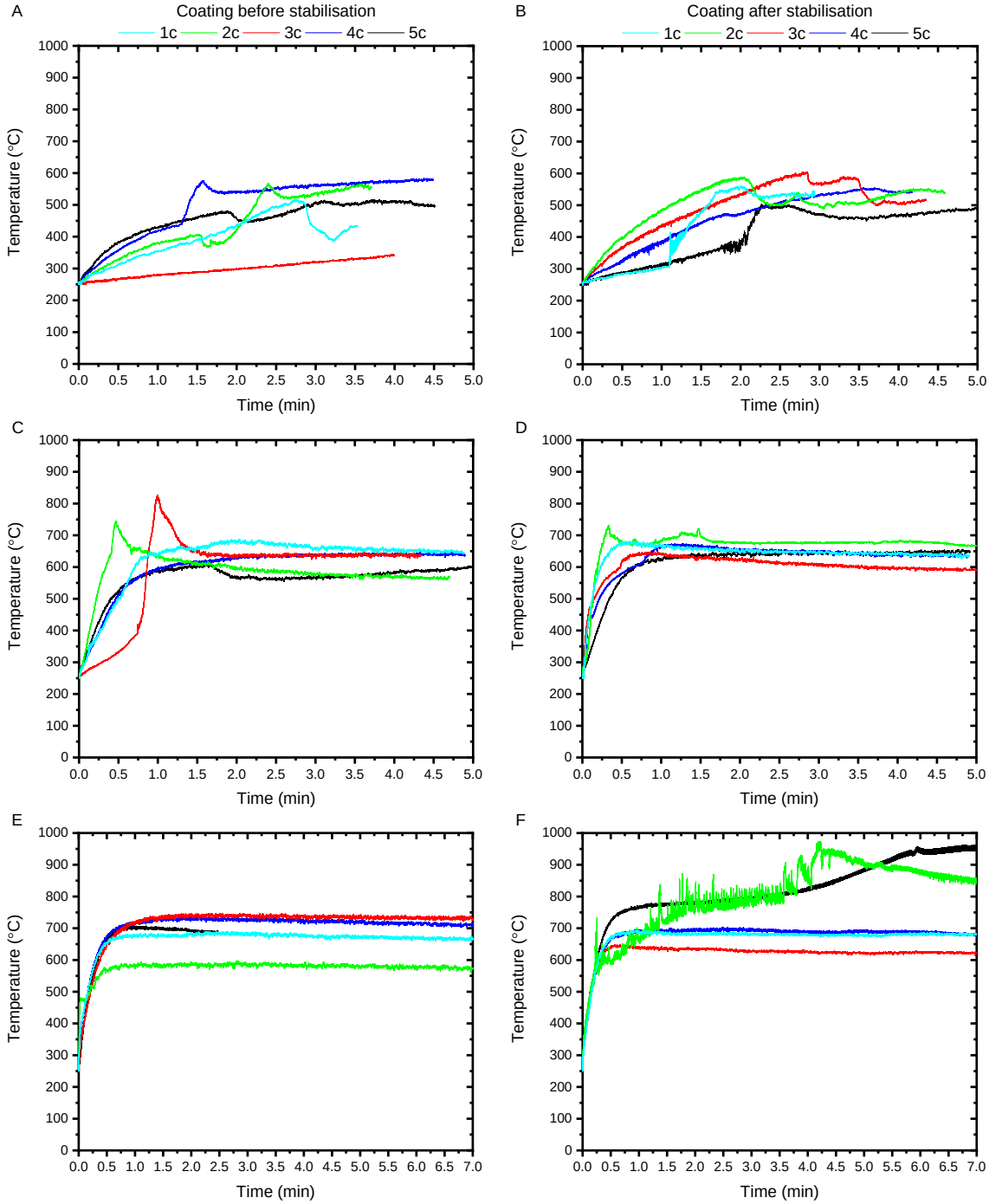

Figure 5.6 Heating profiles of progressive MW carbonisation of PAN precursor. A,B - 165V; C,D - 170-175V; E,F - 230V.

Recorded T_{max} are in the range of 690 – 827°C for fibres coated before stabilisation and 695 - 974°C for fibres coated after stabilisation. T_{max} temperatures are summarised in Table 5.3. Finer tuning of MW power is probably required to reduce the rate further, especially during intermediate stages where transition to higher temperatures is observed.

Wider range and higher values of T_{max} are observed for fibres coated after stabilisation. It was explained in the previous section that this coating sequence results in formation of susceptor layer which absorbs MWs more efficiently and this increases T_{max}. Also, coating before stabilisation decreases variation in T_{max}, through incorporation of the susceptor layer during stabilisation.

Heating lags omitted in low level graphs decrease with increasing number of coating cycles, similarly to lags described for PAN carbonisation at high power level only (5.2).

Temperature changes in the form of peaks are generally more pronounced in the initial stage of heating. This is attributed to reactions taking place during carbonisation of PAN (1.5.1) and evolution of corresponding gaseous products. Sharp peaks and periodic signal noise/vibration is observed in the final heating stage of at least two samples coated after stabilisation (2c and 5c), as it was observed in the previous section (5.2).

Table 5.3 Maximum temperatures recorded during progressive MW carbonisation of PAN precursor.

Sample	Maximum temperature, T_{max} (°C)
Coated before stabilisation	
1c	690
2c	744
3c	827
4c	735
5c	707
Coated after stabilisation	
1c	695
2c	974
3c	717
4c	704
5c	962

5.3.2 Morphology

Representative SEM images of CFs produced via progressive MW carbonisation from PAN precursor are shown in Figure 5.7. Average diameter of the fibre is in the range of 7.44-8.6 μm for CF coated before stabilisation and 7.45-8.72 μm for CF coated after stabilisation. In both groups, diameter is smaller compared to stabilised fibre (10.62 ±

1.05 μm). Diameter of samples coated after stabilisation decreases with increasing T_{max} of MW carbonisation (Table 5.3).

Cross-sections of CFs show characteristics of brittle fracture. Oval pores/defects are still found in majority of cross-sections but they are much less numerous. The length of defects is up to about 1.3 μm but they are narrower, sometimes needle-shaped. This can be explained by lower heating rates during initial stages of heating and also lower T_{max} (Table 5.3) compared to counterparts carbonised at high power only (Table 5.1), which limits radial residual stress in the fibre and development of cavities. Partial preservation of defect length could be an indication that the zone of void formation is comparable in size to the one reported in 5.2, and it is mainly the circumferential dimension that is limited by slower heating.

Fibres retain their overall shape and there are signs of Mrozowski cracks (red arrows) running in longitudinal direction on the outer surface [36,146,148]. Similar defects are observed on fibres from previous section (5.2.2), but here they are much less pronounced and resemble those found on the surface of CF produced via conventional carbonisation at 1000°C (Conv). Bright contrast particles on the surface of the fibres, which might be attributed to loose fragments of susceptor coating are scarce. This is probably due to reduced heating rates and milder carbonisation conditions in general (lower T_{max} - Table 5.3), which lead to slower evolution of volatiles during MW carbonisation and restrict damage of the coating.

Generally, it is possible to find similar amounts of defect-free cross-sections within both sample groups. This is probably due to the methodology used in this section, where heating was shortened or prolonged on individual basis. Different carbonisation conditions are used in order to improve mechanical properties, but could also result in sort of averaged results for samples with different coating numbers and from different groups. Furthermore, during cross-section preparation used in this study, the CF is most likely to break at the weakest points along the fibre length (i.e. pores and defects) and this can lead to apparent higher number of cross-sections with defects observed through SEM.

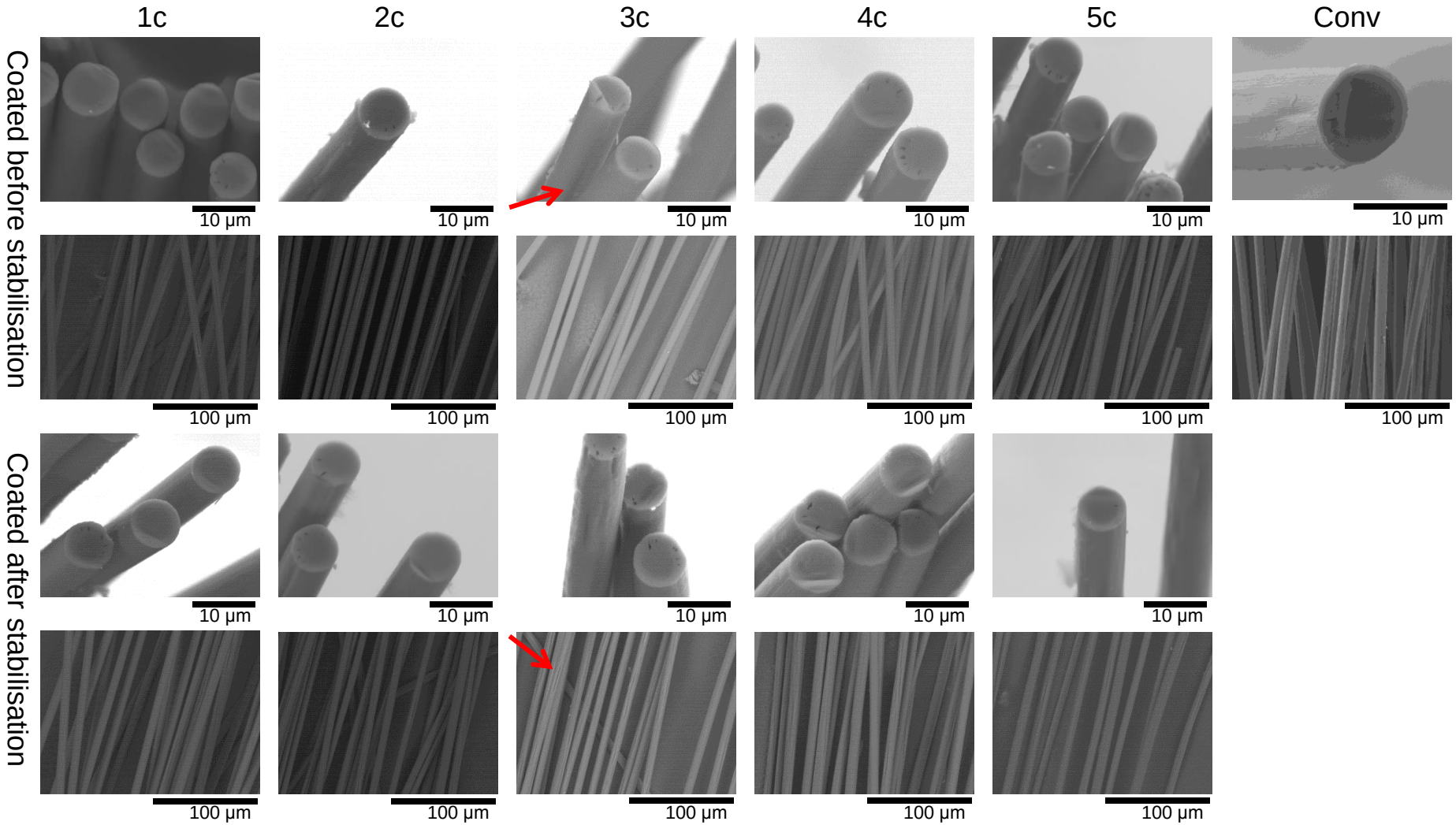

Figure 5.7 SEM images of CF produced via progressive MW carbonisation from PAN precursor. Red arrows – Mrozowski cracks.

5.3.3 TGA

Thermogravimetric analysis of CFs produced via progressive MW carbonisation from PAN precursor is shown in Figure 5.8. Conversion rate evaluated from TGA is in the

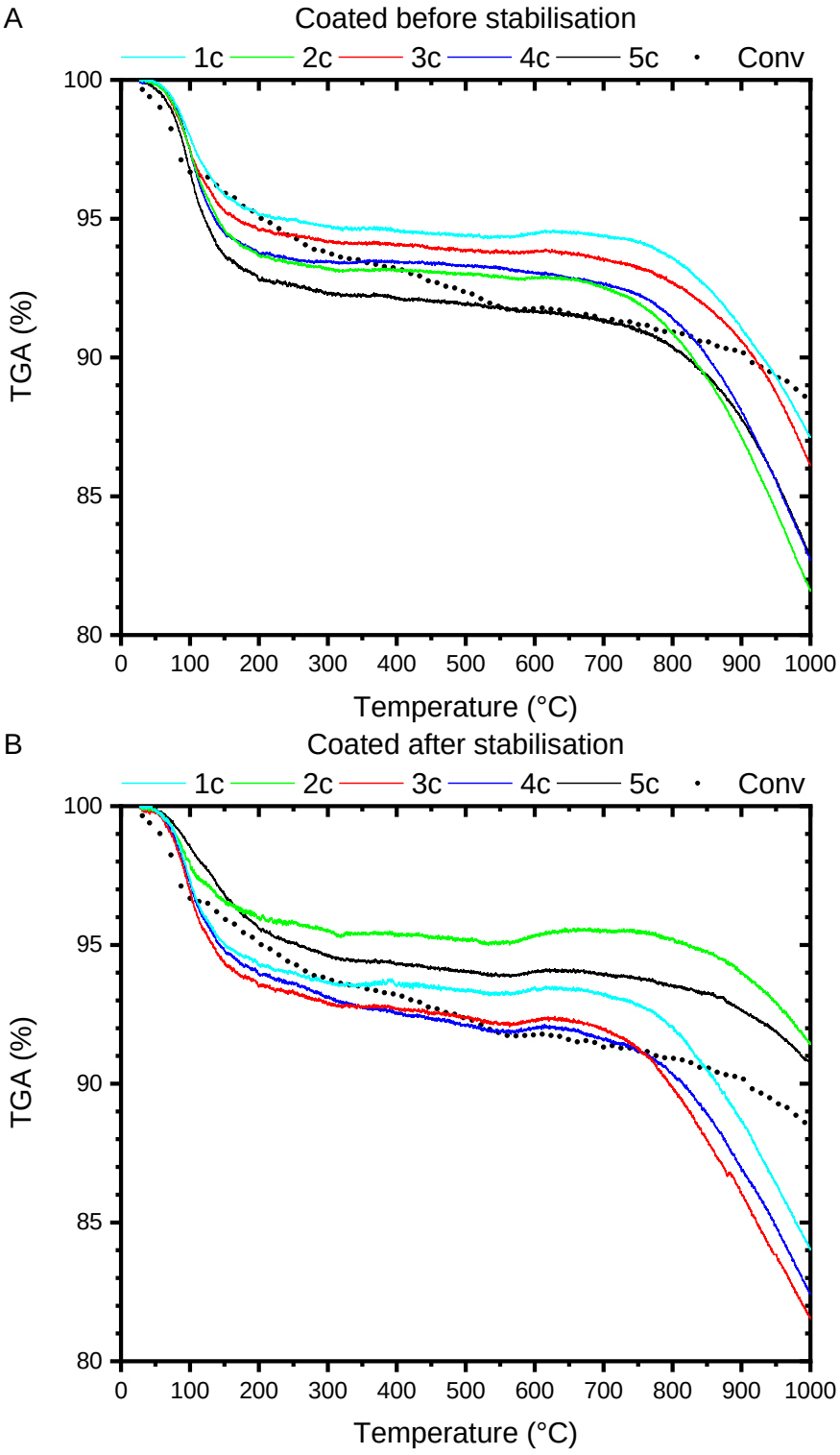

Figure 5.8 TGA of CF produced via progressive MW carbonisation from PAN precursor coated before (A) and after stabilisation (B).

range of 80.9-86.6% for fibres coated before stabilisation and 81-91.1% for fibres coated after stabilisation. Increased conversion rate is associated with higher T_{max} (Table 5.3), which is more evident in the group of samples coated after stabilisation (2c and 5c).

On average, conversion rate is about 8% lower compared to fibres carbonised in MW at high power only (5.2.3). This is in agreement with lower T_{max} temperatures observed during progressive heating (Table 5.3). However, it is clear from Figure 5.8, that significant fraction of mass (4-7%) is lost between 0-200°C, which could be attributed to moisture content [38,150,151] and bring the final values much closer to their counterparts (5.2.3). After the initial mass loss below 200°C, the remaining fraction is evolved from about 750°C, which is explained by evolution of gases during TGA [3,39]. This is in very good agreement with lower T_{max} temperatures observed, which result in incomplete carbonisation.

5.3.4 Raman

Raman spectra of CFs produced via progressive MW carbonisation from PAN precursor are shown in Figure 5.9. Characteristic D and G bands are observed in the range of 1339-1357 cm^{-1} and 1577-1589 cm^{-1}, respectively. Slight red-shift (compared to 5.2.4) observed for both bands could be connected to changes in T_{max} (Table 5.3) or crystallite size L_a [154], but there is no obvious trend to confirm. This is possibly due to differences in total carbonisation times.

The calculated graphitic crystallite size (L_a) is in the range of 4.65-6.75 nm for CFs coated before stabilisation and 4.25-7.78 nm for CFs coated after stabilisation. The values are lower than L_a of their counterparts (5.2.4), which is attributed to lower T_{max} (Table 5.3) and the resulting lower degree of orientation in CFs. Higher spread in L_a is observed in fibres coated after stabilisation, which is in agreement with other results for this coating sequence.

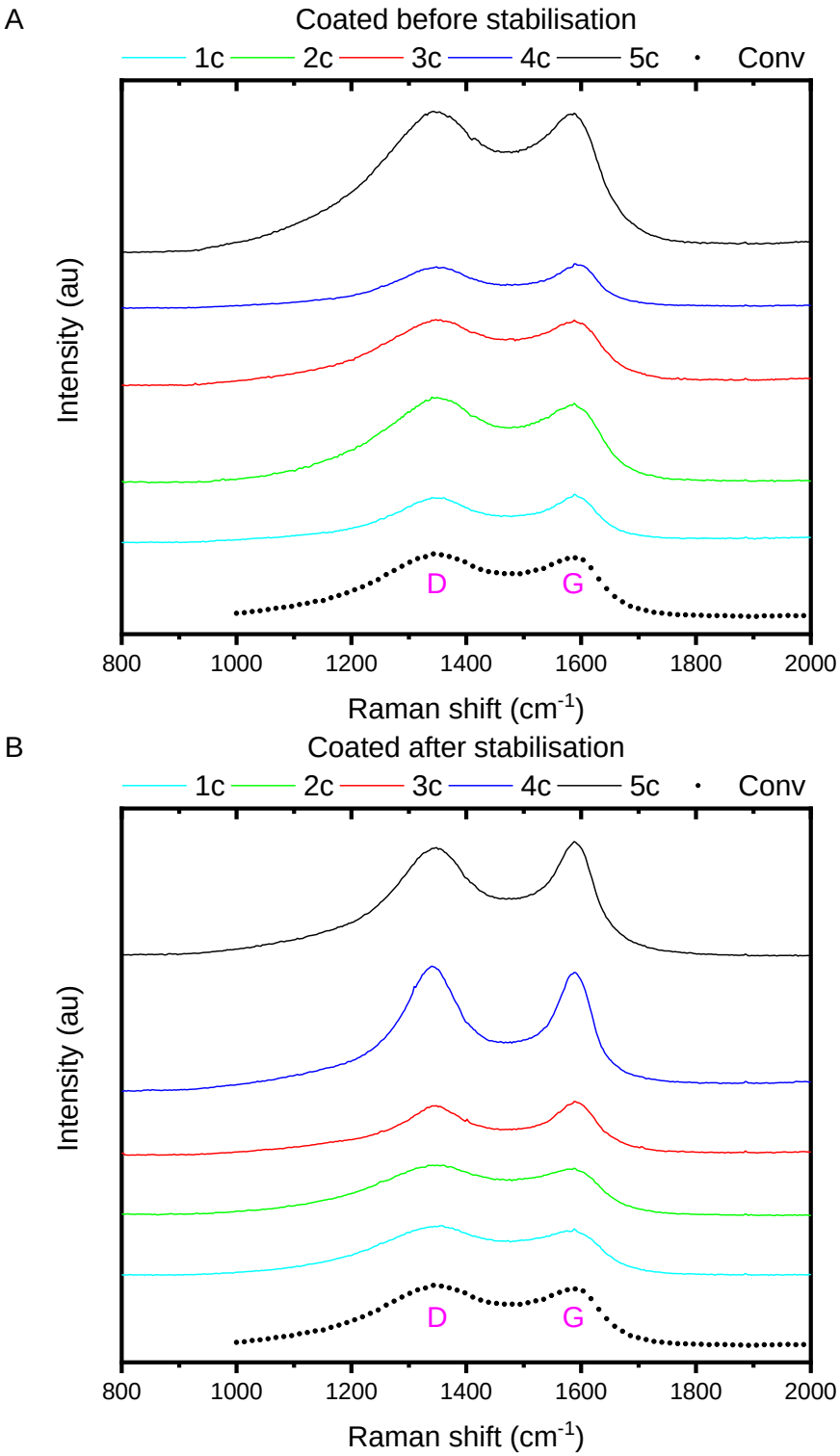

Figure 5.9 RAMAN spectra of CF produced via progressive MW carbonisation from PAN precursor coated before (A) and after stabilisation (B).

5.3.5 Mechanical properties

Mechanical properties of CFs produced via progressive MW carbonisation from PAN precursor are shown in Figure 5.10. Average TS, YM and strain of samples coated

before stabilisation are in the range of 0.42-0.88 GPa, 60.73-82 GPa and 0.56-1.26 %, respectively. Average TS, YM and strain of samples coated after stabilisation are in the range of 0.23-1.18 GPa, 43-100 GPa and 0.34-1.31 %, respectively. The values are generally lower compared to TS of 1.42 GPa, YM of 114.8 GPa and strain of 1.24 % recorded for conventional carbonisation at 1000°C. This is attributed to pores/defects observed through SEM (5.3.2), which are responsible for deterioration of properties [3], especially of TS. This is also observed for PAN samples carbonised at high MW power (5.2.5) and is most likely caused by high heating rates. Although mechanical performance is in most cases inferior to that of the fibre carbonised via conventional method (Conv), there some promising exceptions. Good performance of samples 1c (before and after) and 5c (after) suggests that it is possible to produce CF with properties comparable to control (Conv).

The values are somewhat lower than those of the counterparts (5.2.5), which can be explained by lower recorded T_{max} temperatures [36,95,97] (see Table 5.3 vs Table 5.1). Kim, Kim, Choi, *et al.* also reported that excessive carbonisation of PAN at lower temperatures leads to decrease in TS [94]. Furthermore, smaller number of samples was successfully tested compared to 5.2.5. This suggests fibre brittleness and is most likely caused by an attempt to separate relatively large bundles of these fibres prior to shipment for mechanical testing, which easily results in breakage of the fibre (Figure 5.11). Also, some damage could have been induced during shipment for testing in Germany.

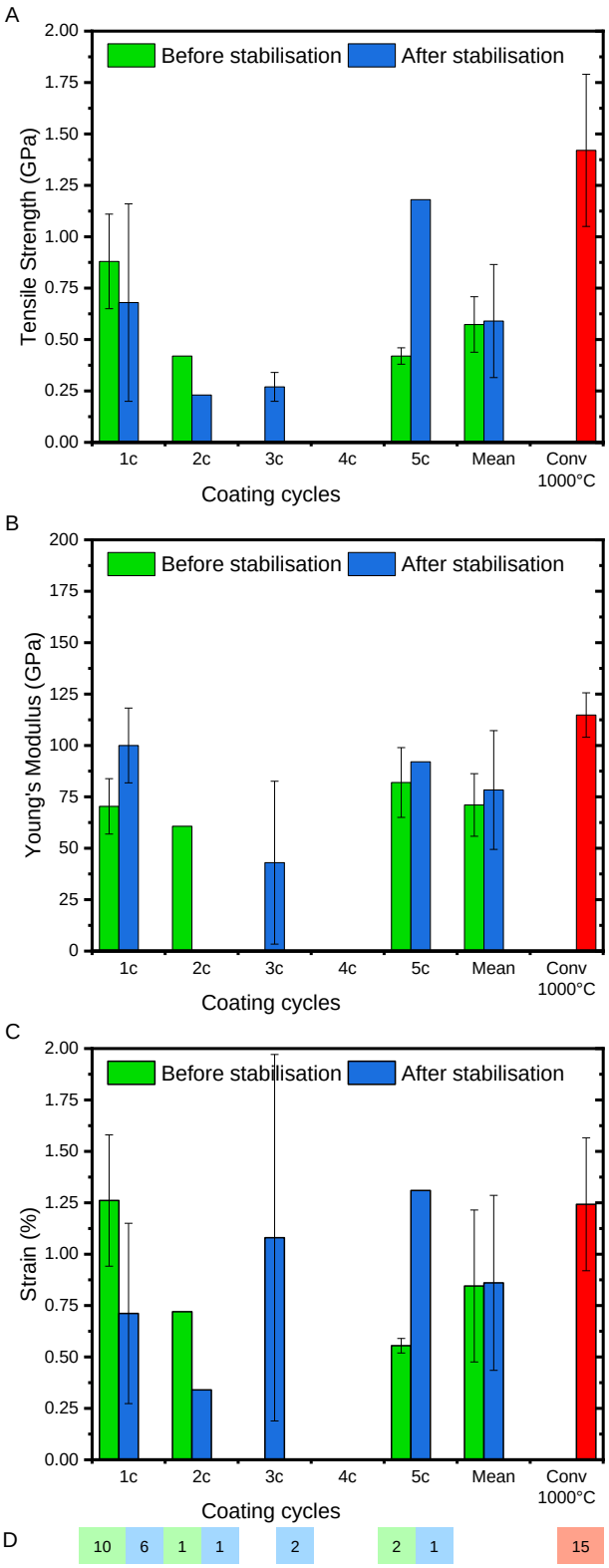

Figure 5.10 Mechanical properties of CF produced via progressive MW carbonisation from PAN precursor and conventional (Conv) at 1000°C. Tensile strength – A, Young's Modulus – B, Strain at break – C, number of fibres successfully tested - D.

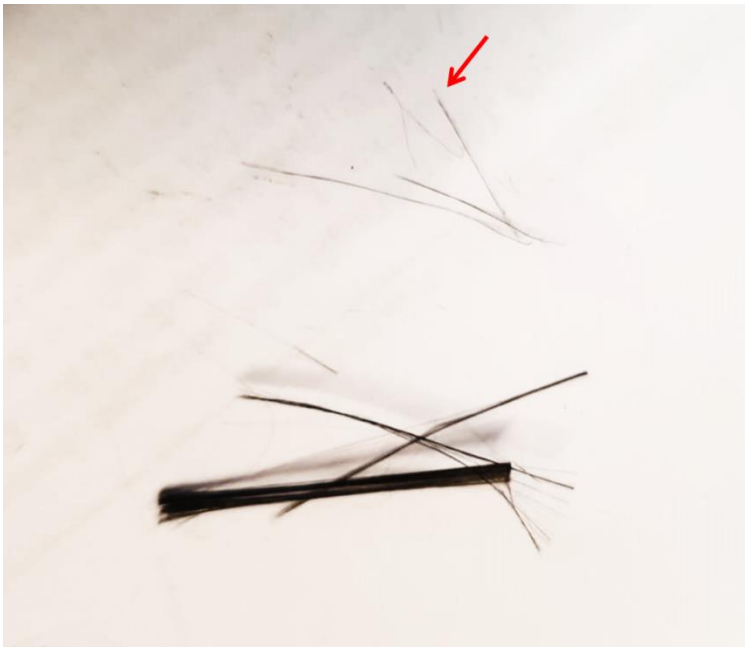

Figure 5.11 PAN based CFs breaking during separation.

5.3.6 Summary

Carbonisation conditions and properties of CFs produced via progressive MW carbonisation from PAN precursor are summarised in Table 5.4, where the data described above may be easily followed and values compared to conventional carbonisation at 1000°C. Standard deviation is reported where possible.

MW carbonisation at progressive power results in improvement of morphology observed through SEM. This can be attributed to lower initial heating rates and recorded T_{max}.temperatures compared to 5.2.1. Similarly to previous data (5.2.6), coating samples before stabilisation results in lower T_{max} and conversion rate. Coating samples after stabilisation results in higher T_{max} and conversion rates. The lack of clear improvement in strength over previous samples (5.2.5) and promising properties recorded for sample 5c coated after stabilisation (Table 5.4) suggest that the coating sequence might be less critical for progressive MW carbonisation of PAN. Instead, reduction of heating rates through finer tuning of MW power may be required in order to fully eliminate porosity and compare mechanical performance more reliably. Since the progressive MW carbonisation results in lowering of recorded T_{max} and conversion rates, it is decided to apply high MW power for subsequent initial tests with lignin/TPU precursor.

Table 5.4 Carbonisation conditions and properties of PAN-based CFs. Samples carbonized at progressive power levels.

Sample	Maximum temperature, T_{max} (°C)	Carbonisation time (min)	Fibre diameter (μm)	Conversion rate (%)	L_a (nm)	Tensile Strength (GPa)	Modulus (GPa)	Strain (%)
Coated before stabilisation								
1c	690	30	7.83 ± 0.57	86.6	6.75 ± 0.15	0.88 ± 0.23	70.40 ± 13.46	1.26 ± 0.32
2c	744	30	7.90 ± 0.38	80.9	6.32 ± 1.14	0.42	60.73	0.72
3c	827	35.5	8.60 ± 0.36	85.4	4.65 ± 1.35	-	-	-
4c	735	20	7.44 ± 0.74	82.0	6.25 ± 0.05	-	-	-
5c	707	20	7.68 ± 0.35	82.1	6.16 ± 2.98	0.42 ± 0.04	82.00 ± 16.97	0.56 ± 0.04
Coated after stabilisation								
1c	695	30	8.72 ± 0.38	83.5	4.25 ± 0.07	0.68 ± 0.48	100.00 ± 18.18	0.71 ± 0.44
2c	974	28	7.66 ± 1.02	91.1	4.27 ± 0.37	0.23	-	0.34
3c	717	30	7.68 ± 0.50	81.0	7.78 ± 0.19	0.27 ± 0.07	43.00 ± 39.6	1.08 ± 0.89
4c	704	30.5	8.26 ± 0.25	81.9	6.42 ± 0.22	-	-	-
5c	962	32	7.45 ± 0.69	90.5	4.96 ± 1.45	1.18	92.04	1.31
Conventional furnace	1000	130+	9.80 ± 1.21	88.2	9.61 ± 1.05	1.42 ± 0.37	114.80 ± 10.79	1.24 ± 0.32

5.4 Conclusions

In this chapter, susceptor assisted MW carbonisation of PAN precursor was demonstrated. The effects of MW power level, sample preparation sequence and susceptor coating thickness on carbonisation conditions and properties of produced CFs were investigated. The following conclusions can be drawn from the results:

1) MW carbonisation at high power (20 min) results in high heating rates and T_{max} of up to 1076°C. This results in creation of defects detected by SEM, probably due to differential shrinkage or evolution of volatiles during carbonisation at high heating rates. CFs produced via MW carbonisation from PAN precursor results in reduction of fibre diameter down to 6.35 μm, conversion rates (TGA) of up to 98%, L_a sizes (Raman) of up to 11.43 nm, TS of up to 1.18 GPa, YM of up to 160.7 GPa and strain of up to 1.31 %.

2) Carbonisation at progressive power levels (up to 36 min) results in reduction of initial heating rates, T_{max} temperatures and visible reduction of defect size and abundance at the expense of diameter reduction, conversion rate and L_a size. Reduction of heating rates through finer tuning of MW power is required to produce CF with mechanical properties comparable with conventional carbonisation. Further improvements could also be achieved via carbonisation under tension.

3) Coating samples before stabilisation results in lower T_{max} and consequently to lower conversion rate and L_a size, but produces CFs with superior mechanical properties. This is most likely due to the fusion/melting of the susceptor layer during stabilisation, which results in reduced efficiency in MW absorption. Coating samples after stabilisation results in higher T_{max}, conversion rate and L_a size. This should lead to improvement, but leads to deterioration of mechanical properties instead, probably due to more harsh conditions of carbonisation as suggested by defect-size (SEM). Furthermore, the susceptor layer applied after stabilisation may be more prone to damage during handling and by the volatile products of carbonisation, which may result in uneven heating, as suggested by temperature jumps recorded during MW carbonisation. Coating samples before stabilisation appears to be more reliable procedure for MW carbonisation at high power, but the difference is less clear when progressive power is used.

4) Increasing the number of MW susceptor coating cycles generally improves absorption of MWs and increases T_{max}. These differences are reduced for carbonisation at progressive power levels and if coating is applied before stabilisation. Relatively high conversion rates achieved for CF coated with a single layer of susceptor (1c) lead to a conclusion that even finer tuning is required. This could be achieved by reduction of susceptor coating thickness or concentration of MWCNTs in suspension.

Reduction of heating rates through finer tuning of MW power may be required in order to fully eliminate porosity from PAN based CFs and compare mechanical performance more reliably. Since the progressive MW carbonisation results in lowering of recorded T_{max} and conversion rates, it is decided to apply high MW power for subsequent initial tests with lignin/TPU precursor.

Chapter 6

Microwave carbonisation of lignin/TPU fibres

6.1 Introduction

As previously described, a blend of lignin and polyurethane (50:50 - lignin/TPU) was recently developed at UL and identified as a promising precursor for CF production [38]. Melt-spun lignin/TPU precursor fibres were coated with MW susceptor according to procedure from 3.2. This enabled achievement of carbonisation temperatures during MW heating and conversion of sustainable lignin/TPU precursor into CF.

It was previously found that coating before stabilisation and progressive MW heating result in lower T_{max} and conversion rates. Therefore, it was initially decided to use high MW power for carbonisation of samples coated after stabilisation. Also this coating sequence was preferred due to the ongoing work optimising stabilisation process of lignin/TPU precursor. First tests showed that 5 cycles of susceptor coating are sufficient for heating of lignin/TPU fibres and therefore 1-5 cycles were used to enable comparison to PAN.

In the first section, high power MW carbonisation is used to convert lignin/TPU fibres coated after stabilisation, to investigate the effects of increasing number of coating cycles. In the second part, progressive MW carbonisation is used to convert fibres coated before and after stabilisation, in order to find optimum conditions and improve mechanical performance of CFs produced from lignin/TPU precursor.

6.2 Carbonisation at high power level

6.2.1 Heating profiles

Heating profiles of high power MW carbonisation of lignin/TPU precursor are shown in Figure 6.1. Most of the samples experienced extremely fast heating to temperatures close to their T_{max}, in the first 15 s of MW heating. This was followed by a sudden drop to 300-500°C and subsequent rise to a stable temperature between 400 - 950°C. This initial disruption can be attributed to carbonisation reactions and release of gases. This corresponds well with increased evolution of methane and methanol recorded in the same temperature range (300-500°C) for the same organosolv hardwood lignin [57].

The disruption is longer and more pronounced compared to PAN carbonised at high power (5.2.1), most likely due to fibre diameter difference. Minor signal disruptions observed at higher temperatures can be attributed to evolution of volatiles (e.g. increased CO_2 release), as well as diameter changes due to shrinkage, similarly to 5.2.1.

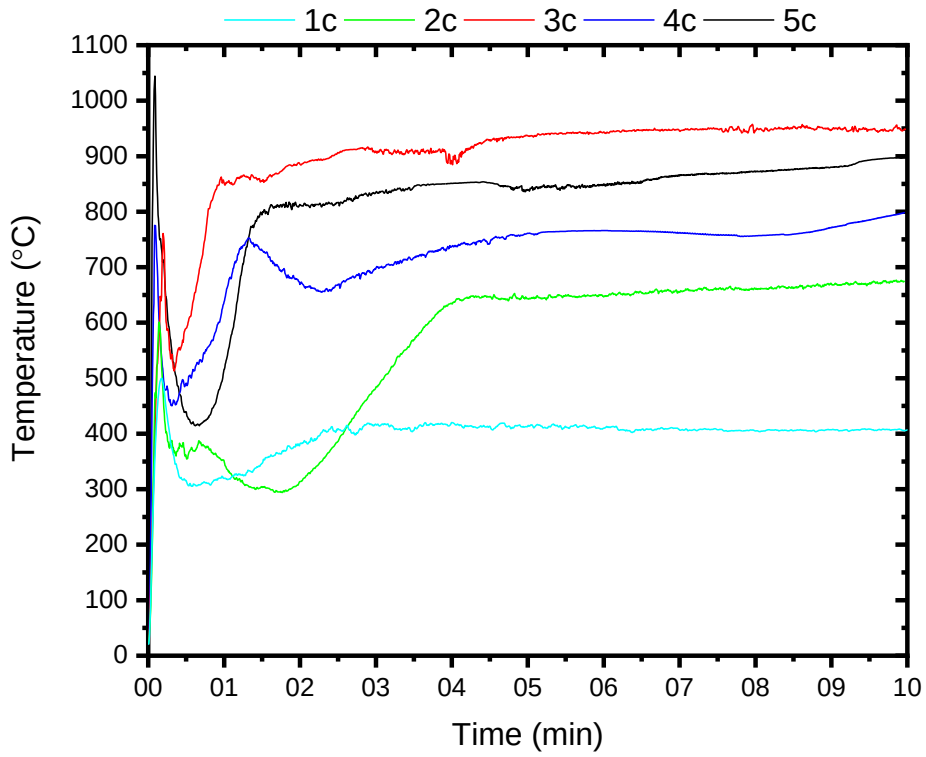

Figure 6.1 Heating profiles of high power MW carbonisation of lignin/TPU precursor.

Recorded T_{max} are in the range of 500 - 1044°C (Table 6.1). Rates and maximum temperatures were observed to be more dependent on the number of the susceptor coating cycles compared to MW heating of PAN (5.2). This can be attributed to larger diameter of lignin/TPU fibres (~100 vs ~10 μm). This leads to smaller surface area covered by MW susceptor coating and smaller number of individual fibres mounted for MW carbonisation. Consequently, there is less MW susceptor present during heating of lignin/TPU compared to PAN carbonisation, which results in enhancement of differences between cycles of susceptor coating and should enable easier optimisation of the MW heating.

Table 6.1 Maximum temperatures recorded during high power MW carbonisation of lignin/TPU precursor.

Sample	Maximum temperature, T_{max} (°C)
Coated after stabilisation	
1c	500
2c	677
3c	958
4c	798
5c	1044

6.2.2 Morphology

Representative SEM images of CFs produced via high power MW carbonisation from lignin/TPU precursor are shown in Figure 6.2. Average diameters of the CFs are in the range of 67.47-100.42 μm. Diameter tends to decrease as the T_{max} increases (Table 6.1), which is attributed to fibre shrinkage during conversion to CF.

Cross-sections show brittle fracture of the fibres with highly porous structures observed for samples with 2 or more layers of susceptor coating. Porous cross-sections present a structure of interconnected pores (mostly oval pores with diameter of up to about 20 μm in the longer dimension and some long cavities and cracks with lengths of up to about 50 μm) surrounded by a sheath/skin with thickness of up to 3 μm. The skin-core structure could be predefined during stabilisation [155,156] and this is enhanced for fibres with larger diameters due to incomplete stabilisation [157].

High porosity observed for samples 2c – 5c can be attributed to the release of volatiles during carbonisation [36,158,159], gasification of oxygen or blending polymers [160]. High heating rate leads to fast release of volatiles such as methane and methanol [57], which results in highly porous morphology. Similarly, the evolution of volatile solvents from the fibre can be used to prepare porous fibres via electrospinning [161]. The porosity is more severe compared to PAN at high power (5.2.2), which could be attributed to higher volume of released gases.

Smooth and homogeneous cross-sections of samples 1c and Conv (conventional carbonisation at 1000°C) suggest that the porosity is induced if the temperature is increases too rapidly above 500°C (T_{max} for sample 1c), which is in agreement with the range of increased gas evolution [57].

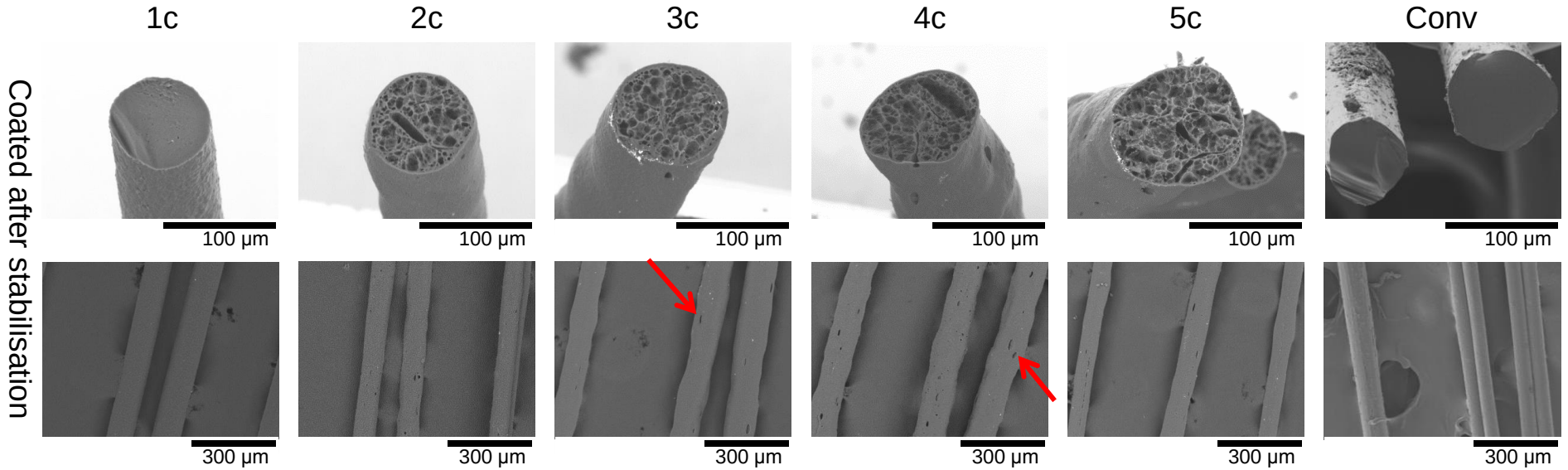

Figure 6.2 SEM images of CF produced via high power MW carbonisation from lignin/TPU precursor. Red arrows – open pores.

Open pores (red arrows) and waviness of the outer surface are also observed for samples with 2 or more layers of susceptor coating. This is due to the porosity induced during carbonisation, which manifests itself in the form of open pores and distorted shapes of produced CFs. This is confirmed by previous reports, where prolonged heating at higher temperatures leads to destruction of walls between pores and their appearance on the surface [162]. Samples 1c and Conv remain straight after the heat treatment.

6.2.3 TGA

Thermogravimetric analysis of CFs produced via high power MW carbonisation from lignin/TPU precursor is presented in Figure 6.3. Conversion rate evaluated from TGA is in the range of 84.7 - 87% for samples 2-5c, which is comparable to conventional carbonisation, even for sample 2c with recorded T_{max} of 677°C. This suggests that during carbonisation most of the mass is lost below this temperature. TGA traces of samples 2-5c and Conv (conventional carbonisation at 1000°C) show a mass loss of up 8% at temperatures below 200°C, which can be attributed to moisture [38,150,151] absorbed during sample preparation or storage due to high porosity. This is confirmed by lower mass loss observed in the same range for non-porous sample (1c). TGA trace of sample 1c presents a significant mass loss at temperatures above 400°C, which is attributed to gas release during carbonisation [38] and results in the final yield of 55%. The low yield can be attributed to the lowest T_{max} reached by the fibre during MW heating (500°C), which was not sufficient for carbonisation of the fibre (Table 6.1). The lack of porosity on SEM images of this sample confirms that it was not exposed to conditions, experienced by the rest of the group. This also suggests that the pores observed in other samples were mostly formed at temperatures above 500°C.

Conversion rate values for samples 2-5c are lower compared to PAN carbonised at high power (5.2.3) and do not follow trends of corresponding T_{max}. This is probably due to larger diameter of lignin/TPU precursor, which leads to incomplete carbonisation of fibres. Consequently, the presence of fibres with different diameters increases the error of TGA measurements.

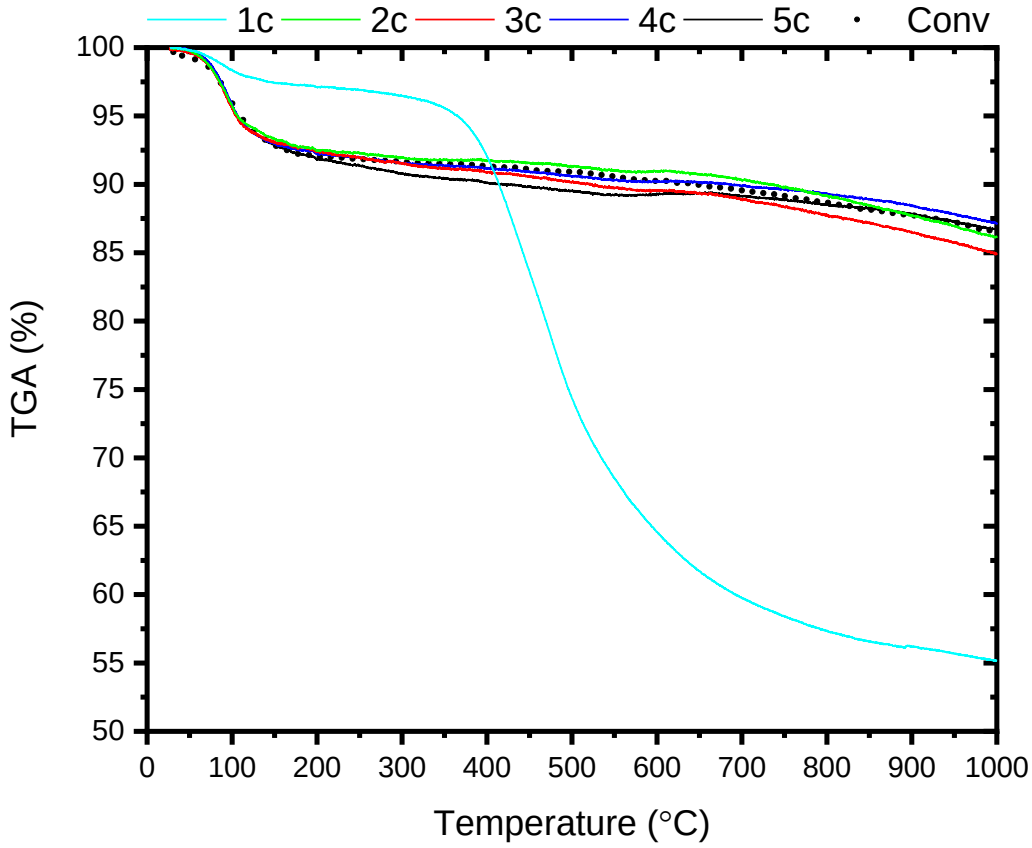

Figure 6.3 TGA of CF produced via high power MW carbonisation from lignin/TPU precursor.

6.2.4 Raman

Raman spectra of CFs produced via high power MW carbonisation from lignin/TPU precursor are shown in Figure 6.4. Characteristic D and G bands are observed in the range of 1344-1354 cm^{-1} and 1579-1588 cm^{-1}, respectively. D and G bands of CF produced via conventional carbonisation at 1000°C (Conv) are in the range of 1346-1350 cm^{-1} and 1583-1586 cm^{-1}, respectively. Spectra of samples 2-5c and Conv present overlapping of peaks which is characteristic for CFs with highly disordered graphitic structure after low temperature carbonisation [152–154]. Both bands are also present in the spectrum of sample 1c, but the intensity of signal is very low. This is in agreement with incomplete carbonisation of the fibre (TGA).

The calculated graphitic crystallite size (L_a) for samples 2-5c is in the range of 5.32-6.24 nm compared to 6.71 nm for sample Conv (conventional at 1000°C). This is in consensus with T_{max} temperatures (Table 6.1) and analogous to findings reported for PAN (5.4), where most of the samples have smaller L_a compared to Conv due to T_{max}<1000°C. Although it is possible to calculate L_a value (6.58 nm) for sample 1c, it is only theoretical. The sample is not fully carbonised, as suggested by TGA and low

intensity of Raman spectrum. Furthermore, the method used here for L_a calculation applies only for crystallite size >2 nm [138,154].

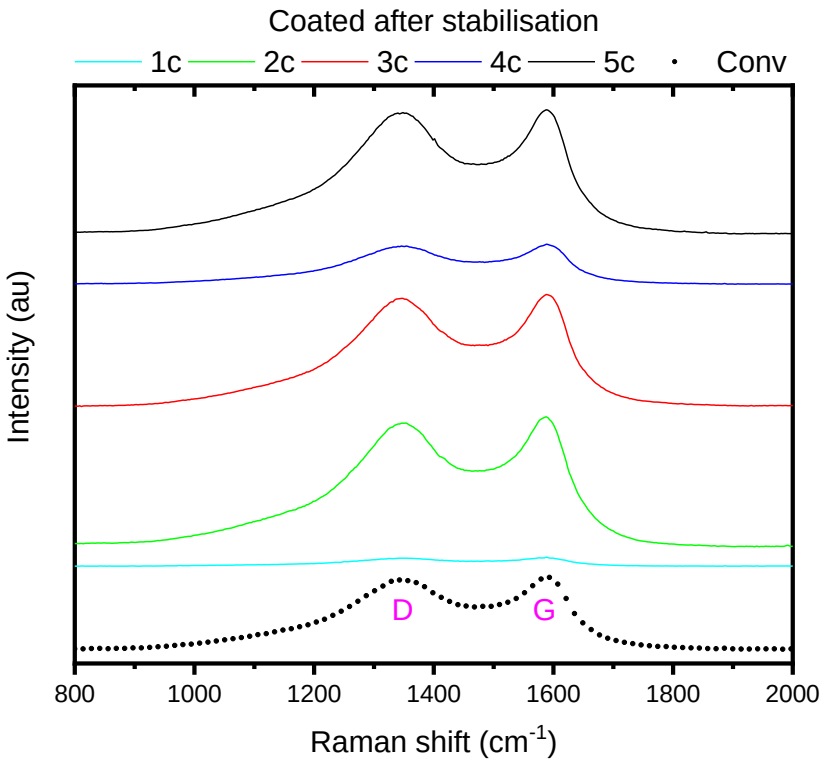

Figure 6.4 RAMAN spectra of CF produced via high power MW carbonisation from lignin/TPU precursor.

6.2.5 Summary

Carbonisation conditions and properties of CFs produced via high power MW carbonisation from lignin/TPU precursor are summarised in Table 6.2, where values can be compared to conventional carbonisation at 1000°C.

High power MW carbonisation results in highly porous morphology of samples produced from lignin/TPU precursor, which is attributed to high heating rates and release of volatiles. In general, recorded T_{max} increases with the coating thickness. Conversion rates are comparable to conventional carbonisation, even for sample 2c with recorded T_{max} of 677°C. CFs presented in this section are too brittle for measurement of mechanical properties. Reduction of initial heating rates is required to produce lignin based samples for mechanical testing. It was previously found that progressive carbonisation of PAN improved morphology of produced fibres, but slightly decreased recorded T_{max} and conversion rates. However, due to high porosity, it was decided not to increase number of cycles over 5 in the subsequent experiments with lignin/TPU precursor.

Table 6.2 Carbonisation conditions and properties of lignin/TPU CFs. Samples carbonized at high power level.

Sample	Maximum temperature, T_{max} (°C)	Carbonisation time (min)	Fibre diameter (μm)	Conversion rate (%)	L_a (nm)
Coated after stabilisation					
1c	500	10	91.39 ± 8.88	55.0	6.58 ± 1.25
2c	677	10	78.46 ± 12.64	86.0	6.24 ± 0.43
3c	958	10	86.10 ± 15.81	84.7	5.60 ± 0.19
4c	798	10	100.42 ± 16.92	87.0	5.32 ± 0.20
5c	1044	10	67.47 ± 8.63	86.6	6.13 ± 1.43
Conventional furnace	1000	130+	66.61 ± 16.04	86.3	6.71 ± 0.10

6.3 Carbonisation at progressive power levels

MW carbonisation of lignin/TPU fibres at high power level resulted in production of highly porous fibres. Previous experiments with PAN showed that progressive carbonisation improved morphology of produced fibres, but it was inconclusive whether one or the other coating sequence produces better CFs. Therefore both procedures are also applied in this section.

In this part, an input voltage of the MW setup was changed in an effort to reduce high initial heating rates during MW carbonisation of lignin/TPU precursor, reduce porosity and improve properties of the produced CFs. The voltage was increased incrementally, following similar procedure described for PAN (5.3).

Precursor with slightly smaller diameter was used (~ 72 μm) in order to improve flexibility of samples, simplify mounting of samples for MW carbonisation and prevent damage by manual handling. Lignin/TPU precursor fibres were coated with 1-5c (coating cycles) before and after stabilisation (according to 3.2) and stabilised prior to carbonisation. It was decided not to increase number of cycles over 5 to enable easier optimisation of progressive MW carbonisation. Promising conversion rates reported in the previous section (6.2.3) suggested that the thickness should be sufficient.

6.3.1 Heating profiles

Heating profiles of lignin/TPU precursor samples carbonised at progressive power levels are shown in Figure 6.5. Noticeably lower heating rates are observed during the initial stage at lowest power (Figure 6.5 A and B). After 5 minutes of heating, most of the samples reach temperatures between 300-450°C, which is usually higher for samples coated after stabilisation. This correlates with improved MW absorption observed previously for the susceptor layer prepared via this sequence (5.2). Increasing the MW power increases the rate of heating significantly as illustrated in (Figure 6.5 C and D). It has been observed that at a certain point during initial and intermediate stages of heating, sample temperature suddenly increases from about 400°C to about 600-800°C at which it tends to stabilise again. This sudden rise is recorded earlier in the process for samples with thicker susceptor coating (see 3-5c vs 2c in Figure 6.5 C). Reduction of heating rate before this transition is probably the key to process optimisation, as suggested by similar practice for conventional carbonisation of other hardwood lignin fibres [156]. After this, relatively stable reading of temperature

(sometimes preceded by a sharp peak instead of round shoulder) is recorded and the temperature scales with MW power until the final stage at 230V, 700W (Figure 6.5 E and F).

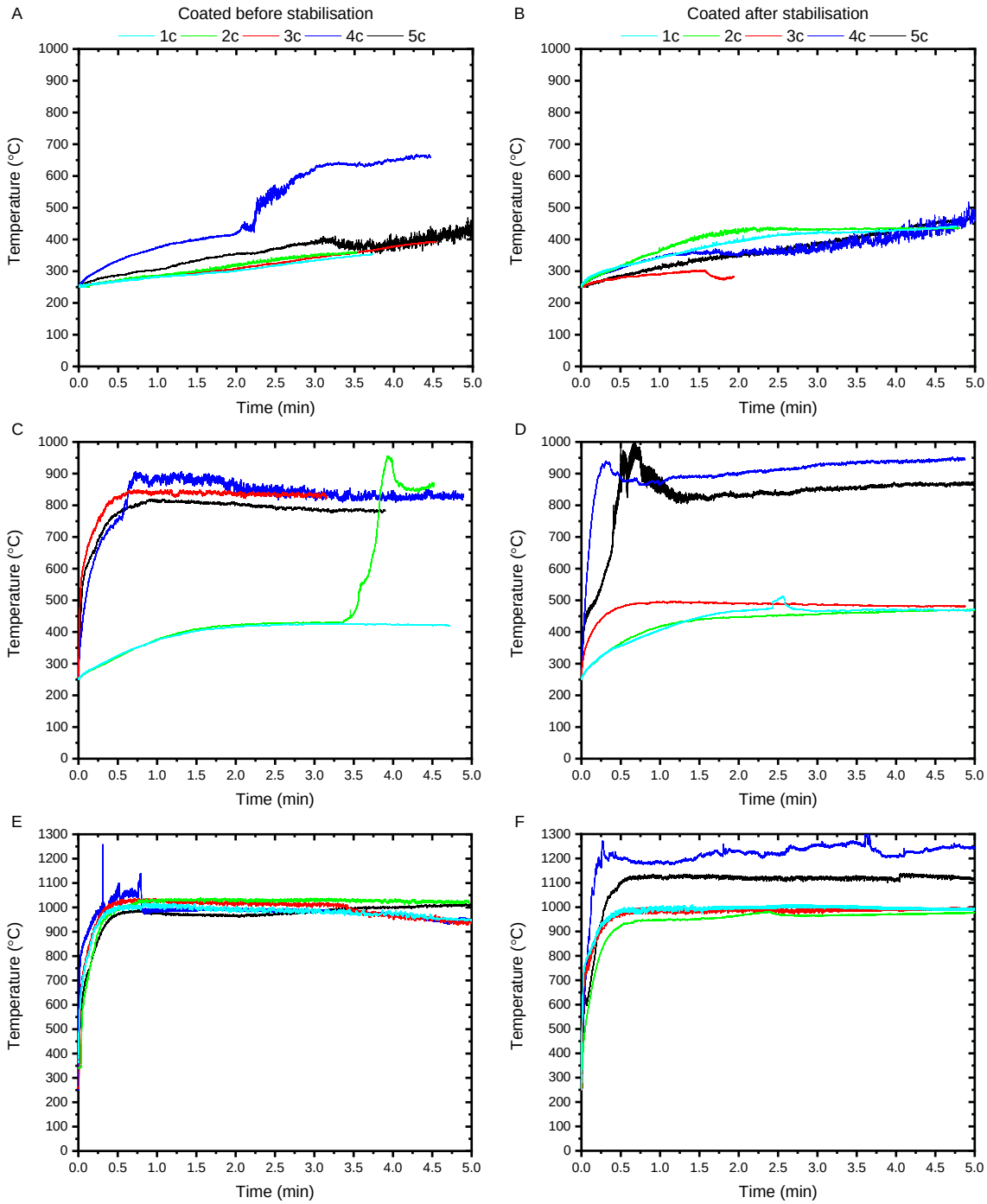

Figure 6.5 Heating profiles of progressive MW carbonisation of lignin/TPU precursor. A,B – 165-170V; C,D - 175V; E,F - 230V.

Recorded T_{max} are in the range of 1020 – 1259°C for fibres coated before stabilisation and 1000 – 1346°C for fibres coated after stabilisation. Highest temperatures are recorded for samples after 4 cycles of susceptor coating (4c). Wider range and higher T_{max} is observed for samples coated after stabilisation, which could be explained by

improved MW absorption of these samples. Similarly to previous findings for PAN (5.2.1), there is an increased difference of T_{max} between 3c and 4c samples coated after stabilisation, which might be correlated with an increase of electrical conductivity (4.2). T_{max} temperatures are summarised in **Error! Not a valid bookmark self-reference.**.

Finally, sharp peaks and signal vibrations are observed at different stages of heating. These features are observed in heating profiles of samples with thicker susceptor coatings and can be explained by one or combination of: evolution of volatiles, coating damage, plasma formation or noise due to alternating electromagnetic field [21,36,92].

Table 6.3 Maximum temperatures recorded during progressive MW carbonisation of lignin/TPU precursor.

Sample	Maximum temperature, T_{max} (°C)
Coated before stabilisation	
1c	1020
2c	1040
3c	1037
4c	1259
5c	1020
Coated after stabilisation	
1c	1010
2c	1056
3c	1000
4c	1346
5c	1139

6.3.2 Morphology

Representative SEM images of CFs produced via progressive MW carbonisation from lignin/TPU precursor are shown in Figure 6.6. Average diameter of the fibre is in the range of 44.84-50.49 μm for CF coated before stabilisation and 43.9-53.87 μm for CF coated after stabilisation. For both sequences, diameter is smaller compared to stabilised fibre (65.48 ± 8.45 μm) and in most cases smaller than diameter of Conv (conventional carbonisation at 1000°C). This is in agreement with T_{max} ≥1000°C recorded for all samples (Recorded T_{max} are in the range of 1020 – 1259°C for fibres coated before stabilisation and 1000 – 1346°C for fibres coated after stabilisation. Highest temperatures are recorded for samples after 4 cycles of susceptor coating (4c). Wider range and higher T_{max} is observed for samples coated after stabilisation, which could be explained by improved MW absorption of these samples. Similarly to previous findings

for PAN (5.2.1), there is an increased difference of T_{max} between 3c and 4c samples coated after stabilisation, which might be correlated with an increase of electrical conductivity (4.2). T_{max} temperatures are summarised in **Error! Not a valid bookmark self-reference.**.

Finally, sharp peaks and signal vibrations are observed at different stages of heating. These features are observed in heating profiles of samples with thicker susceptor coatings and can be explained by one or combination of: evolution of volatiles, coating damage, plasma formation or noise due to alternating electromagnetic field [21,36,92].

Table 6.3), which enhances shrinkage during carbonisation.

Cross-sections of CFs present evidence of brittle fracture. Majority of observed defects are small, circular pores of up to 4 μm or much smaller. About an equal amount of cross-sections show a smooth and homogeneous morphology, which is almost identical to the control (Conv) and very similar to the one reported previously for the same precursor [38] or other compatible lignin-based precursors [130]. This is a clear improvement over high power MW carbonisation of lignin/TPU fibre (6.2) and even over MW carbonisation of PAN fibre discussed in the previous chapter. The main reason is undoubtedly reduction of heating rates during initial carbonisation stage, especially in the range of 400-800°C which allows more time for carbonisation reactions, slower evolution of volatile products [57] and improves morphology. This is achieved more easily in MW carbonisation of lignin/TPU, most likely due to larger diameter (almost an order of magnitude compared to PAN) and resulting lower volume ratio of the MW susceptor to the fibre. Further improvements can be achieved via reduction of heating rate during intermediate stages (under 600-800°C), reduction of fibre diameter and carbonisation under tension.

Fibres retain their overall shape and signs of defects or waviness of external surface are scarcely found. This confirms that distorted shapes observed in 6.2.2 are closely related to internal porosity of the fibre. Loose fragments of susceptor coating are rarely observed and usually as a result of fibre breakage to reveal a cross-section.

It is difficult to uncover trends in morphology caused by coating thickness and sequence order. This is probably due to varying carbonisation times, which has an averaging effect.

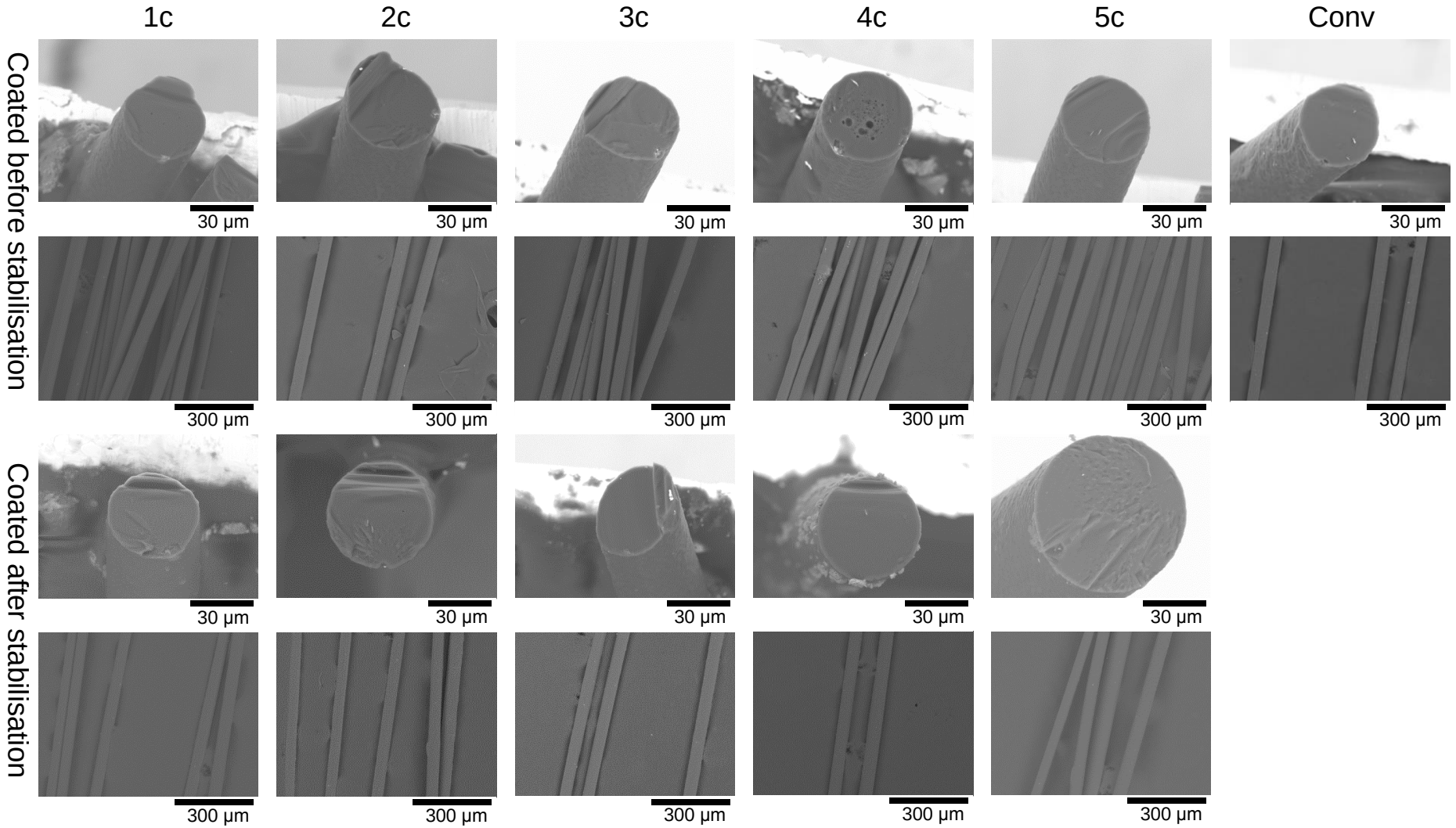

Figure 6.6 SEM images of CF produced via progressive MW carbonisation from lignin/TPU precursor.

6.3.3 TGA

Thermogravimetric analysis of CFs produced via progressive MW carbonisation from PAN precursor is shown in Figure 6.7. Conversion rate evaluated from TGA is in the range of 91.9 – 94.4% for fibres coated before stabilisation and 78.8 – 98.6% for fibres

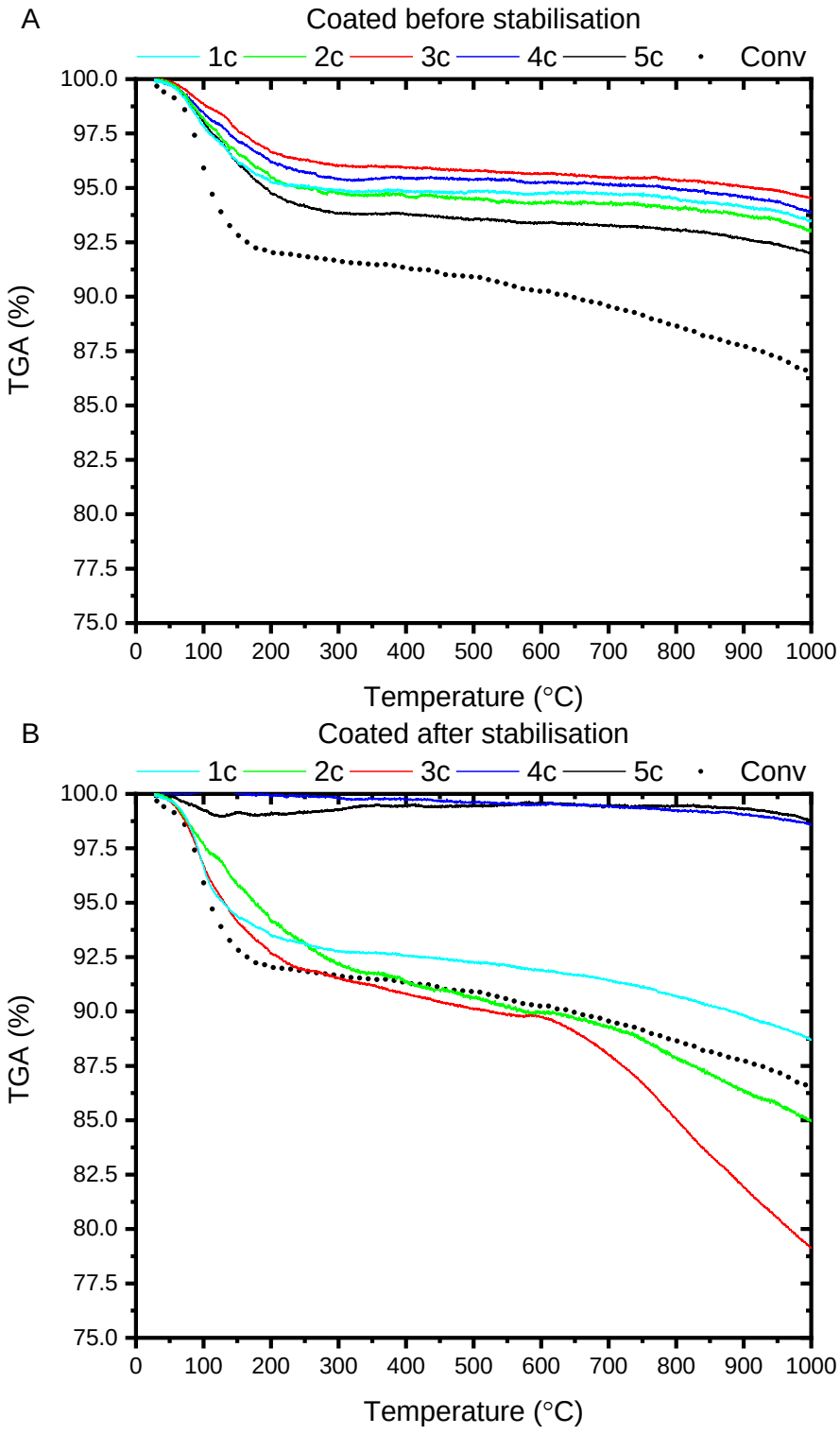

Figure 6.7 TGA of CF produced via progressive MW carbonisation from lignin/TPU precursor coated before (A) and after stabilisation (B).

coated after stabilisation. Conversion rates are generally higher than those reported for carbonisation at high power (6.2.3), which is in agreement with higher recorded T_{max} temperatures (Table 6.3). This is in agreement with the lack of significant mass loss in the range of 300-600°C, which is attributed to release of volatiles in the previous section [57]. Loss of up to 8% is observed below 200°C, probably due to moisture content [38,150,151], which is also observed in the previous sections (5.3.3 and 6.2.3). This brings conversion rate of fibre carbonised via conventional method down to only 86.3%. The moisture content is higher in CFs coated after stabilisation, which could indicate that melting of the susceptor coating during stabilisation reduces moisture intake of the CF after carbonisation.

Coating before stabilisation results in more consistent results, probably due to the same phenomenon of the coating fusion/degradation during stabilisation. Highest conversion rates are observed for coating after stabilisation (especially 4c and 5c), which is in good agreement with previous findings (5.2.3). Significant improvement over high power carbonisation of lignin/TPU can be explained by smaller diameter of PF (~ 72 μm). This could change ratio of the MW susceptor and is in agreement with T_{max} recorded at temperatures ≥1000°C for all samples (Recorded T_{max} are in the range of 1020 – 1259°C for fibres coated before stabilisation and 1000 – 1346°C for fibres coated after stabilisation. Highest temperatures are recorded for samples after 4 cycles of susceptor coating (4c). Wider range and higher T_{max} is observed for samples coated after stabilisation, which could be explained by improved MW absorption of these samples. Similarly to previous findings for PAN (5.2.1), there is an increased difference of T_{max} between 3c and 4c samples coated after stabilisation, which might be correlated with an increase of electrical conductivity (4.2). T_{max} temperatures are summarised in **Error! Not a valid bookmark self-reference.**.

Finally, sharp peaks and signal vibrations are observed at different stages of heating. These features are observed in heating profiles of samples with thicker susceptor coatings and can be explained by one or combination of: evolution of volatiles, coating damage, plasma formation or noise due to alternating electromagnetic field [21,36,92].

Table 6.3).

6.3.4 Raman

Raman spectra of CFs produced via progressive MW carbonisation from lignin/TPU precursor are shown in Figure 6.8. Characteristic D and G bands are observed in the range of 1341-1353 cm^{-1} and 1582-1593 cm^{-1}, respectively. For conventional carbonisation at 1000°C (Conv) they appear in the range of 1346-1350 cm^{-1} and 1583-1586 cm^{-1}, respectively. All spectra present overlapping of peaks which is attributed to highly disordered graphitic structures after low temperature carbonisation [152,153]. Slight red-shift of D band and blue-shift of G band are observed, compared to high power process (6.2.4). This could be associated with the structural changes and suggest fuller carbonisation [154,160].

The calculated graphitic crystallite size (L_a) is in the range of 5.12-7.12 nm for CFs coated before stabilisation, 5.02-6.73 nm for CFs coated after stabilisation and 6.71 nm for conventional carbonisation at 1000°C. This is an improvement over high power carbonisation (6.2.4) and is in general agreement with trends observed for T_{max} (Recorded T_{max} are in the range of 1020 – 1259°C for fibres coated before stabilisation and 1000 – 1346°C for fibres coated after stabilisation. Highest temperatures are recorded for samples after 4 cycles of susceptor coating (4c). Wider range and higher T_{max} is observed for samples coated after stabilisation, which could be explained by improved MW absorption of these samples. Similarly to previous findings for PAN (5.2.1), there is an increased difference of T_{max} between 3c and 4c samples coated after stabilisation, which might be correlated with an increase of electrical conductivity (4.2). T_{max} temperatures are summarised in **Error! Not a valid bookmark self-reference.**.

Finally, sharp peaks and signal vibrations are observed at different stages of heating. These features are observed in heating profiles of samples with thicker susceptor coatings and can be explained by one or combination of: evolution of volatiles, coating damage, plasma formation or noise due to alternating electromagnetic field [21,36,92].

Table 6.3). Calculated values are higher than L_a size reported for the same precursor, but this is due to different calculation methods being employed [38].

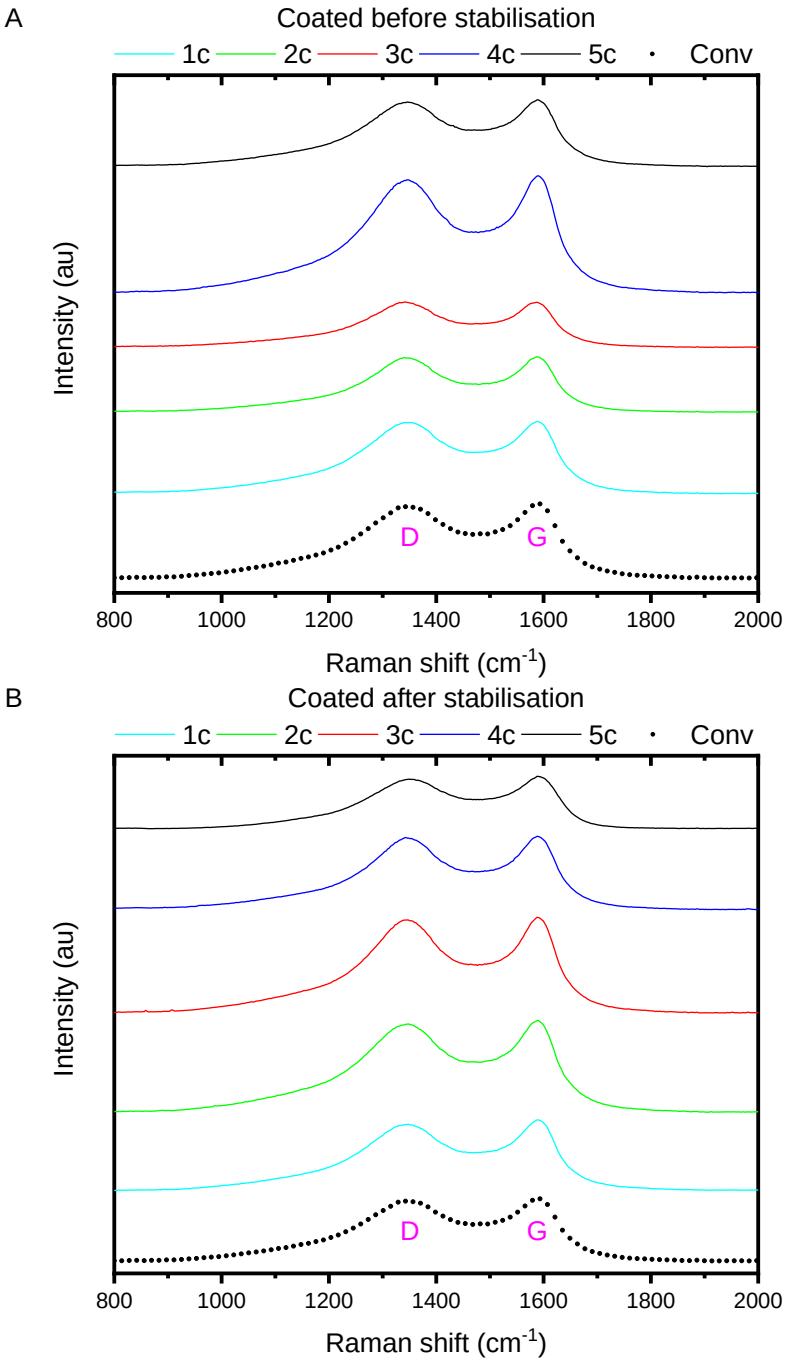

Figure 6.8 RAMAN spectra of CF produced via progressive MW carbonisation from lignin/TPU precursor coated before (A) and after stabilisation (B).

6.3.5 Mechanical properties

Mechanical properties of CFs produced via progressive MW carbonisation from lignin/TPU precursor are shown in Figure 6.9. Properties are compared to conventional carbonisation (Conv) at 1000, 1400 1600 and 2000°C.

Average TS, YM and strain of samples coated before stabilisation are in the range of 0.13-0.31 GPa, 51-81 GPa and 0.23-0.5 %, respectively. Average TS, YM and strain of

samples coated after stabilisation are in the range of 0.08-0.33 GPa, 34.67-64.67 GPa and 0.21-0.57 %, respectively.

TS of fibres (Figure 6.9 A) carbonised in MW exceeded performance of 0.25 ± 0.05 GPa for conventional carbonisation (Conv) at 1000°C. Even a single layer of susceptor (1c) is sufficient to produce CFs in MW which are comparable with this result. Furthermore, most of the values overlap with result of 0.36 ± 0.06 GPa for conventional carbonisation (Conv) at 1400°C, with closest values reported for 5 cycles of susceptor coating. This improvement can be attributed to reduction of heating rates and temperatures during initial heating stage and is in good agreement with improved morphology revealed by SEM. Similarly, mechanical properties of CFs produced in microwave plasma were improved by addition of low temperature pre-carbonisation step [94].

Values of YM (Figure 6.9 B) match those of samples carbonised conventionally (Conv) at temperatures of 1400°C or higher, which implies that an improvement of the YM could be achieved by optimisation of MW carbonisation through power, time or temperature variation.

Strain at failure (Figure 6.9 C) averaged at values of conventional carbonisation at 1400 – 1600°C, and in some cases was found superior than sample Conv carbonised at 2000°C.

This is an excellent result illustrating that, if proper conditions are used, susceptor assisted MW carbonisation proposed in this work can be successfully applied for rapid carbonisation of CFs with mechanical performance comparable with conventional carbonisation. In this case, progressive MW carbonisation appears to improve properties more efficiently compared to PAN (5.3.5), probably due to diameter difference. Reduction of high heating rates observed during intermediate stages of MW carbonisation (Figure 6.5 C and D) will most likely eliminate pores observed in some of the cross-sections (Figure 6.6). This will improve reliability of the process and increase the average mechanical properties.

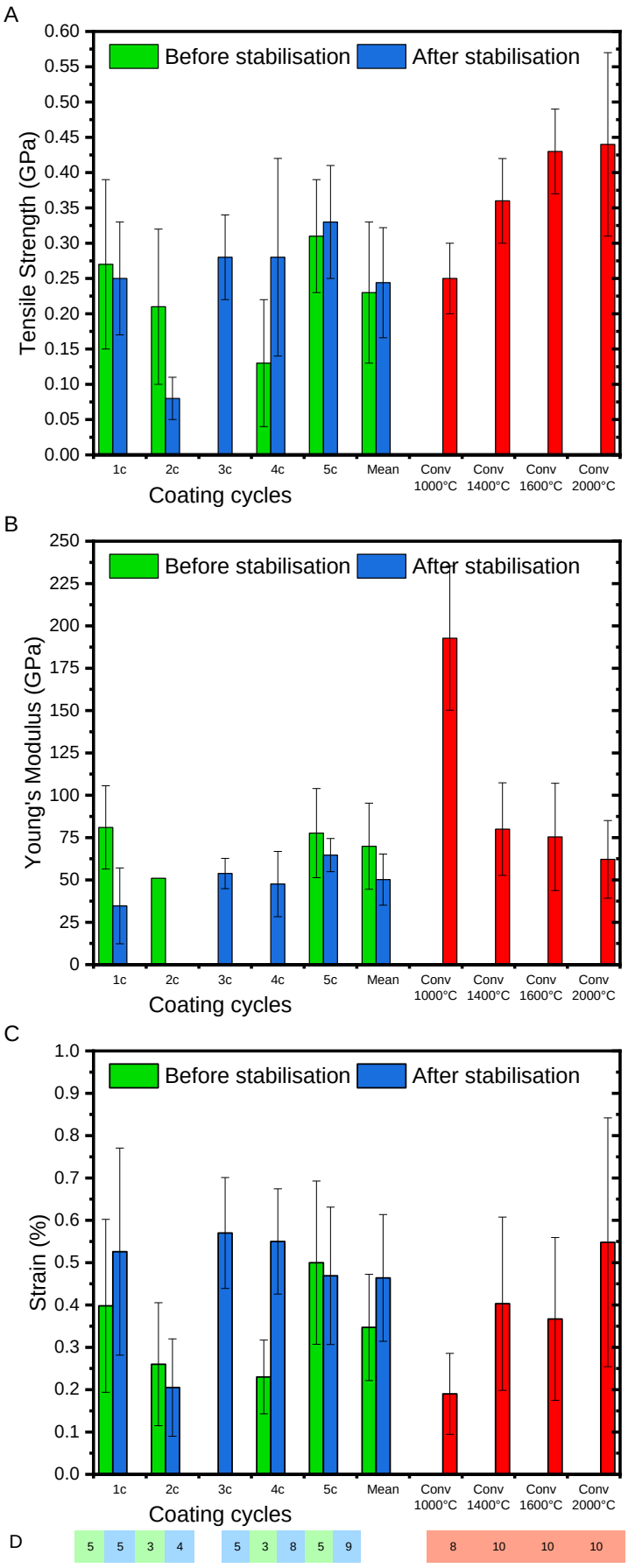

Figure 6.9 Mechanical properties of CF produced via progressive MW carbonisation from lignin/TPU precursor. Tensile strength – A, Young's Modulus – B, Strain at break – C, number of fibres successfully tested - D.

Further improvement of mechanical performance of the presented lignin/TPU CFs could be achieved by reduction of fibre diameter [3,36,38], as illustrated by reported TS of 1.1 ± 0.1 GPa for the same precursor with a final diameter of 25 ± 3 μm.

On the other hand, the tuning of MW heating conditions and improvement of mechanical properties achieved more easily for lignin/TPU precursor is mostly attributed to this larger fibre diameter compared to PAN. As discussed previously, this leads to lower amount of MW susceptor used and results in milder conditions. Application of fibre with much lower diameter will require closer control of susceptor coating thickness, MW power and other process conditions.

6.3.6 Summary

Carbonisation conditions and properties of CFs produced via progressive MW carbonisation from lignin/TPU precursor are summarised in Table 6.4, where the trends described above can be followed. Standard deviation is reported where possible.

MW carbonisation at progressive power results in remarkable improvement of morphology and mechanical properties of CFs derived from lignin/TPU precursor. This can be attributed to lower initial heating rates to allow carbonisation reactions and slower evolution of volatiles, especially methane and methanol. The highest conversion rates are recorded for samples 4c and 5c coated after stabilisation, which is in agreement with recorded T_{max}. Melting of the susceptor layer during stabilisation (4.2) results in slightly lower, but more repetitive conversion rates observed for samples coated before heat treatments. Most of the samples outperform conventional carbonisation at 1000°C, which is in agreement with T_{max} values ≥1000°C. Good performance of both 1c samples is very promising from an LCA perspective.

Table 6.4 Carbonisation conditions and properties of lignin/TPU CFs. Samples carbonised at progressive power levels.

Sample	Maximum temperature, T_{max} (°C)	Carbonisation time (min)	Fibre diameter (μm)	Conversion rate (%)	L_a (nm)	Tensile Strength (GPa)	Modulus (GPa)	Strain (%)
Coated before stabilisation								
1c	1020	30	50.49 ± 6.16	93.3	5.12 ± 1.33	0.27 ± 0.12	81.00 ± 24.56	0.40 ± 0.20
2c	1040	30	48.14 ± 5.28	92.9	7.06 ± 1.23	0.21 ± 0.11	51.00	0.26 ± 0.15
3c	1037	29	44.84 ± 1.75	94.4	7.12 ± 0.85	-	-	-
4c	1259	22	46.45 ± 5.62	93.8	5.51 ± 0.12	0.13 ± 0.09	-	0.23 ± 0.09
5c	1020	34	48.41 ± 5.23	91.9	6.33 ± 1.65	0.31 ± 0.08	77.67 ± 26.31	0.50 ± 0.19
Coated after stabilisation								
1c	1010	31	43.90 ± 3.06	88.5	5.73 ± 0.77	0.25 ± 0.08	34.67 ± 22.37	0.53 ± 0.24
2c	1056	37	47.72 ± 6.20	84.8	6.21 ± 0.89	0.08 ± 0.03	-	0.21 ± 0.12
3c	1000	25	45.64 ± 1.73	78.8	5.02 ± 0.82	0.28 ± 0.06	53.80 ± 8.96	0.57 ± 0.13
4c	1346	25	49.08 ± 2.28	98.5	6.10 ± 0.62	0.28 ± 0.14	47.57 ± 19.25	0.55 ± 0.12
5c	1139	40	53.87 ± 15.66	98.6	6.73 ± 0.48	0.33 ± 0.08	64.67 ± 9.79	0.47 ± 0.16
Conventional furnace	1000	130+	48.37 ± 2.20	86.3	6.71 ± 0.10	0.25 ± 0.05	192.75 ± 42.55	0.19 ± 0.10
	1400			-	-	0.36 ± 0.06	80.00 ± 27.33	0.40 ± 0.20
	1600			-	-	0.43 ± 0.06	75.40 ± 31.70	0.37 ± 0.19
	2000			-	-	0.44 ± 0.13	62.14 ± 22.97	0.55 ± 0.29

6.4 Conclusions

In this chapter, susceptor assisted MW carbonisation of lignin/TPU precursor was demonstrated. The effects of MW power level, sample preparation sequence and susceptor coating thickness on carbonisation conditions and properties of produced CFs were investigated. The following conclusions can be drawn from the results:

1) MW carbonisation at high power (10 min) results in high heating rates and T_{max} of up to 1044°C. This results in brittle CFs with high porosity observed through SEM. This is attributed to evolution of volatiles during carbonisation at high heating rates.

2) Carbonisation at progressive MW power levels (up to 40 min) results in T_{max} of up to 1346°C at the high power stage. This results in conversion rates (TGA) of up to 98.6%, L_a sizes (Raman) of up to 7.12 nm. Reduction of initial heating rates results in great improvement of morphology of fibres observed via SEM. Most importantly, the highest average values of TS, YM and strain of up to 0.33 GPa, 81 GPa and 0.57 % are recorded, respectively. This mechanical performance is comparable or superior to CFs produced via conventional method at temperature range of 1000-2000°C. Reduction of heating rate during intermediate stages (under 600-800°C) is required to ensure reliability of the process. Further improvements can be achieved via reduction of fibre diameter and carbonisation under tension.

3) Coating samples before stabilisation results in slightly lower T_{max}, but more reliable conversion rates and higher L_a sizes. This can be explained by the fusion/melting of the susceptor layer during stabilisation, which results in reduced efficiency in MW absorption and more durable susceptor layer. Coating samples after stabilisation results in more harsh conditions of carbonisation with highest T_{max} temperatures. Furthermore, the susceptor layer applied after stabilisation may be more prone to damage during handling and carbonisation. This results in wider range of conditions, properties and could contribute to increased absorption of moisture after carbonisation.

4) Increasing the number of MW susceptor coating cycles generally improves absorption of MWs and increases T_{max} and enables fuller carbonisation to CF. The differences are reduced for MW carbonisation at progressive power levels

and if coating is applied before stabilisation. This is probably due to averaging effects of these heat treatments on MW absortion efficiency. Even a single cycle of susceptor coating results in T_{max} of up to 1020°C, conversion rate of up to 93.3%, TS of up to 0.27 GPa, YM of up to 81 GPa and strain of up to 0.4%.

5) Higher diameter of lignin/TPU precursor reduces the ratio of the susceptor coating to the fibre volume. This results in highlighted effect of coating thickness observed for high power MW carbonisation. Furthermore, it allows easier optimisation of MW carbonisation leading to improvement of morphology and mechanical properties of CFs produced from lignin/TPU precursor.

MW carbonisation at progressive power results in remarkable improvement of morphology and mechanical properties of CFs derived from lignin/TPU precursor. MW heating model is presented in the next chapter to verify the experimental data and improve understanding of the differences observed for PAN and lignin/TPU precursors. This is followed by life cycle assessment, which illustrates benefits of susceptor assisted MW carbonisation.

Chapter 7

Linear model, LCA and alternative applications of MW heating

In this chapter, a linear model of MW carbonisation is described in order to verify some of the concepts and improve understanding of the heating mechanism. Furthermore, life cycle assessment is presented to illustrate the breakthrough in terms of energy use and environmental impact reduction. Finally, adaptability of susceptor assisted MW heating as preparation method of other carbon materials is briefly evaluated.

This chapter presents results of collaboration of the main author with other researchers. In collaboration with Timothy J. Conroy a model for microwave heating was developed. Life cycle analysis was a collaboration with Frida Hermansson, Matty Janssen, and Magdalena Svanström. Finally, MW carbonisation of other materials was a collaboration with Anne Beaucamp and Mario Culebras Rubio.

7.1 Linear model of microwave heating

In this section, MATLAB calculation results of MW heating model are presented. For more detailed description of equations used in the model, the reader is referred to an Appendix A of the thesis. The author of this thesis is not responsible for creation of the MATLAB code and detailed description of equations. Therefore, a summary of assumptions is presented below. The author of this thesis is responsible for proposing assumptions related to MW heating mechanism, provision of necessary information such as material properties, geometry of the sample and setup, as well as running MATLAB simulations and creation of plots and figures.

7.1.1 Coupled electromagnetic - heat transfer model

The microwave heating process proposed here involves raising the temperature of precursor fibres using electromagnetic waves, via a lossy dielectric susceptor coating. The electromagnetic waves are generated by a 1 kW magnetron operating with an assumed efficiency of 60-70%. A waveguide then passes the electromagnetic waves into the microwave cavity with internal dimensions of 0.32 m (height) x 0.45 m (width) x 0.28 m (depth). The electromagnetic fields alternate with a frequency of 2.45 GHz,

which in turn excite the susceptor material. The susceptor material is a conductive nanocomposite containing MWCNTs, which have a high dielectric loss. That means the temperature increases rapidly upon exposure to electromagnetic waves due to conduction of delocalised electrons in MWCNTs. As the temperature of the susceptor increases, heat conducts to the lower temperature precursor material located at the core of the fibre. In order to model the transient temperature distribution on the precursor core, it is necessary to couple the electromagnetic and heat transfer domains.

Recognising the symmetry that exists in heating of the fibre and the size of the geometry in comparison to the wavelength of the electromagnetic field, the heat diffusion, for 3D transient heat conduction in cylindrical coordinates, is reduced to a one dimensional problem by assuming symmetry with respect to the circumferential and axial coordinates. This simplification may be afforded as the cross section of the fibre will not experience a significant variation in electric field strength, due to the size of the fibre diameter relative to the electromagnetic field wavelength (10^{-5}-10^{-4} m vs 10^{-1} m). For simplicity, the fibre is assumed as suspended in the electromagnetic field, with temperatures and heat losses to the environment uniform around the circumference and along the length; embedded in this assumption is the omission of the effects of neighbouring fibres in a bundle, and that conditions are representative of a fibre at the outer surface of a bundle. As the model must be able to describe the transient temperature response of the fibre material as heat is conducted radially through the fibre via the dielectrically heated susceptor material, the temporal and volumetric heat generation terms are retained in the formulation of the one dimensional model.

If constant material properties are assumed, then the model can be linearised, as presented below. Mathematical model for non-linear scheme has also been developed and can be used in the future, when the temperature dependency of material properties is fully studied.

In order to deliver a transient temperature profile over the radial coordinate, it is necessary to define initial and boundary conditions. Upon introduction of the electromagnetic field to the heat transfer domain, it is assumed that the temperature of the PAN fibre is equal to the ambient (20°C). Due to symmetry, a zero temperature gradient exists at the core of the fibre. At the surface of the susceptor, heat losses through radiation and convection are assumed.

Volumetric heat generation is assumed in the susceptor coating only, as the precursor fibre has a negligible dielectric loss. The thickness of susceptor coating is in the order of 100 nm. At such scales, the conventional 'bulk' heat diffusion model no longer holds, as the thickness is likely smaller than the mean free paths of the electrons and phonons that transport heat through the material. In order to circumvent this difficulty in modelling, the volumetric heat generation term is transformed to a heat flux on the fibre surface. The susceptor coating is removed from the model, and the precursor fibre is 10 μm in diameter. Utilising a 1 μm spatial step permits a time step of 10^{-6} s for stability and accuracy, which is over 10^{6} times larger than the limiting temporal increment for modelling at 10-100 nm. When the heat generation term is converted to an incident heat flux on the PAN surface, an energy balance dictates the state of thermal equilibrium of the fibre. An assumption of uniform temperature across the susceptor material and a negligible dielectric loss in the PAN fibre is made.

By reducing the heat diffusion to a one-dimensional radial conduction problem, the transient temperature profile can be solved numerically using implicit finite difference methods with appropriate initial and boundary conditions. This method is unconditionally stable, meaning a solution can be obtained using any temporal step size, and is resolved iteratively with a set of linear algebraic equations. However, the chosen time increment does influence solution accuracy, so caution must be exercised in this regard. The equations needed to build the finite difference model are essentially discrete approximations of the differential terms present in the heat equation, and are formulated using the second-order accurate central difference scheme.

In order to solve the transient heat conduction problem using the finite difference scheme, temperatures are evaluated at a new time, rather than in a previous time, as is the case using conditionally stable explicit solution methods. The Gauss-Seidel iteration technique is employed here to resolve temperatures in the finite difference stencil at new times. This method is robust, efficient, and involves solving a linear set of finite difference equations describing nodal temperatures at new times simultaneously by iterating towards converged solutions, then marching the solution at each time step by setting the outputs at time n as the inputs for time n+1. An acceptable error in temperature of 0.001 K is applied. Due to the cylindrical fibre geometry and imposed boundary conditions, different coefficients exist for modes at the root, the interior, and at the surface.

Maxwell's equations constitute a fundamental model for electromagnetism. These equations are generally represented in integral or differential form to describe the electric and magnetic fields in a three-dimensional space. Numerical techniques such as Finite-difference time-domain (FDTD) and Finite element method (FEM) are commonly used to solve Maxwell's equations in electromagnetic problems. In the present model, the term necessary to resolve the transient temperature field in the PAN fibre is established using a series of analytical expressions that describe peak electric field strength. This simplification is afforded as the location of 'hot spots' in the commercial microwave oven are first identified in the experimental analysis, with the PAN fibre then positioned appropriately. Assuming a fixed input power of 0.7 kW from the magnetron, the average microwave strength over the cavity cross section is calculated and the peak electric field strength can then be obtained.

7.1.2 Material properties

Material properties assumed for modelling of MW heating are presented in Table 7.1.

Table 7.1 Material properties assumed in linear model calculations.

Property	Precursor	CF	Susceptor
Thermal conductivity (W/mK)	0.262	1.36	-
Density (kg/m^3)	1.16 x 10^3	1.80 x 10^3	-
Specific heat capacity (J/kgK)	1.29 x 10^3	9.01 x 10^2	-
Thermal diffusivity (m^2/s)	1.76 x 10^{-7}	8.40 x 10^{-7}	-
Conductivity (S/m)	0	-	10^6
Emissivity	-	-	0.9
Reference	[163–165]	[166–168]	[117,135]

7.1.3 Results

Experimental and modelled MW heating profiles are compared in Figure 7.1. Application of data obtained in Chapter 4 (for susceptor coating conductivity) results in extremely slow rise in modelled temperature. Therefore, a value obtained from literature for MWCNTs is used. This should mimic the real heating mechanism more efficiently, as the MWCNTs should heat in MWs independently, regardless of proximity of other nanoparticles. Experimental MW heating of PAN samples 1 – 5c is compared to modelled MW heating using corresponding susceptor thickness (Figure 7.1 A and B). It is observed that modelled rates are two orders of magnitude higher from experimental heating rates and that modelled T_{max} temperatures (1020 – 1320°C) are higher than those recorded experimentally (910 – 1060°C). The differences have numerous

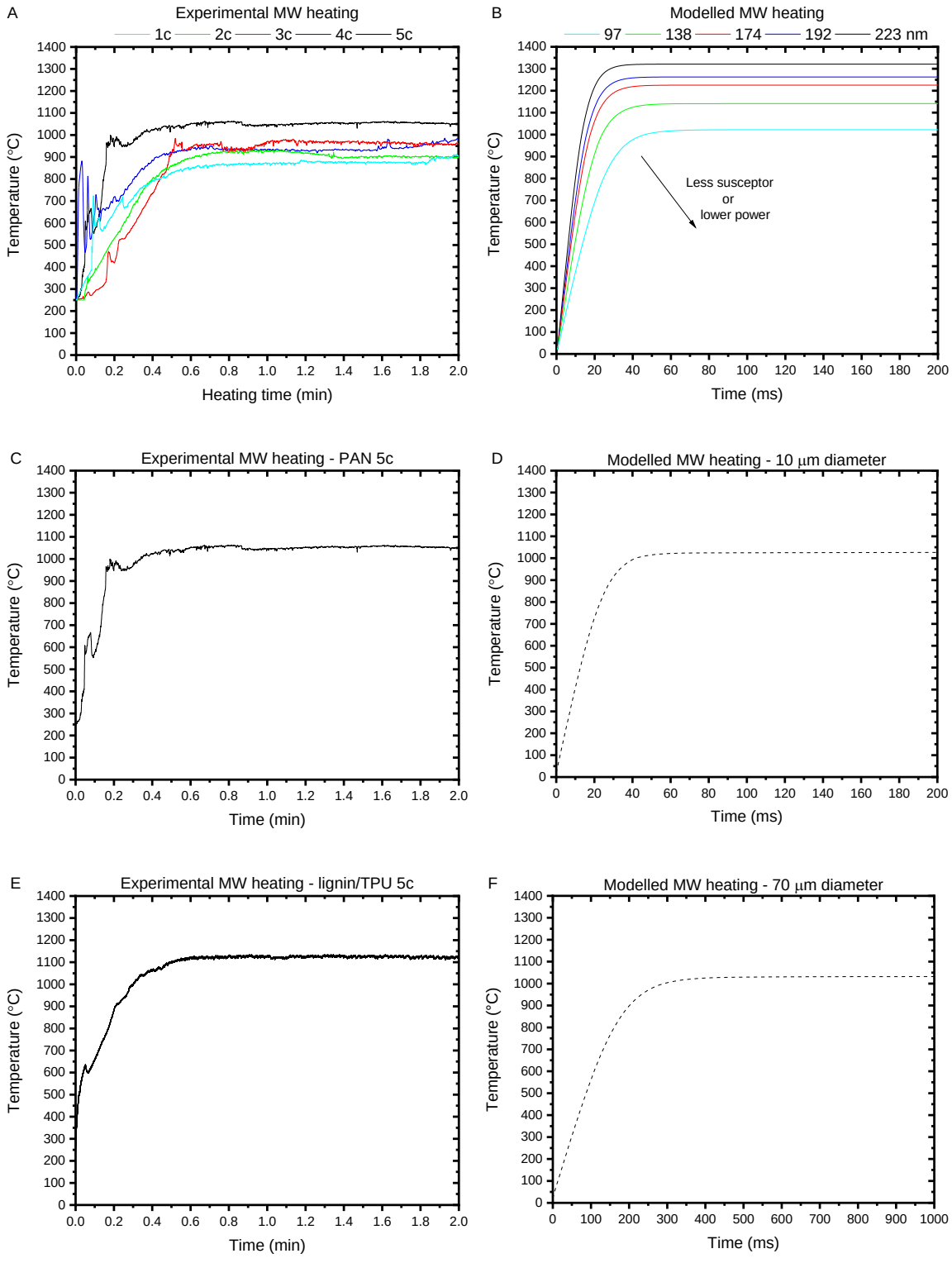

Figure 7.1 Experimental vs modelled MW heating profiles at 2.45GHz, 700W. Experimental PAN 1 – 5c (A), model for diameter 10 μm and susceptor thickness corresponding to 1 – 5c (B), PAN 5c (C), model for PF with 10 μm diameter and 100 nm of susceptor (D), lignin/TPU 5c (E), model for PF with 70 μm diameter and 100 nm of susceptor (F).

explanations, such as inefficiency of the domestic MW. In this scenario, there are several assumptions that could lead to higher predicted temperatures and rates. The susceptor coating is assumed to be entirely made of MWCNTs and no heat transfer occurs within its structure. The peak intensity of electric field is expected to act on each fibre in the bundle. None of the reactions taking place during carbonisation are taken into account, which results in higher rates and the absence of peaks/disruptions, compared to the experimental data. Also, modelled heat loss depends on assumed value of emissivity (ε). The higher the ε value assumed, the lower the predicted rate and T_{max}.

It is worth noting that modelled rates and temperatures could be even higher if other heating mechanisms were included, such as dielectric polarisation, eddy current loss and others [15]. Furthermore, as the carbon phase develops in the fibre, it changes from MW transparent to absorbing material. This increases its contribution in heat generation, provided that it is not completely shielded from electromagnetic field by the susceptor.

Figure 7.1 (C and D) shows that the T_{max} closest to experimental (5c) is obtained for modelled susceptor thickness of 100 nm. This can be compared to results for 70 μm fibre shown in Figure 7.1 (E and F). Modelled temperature rises to 1000°C in 40 and 290 ms for a precursor with a diameter of 10 and 70 μm, respectively. This shows that increasing the diameter of the precursor decreases the rate of MW heating.

Predicted T_{max} close to 1030°C is observed regardless of the fibre diameter. The model does not take into account absorption of MWs by the precursor material itself and therefore the modelled diameter has little effect once the temperature reaches the maximum where equilibrium between the heat generated in the susceptor and the heat lost through radiation/convection is achieved.

Modelling results for 10 μm diameter PF cross-section heated in an electromagnetic field of a microwave are shown in Figure 7.2. Four points in time are chosen to demonstrate temperature distribution at approximately 100, 400, 700 and 1000°C. The maximum edge-to-core temperature difference of nearly 1.5°C is observed at the start of the heating and decreases over time of 43 ms to a difference of 0.02°C at 1000°C.

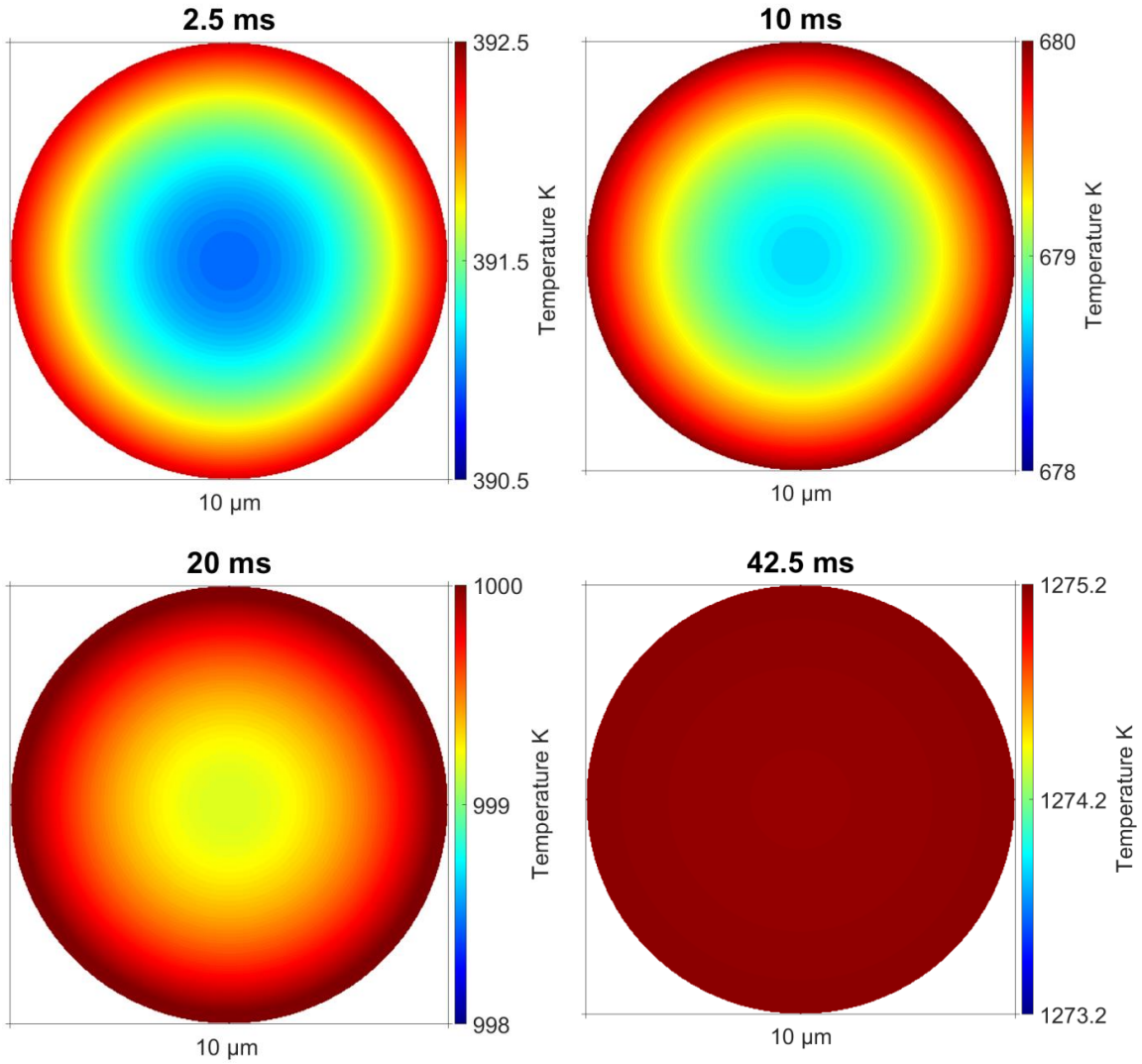

Figure 7.2 Modelled cross-section of PF (10 µm diameter and 100 nm susceptor coating) showing edge-to-core temperature distribution at 2.5, 10, 20 and 42.5 ms of MW heating, which correspond to fibre temperatures of approximately 100, 400, 700 and 1000°C, respectively.

MW heating simulation of 70 µm diameter PF is shown in Figure 7.3. In this case, the edge-to-core difference at the start of the heating reaches nearly 9.9°C and decreases over time of 295 ms to a difference of 0.17°C at 1000°C. This illustrates that increase in diameter results in larger temperature gradient during heating. Addition of heat generation by developed carbon phase in the model should reveal how it could influence this gradient.

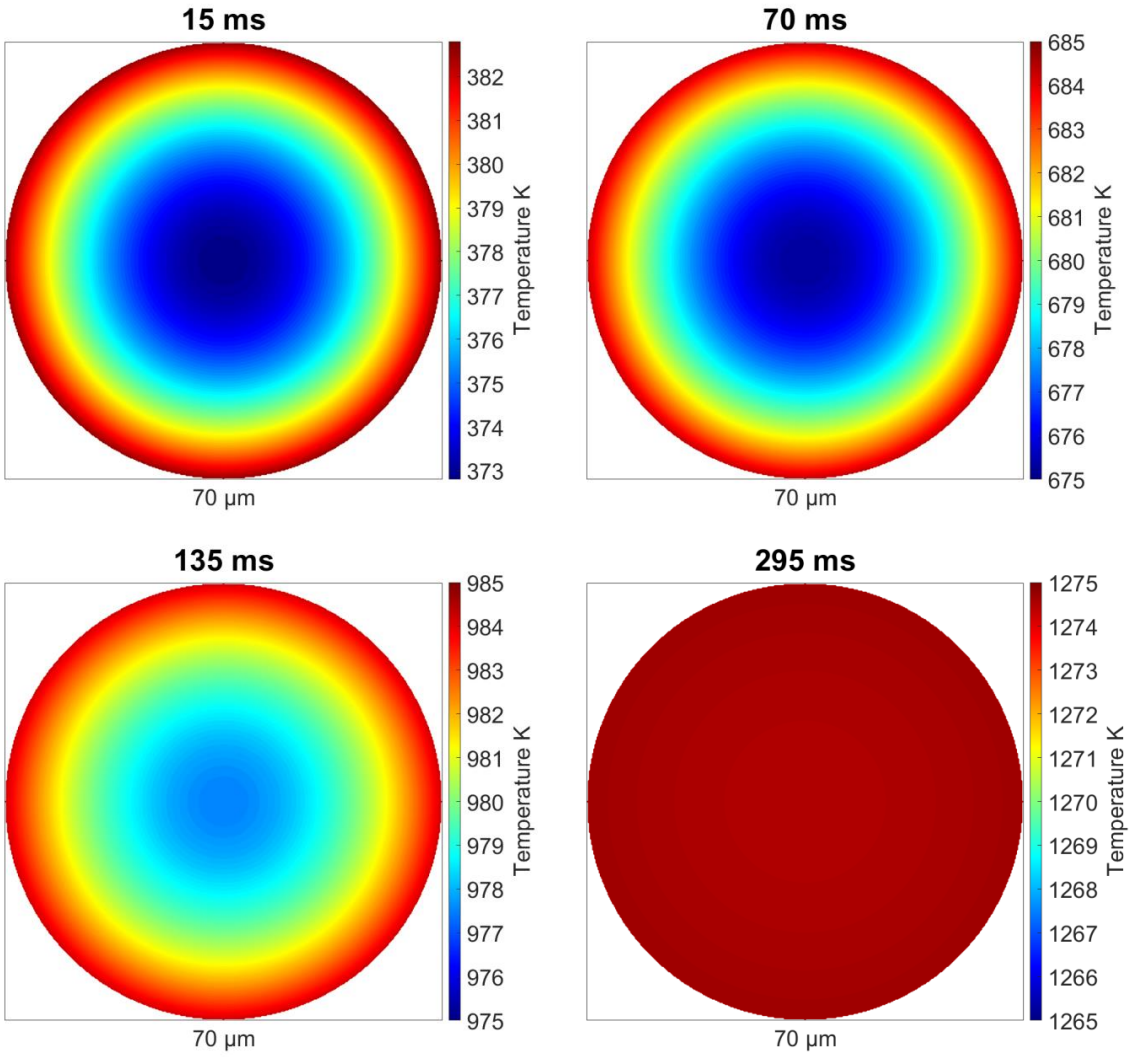

Figure 7.3 Modelled cross-section of PF (70 µm diameter and 100 nm susceptor coating) showing edge-to-core temperature distribution at 15, 70, 135 and 295 ms of MW heating, which correspond to fibre temperatures of approximately 100, 400, 700 and 1000°C, respectively.

7.2 Life cycle assessment of carbon fibre production using microwave technology

In this section, life cycle analysis of MW heating is presented and quantifies the environmental and cost benefits achieved via MW carbonisation. A summary of assumptions is presented below. For more detailed description, the reader is referred to an Appendix B of the thesis, which includes report provided by an external institution. The author of this thesis is responsible for collection of data during lab scale

experiments (Chapters 5 – 6), estimation of susceptor volume/weight fractions and energy savings of MW over conventional carbonisation.

7.2.1 Assumptions

It is assumed that the resulting fibres have the same quality and can fulfil the same function in the final application. The lignin/TPU based fibres are assumed to be produced from 50% lignin and 50% TPU. The production of CF via conventional and MW heating is compared and is assumed to take place in Germany.

There is no large-scale production of CFs using MW heating or lignin/TPU precursor, therefore a prospective approach is needed in the assessment.

This study considers the cradle-to-gate activities of the CF production. This means that the extraction of raw materials, the processing of the materials and the production of the CF which leaves the system at the factory gate. The study does not include the manufacturing of a composite in which the CF is used, the use of the composite or any end-of-life treatment. These are assumed to be the same for the different types of fibres considered.

This study considers climate impact and energy use. These are chosen as they are among the most commonly used impact assessment methods. Also, consideration of the climate impact is motivated by the replacement of fossil based raw material (PAN) to bio-based raw material (lignin and TPU). It is also strongly linked to fossil fuel use, e.g. in electricity generation. The consideration of energy use is motivated by the fact that previous studies have shown that the carbonisation is highly energy intensive (see [169]).

The lignin/TPU precursor fibres are spun using melt spinning, whereas the PAN-based fibres often are spun using wet spinning (Das, 2011). This is followed by CF production which is the same for both types of fibres. This includes stabilisation and carbonisation of the fibres. The carbonisation is done either by means of a conventional furnace or MW technology, followed by subsequent surface treatment and spooling.

The climate impact is assessed using CML2001 and the energy use by cumulative energy demand as provided by Ecoinvent 3.3 [170]. All modelling is done in OpenLCA. When ecoinvent processes are referred to below, it refers to Ecoinvent database 3.3. ELCD refers to the database provided by European Platform on Life Cycle Assessment.

The inventory for lignin/TPU CF is based on primary data collected within the LIBRE project. Data for Organosolv lignin production is taken from [171]. TPU production is based on a polyurethane data set available in Ecoinvent 3.3, where the polyols have been replaced with bio-based polyols based on data from [172].

When needed and possible, literature data have been used to upscale production processes within the LIBRE project from pilot to industrial scale, such as for the spinning process, where the processing electricity for the extrusion is approximated to 0.1 kWh/kg as suggested by Das [173]. Other energy and material inputs related to heating and cleaning are still based on pilot scale data due to data availability. The CF production data using a conventional furnace is provided within the project for industrial scale production of PAN-based CF. However, due to lignin's inherent properties, there are indications that the energy consumption in CF production is around 25% lower than for PAN [173]. Therefore, a 25% reduction in energy used by a conventional furnace for stabilisation and carbonisation is assumed. Blending with TPU could influence this reduction, but to what extent is still unknown.

The available data for carbonisation using MW technology are for lab scale. For the purpose of this life cycle assessment, approximations and assumptions were made. The data provided within the project suggests that the MW carbonisation needs only 6.8% of the energy used for CF production with a conventional furnace. Therefore, the energy use for the microwave oxidation, stabilisation and carbonisation of lignin/TPU based CF production is assumed to be 6.8% of the energy used by conventional furnace. The material yield after stabilisation and carbonisation process is measured to be 40%. The order of magnitude for this energy reduction is in line with what is suggested by Lam *et al.*, who used MW pyrolysis to produce CFs from bamboo [99]. The reduction only applies to oxidation, stabilisation and carbonisation and not to processes such as spooling or any surface treatments of the CF. The dataset "Polyacrylonitrile fibres (PAN), production mix, at plant, from acrylonitrile and methacrylate, PAN without additives" [174] from the ELCD database is used to model the PAN precursor fibre. PAN based CF production is based on data provided within the LIBRE project and the energy consumption when using MW technology is assumed to be reduced to 6.8% of the energy consumption when using conventional furnace. The yield in the PAN-based CF production is measured to be 50%. Both carbonisation processes are assumed to use the same amount of nitrogen produced from compressed air.

7.2.2 Results

Cumulative energy demand to produce 1 kg of CF from PAN and lignin/TPU precursor via conventional and MW heating is compared in Figure 7.4.

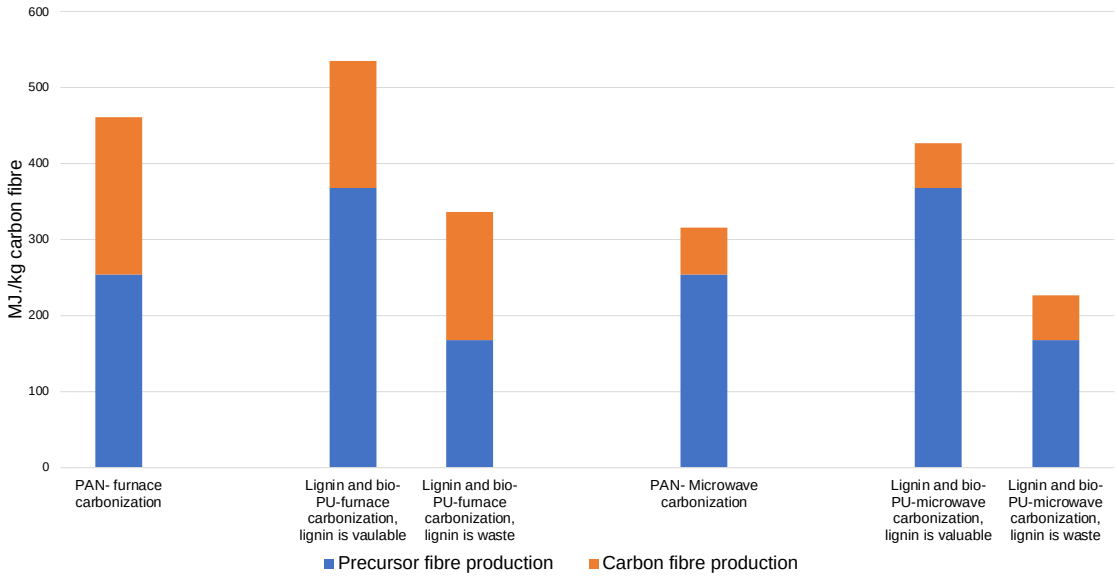

Figure 7.4 Energy demand for production of 1kg of CF using different carbonisation techniques (Conventional vs Microwave) and precursor materials (PAN vs lignin/TPU).

Using MW technology for CF production shows great potential to decrease the cumulative energy demand for both PAN and lignin/TPU fibres. It is predicted that application of MW heating reduces energy demand of CF production by up to 70%. Application of lignin/TPU blend reduces the energy consumption of PF production by up to 26% (if lignin is regarded as waste). This results in 47% reduction in cumulative energy demand if CF is produced via MW heating and from lignin/TPU precursor. Note that the energy use for the PAN-based fibres produced using MW technology consists of approximately 4% renewables, whereas the amount of renewable energy sources used when producing the lignin/TPU fibres using MW technology is between 10% and 44%.

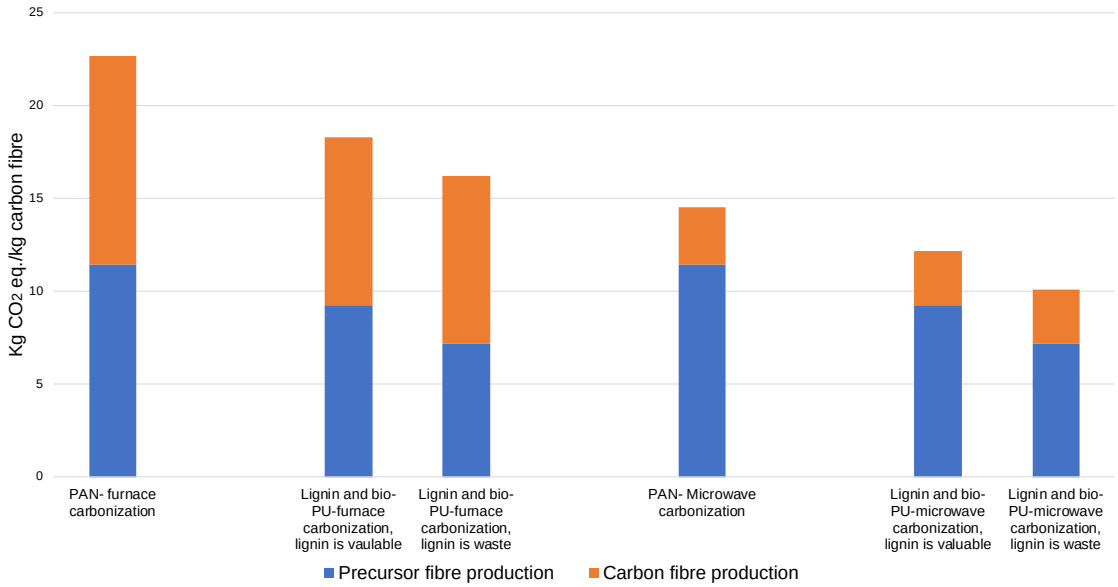

Figure 7.5 Environmental impact of production of 1kg of CF using different carbonisation methods (Conventional vs Microwave) and precursor materials (PAN vs lignin/TPU).

Results in Figure 7.5 show that the climate impact of the CFs production using a conventional furnace is significantly higher for PAN-based fibres compared to lignin-based fibres, despite lower carbon yield of the latter material. This is attributed to lower climate impact of the PF production. Furthermore, lignin's inherent properties in theory reduce the energy consumption in the CF production step by 25%. MW technology reduces CO_2 emission of CF production by up to 73%. Application of lignin/TPU blend reduces the climate impact of PF production by up to 37%. This results in 56% reduction in cumulative environmental impact if CF is produced via MW heating and from lignin/TPU precursor.

7.3 Alternative applications of microwave carbonisation

7.3.1 Introduction

In this section, susceptor assisted MW heating was applied for energy-efficient carbonisation of other materials, especially if the porosity induced by the high heating rates which is detrimental for CF production could be beneficial for other applications.

MW heating was applied for preparation of lignin-based porous materials: electrospun carbon nanofiber mats for bio-sensing as well as foams (derived from hydrogel) for structural or energy storage applications. Lignin-based hydrogels were prepared according to 3.7.1, as previously described by Culebras *et al.* [175]. In this case the

susceptor was applied before stabilisation to enable impregnation of the susceptor into the hydrogel. Prepared samples were carbonised in MW and characterised via SEM, TGA. Nanofibre mats were prepared according to 3.7.2, similarly to procedure described by Beaucamp *et al.* [176]. Nanofiber samples were coated with susceptor after stabilisation. Samples were then carbonised in MW and characterised via SEM.

7.3.2 Results

Heating profiles for high power MW carbonisation of lignin-based foam and nanofiber (NF) electrode are shown in Figure 7.6. Maximum temperatures of 542°C and 1028°C are recorded, respectively. The difference can be attributed to: (i) lower no. of LBL cycles; (ii) difficulty in susceptor impregnation of the foam sample; (iii) small geometry of the foam sample, which results in false temperature reading. Partial carbonisation of the foam sample is confirmed by a conversion rate of 74% (TGA). NF electrode was not analysed via TGA due to very low amount/weight of electrospun fibres.

SEM images of the carbonised foam and NF electrode are shown in Figure 7.7. It is observed that samples retain their overall structure after MW carbonisation, but the susceptor coating could influence the surface area of NF sample by bridging gaps between individual NFs (Figure 7.7 B).

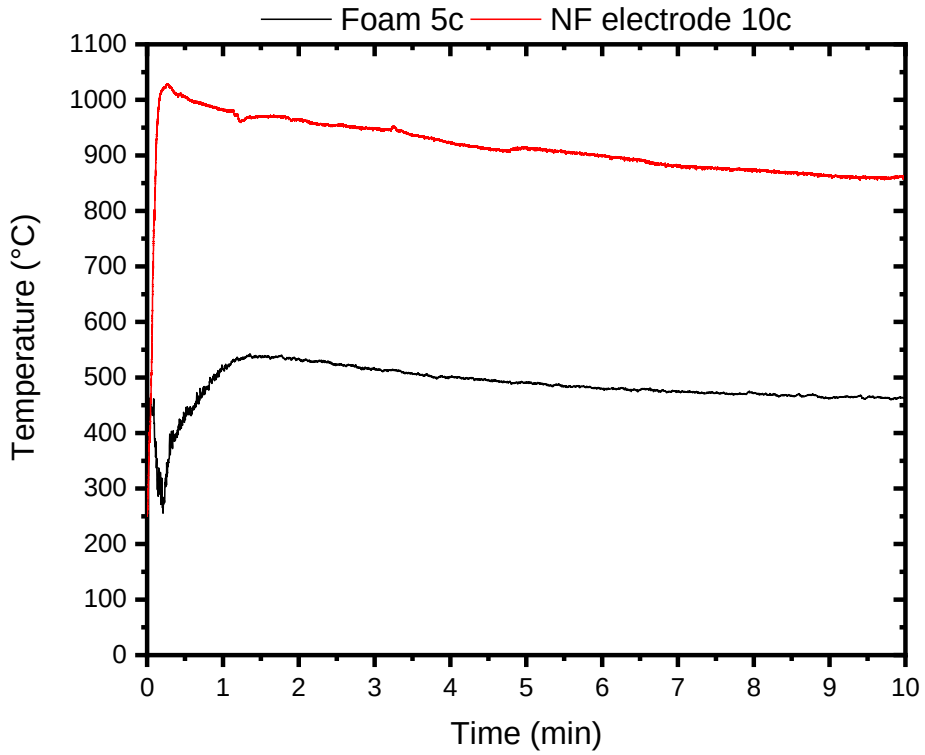

Figure 7.6 High power MW carbonisation of lignin-based foam and electrospun nanofiber (NF) electrode.

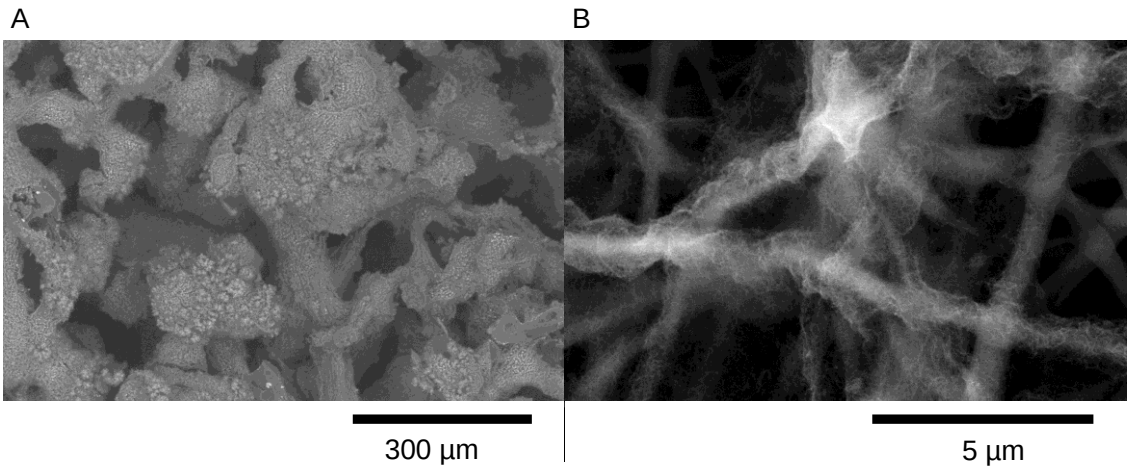

Figure 7.7 SEM images of other lignin-based materials: foam (A) and nanofibre electrode (B).

7.4 Conclusions

The following conclusions can be drawn from the results of each subsection:

1) Proposed coupled electromagnetic - heat transfer model predicts that MW heating rate and T_{max} increase with increasing thickness of susceptor (MWCNTs) and MW power. Predicted initial heating rate is inversely proportional to precursor fibre diameter due to decreased susceptor to fibre volume ratio. These results are in good agreement with data from previous chapters.
2) Life cycle assessment predicts that MW heating reduces the energy demand and environmental impact of CF production by up to 70 and 73%, recpectively. Application of lignin/TPU precursor (lignin considered as waste) is predicted to reduce energy consumption and climate impact of PF production by 26 and 37%, recpectively. Finally, MW carbonisation of lignin/TPU precursor is predicted to reduce the cumulative energy demand and environmental impact of CF production by 47 and 56%, respectively.
3) MW carbonisation can be successfully employed for rapid carbonisation of lignin-based materials for other advanced applications, but the application will determine its effectiveness.

Chapter 8

Conclusions and future work

Susceptor induced dielectric heating in MW is used for energy efficient carbonisation of PAN and lignin/TPU precursors. Produced CFs are characterised via SEM, TGA, RAMAN and tensile testing. The following conclusions can be drawn for MW carbonisation of PAN precursor:

1) MW carbonisation at high power (20 min) results in high heating rates and T_{max} of up to 1076°C. This results in creation of defects detected by SEM, probably due to differential shrinkage or evolution of volatiles during carbonisation at high heating rates. CFs produced via MW carbonisation from PAN precursor results in reduction of fibre diameter down to 6.35 μm, conversion rates (TGA) of up to 98%, L_a sizes (Raman) of up to 11.43 nm, TS of up to 1.18 GPa, YM of up to 160.7 GPa and strain of up to 1.31 %.

2) Carbonisation at progressive power levels (up to 36 min) results in reduction of initial heating rates, T_{max} temperatures and visible reduction of defect size and abundance at the expense of diameter reduction, conversion rate and L_a size. Reduction of heating rates through finer tuning of MW power is required to produce CF with mechanical properties comparable with conventional carbonisation. Further improvements could also be achieved via carbonisation under tension.

3) Coating samples before stabilisation results in lower T_{max} and consequently to lower conversion rate and L_a size, but produces CFs with superior mechanical properties. This is most likely due to the fusion/melting of the susceptor layer during stabilisation, which results in reduced efficiency in MW absorption. Coating samples after stabilisation results in higher T_{max}, conversion rate and L_a size. This should lead to improvement, but leads to deterioration of mechanical properties instead, probably due to more harsh conditions of carbonisation as suggested by defect-size (SEM). Furthermore, the susceptor layer applied after stabilisation may be more prone to damage during handling and by the volatile products of carbonisation, which may result in uneven heating, as suggested by temperature jumps recorded during MW carbonisation. Coating samples before

stabilisation appears to be more reliable procedure for MW carbonisation at high power, but the difference is less clear when progressive power is used.

4) Increasing the number of MW susceptor coating cycles generally improves absorption of MWs and increases T_{max}. These differences are reduced for carbonisation at progressive power levels and if coating is applied before stabilisation. Relatively high conversion rates achieved for CF coated with a single layer of susceptor (1c) lead to a conclusion that even finer tuning is required. This could be achieved by reduction of susceptor coating thickness or concentration of MWCNTs in suspension.

The following conclusions can be drawn for MW carbonisation of lignin/TPU precursor:

5) MW carbonisation at high power (10 min) results in high heating rates and T_{max} of up to 1044°C. This results in brittle CFs with high porosity observed through SEM. This is attributed to evolution of volatiles during carbonisation at high heating rates.

6) Carbonisation at progressive MW power levels (up to 40 min) results in T_{max} of up to 1346°C at the high power stage. This results in conversion rates (TGA) of up to 98.6%, L_a sizes (Raman) of up to 7.12 nm. Reduction of initial heating rates results in great improvement of morphology of fibres observed via SEM. Most importantly, the highest average values of TS, YM and strain of up to 0.33 GPa, 81 GPa and 0.57 % are recorded, respectively. This mechanical performance is comparable or superior to CFs produced via conventional method at temperature range of 1000-2000°C. Reduction of heating rate during intermediate stages (under 600-800°C) is required to ensure reliability of the process. Further improvements can be achieved via reduction of fibre diameter and carbonisation under tension.

7) Coating samples before stabilisation results in slightly lower T_{max}, but more reliable conversion rates and higher L_a sizes. This can be explained by the fusion/melting of the susceptor layer during stabilisation, which results in reduced efficiency in MW absorption and more durable susceptor layer. Coating samples after stabilisation results in more harsh conditions of carbonisation with highest T_{max} temperatures. Furthermore, the susceptor layer applied after

stabilisation may be more prone to damage during handling and carbonisation. This results in wider range of conditions, properties and could contribute to increased absorption of moisture after carbonisation.

8) Increasing the number of MW susceptor coating cycles generally improves absorption of MWs and increases T_{max} and enables fuller carbonisation to CF. The differences are reduced for MW carbonisation at progressive power levels and if coating is applied before stabilisation. This is probably due to averaging effects of these heat treatments on MW absortion efficiency. Even a single cycle of susceptor coating results in T_{max} of up to 1020°C, conversion rate of up to 93.3%, TS of up to 0.27 GPa, YM of up to 81 GPa and strain of up to 0.4%.

9) Higher diameter of lignin/TPU precursor reduces the ratio of the susceptor coating to the fibre volume. This results in highlighted effect of coating thickness observed for high power MW carbonisation. Furthermore, it allows easier optimisation of MW carbonisation leading to improvement of morphology and mechanical properties of CFs produced from lignin/TPU precursor.

Susceptor assisted dielectric heating is a promising alternative method for carbonisation of both PAN and lignin-based fibres. Comparison of CFs derived from both precursors using different power modes is shown in Figure 8.1. It is observed that reduction of initial heating rates results in improvement of morphology. Improvement of mechanical performance is achieved more easily for lignin/TPU, most likely due to fibre diameter difference. Improved control over MW power is expected to improve reliability of MW carbonisation of PAN and precursor fibres with smaller diameter in general.

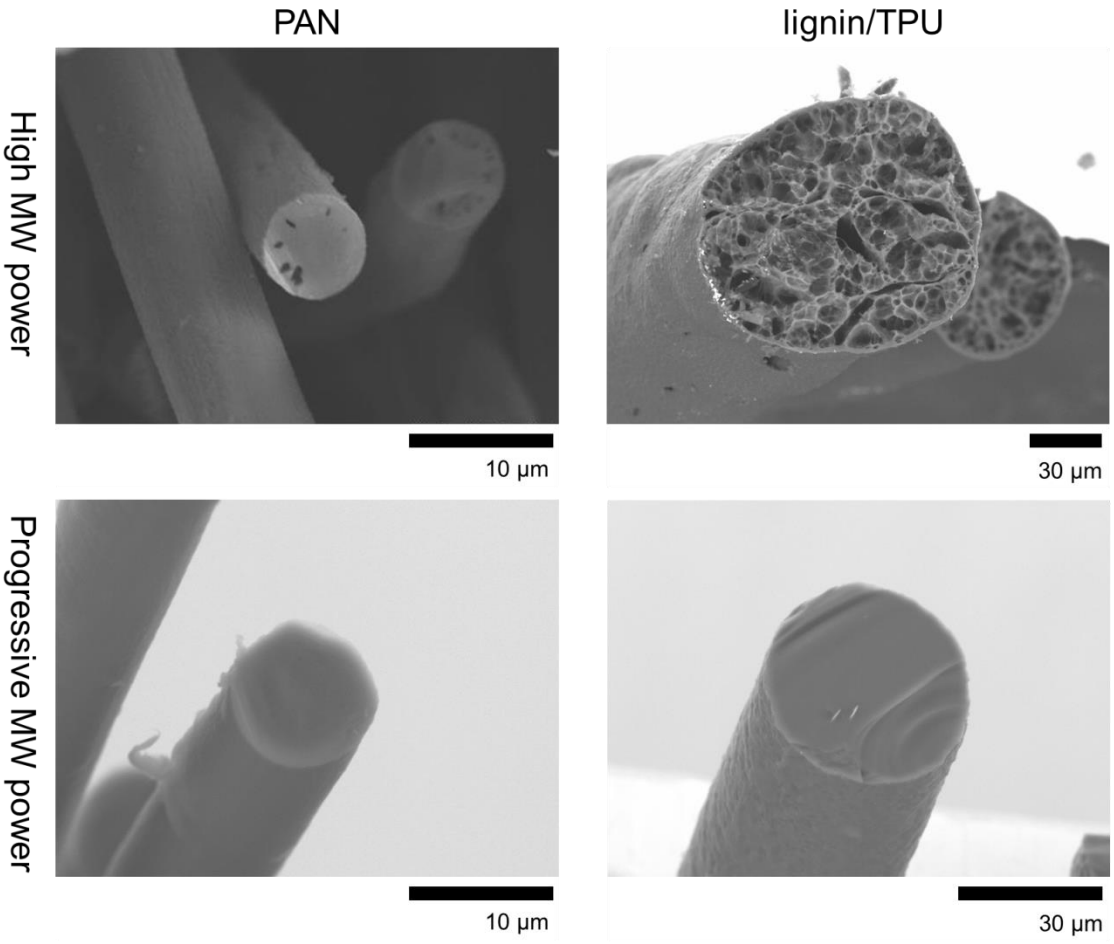

Figure 8.1 Comparison of cross-sections of fibres carbonised in MW using 5 cycles of susceptor coating. Samples coated before stabilisation, except for lignin/TPU at high MW power.

Further research may be required before successful application of MW carbonisation in industry:

1) Real-time tuning of MW power is required in order to achieve finer control over heating rates and ensure defect free CF. Reduction in coating thickness may be necessary, especially for precursor with smaller diameter.

2) CF production presented here including coating with susceptor, stabilisation and MW carbonisation operated on batch basis and involved manual handling of fibre samples. Small-scale continuous line can improve repeatability of the process and improve mechanical performance through proper tension control. This will also provide data for life cycle assessment of continuous MW carbonisation.

3) The effects of porosity/mesoporosity on mechanical properties can be systematically studied to find optimum MW heating conditions for CF with desired microstructure and properties.

4) In the future, the carbonisation chamber could be insulated to avoid overheating of equipment, prevent heat loss and reduce the cooling rate of CF.

5) Other LBL techniques and susceptors can be used to optimise MW heating. Once enough fibre is produced via MW heating, CF can be applied in CFRP. Especially, the effects of different susceptor coatings on the adhesion between fibres and the resin can be studied.

6) MW heating model can be improved by including of other heating mechanisms. Non-linear material properties can also be evaluated to improve model accuracy.

References

[1] P.K. Mallick, Fiber-reinforced composites: materials, manufacturing, and design, CRC press, 2007.

[2] N. Hu, ed., Composites and Their Applications, InTech, 2012. https://doi.org/10.5772/3353.

[3] P. Morgan, Carbon fibers and their composites, CRC press, 2005.

[4] D. Chung, Carbon fiber composites, Elsevier, 2012.

[5] Carbon Fiber Market Global Forecast to 2026 | MarketsandMarkets, (n.d.). https://www.marketsandmarkets.com/Market-Reports/carbon-fiber-396.html (accessed July 23, 2021).

[6] N. Hiremath, S. Young, H. Ghossein, D. Penumadu, U. Vaidya, M. Theodore, Low cost textile-grade carbon-fiber epoxy composites for automotive and wind energy applications, Compos. Part B Eng. 198 (2020) 108156. https://doi.org/10.1016/j.compositesb.2020.108156.

[7] A. Dér, N. Dilger, A. Kaluza, C. Creighton, S. Kara, R. Varley, C. Herrmann, S. Thiede, Modelling and analysis of the energy intensity in polyacrylonitrile (PAN) precursor and carbon fibre manufacturing, J. Clean. Prod. 303 (2021) 127105. https://doi.org/10.1016/j.jclepro.2021.127105.

[8] C.D. Warren, Low cost carbon fiber overview, Oak Ridge Natl. Lab. Oak Ridge Tenn. (2011).

[9] H. Mainka, O. Täger, E. Körner, L. Hilfert, S. Busse, F.T. Edelmann, A.S. Herrmann, Lignin – an alternative precursor for sustainable and cost-effective automotive carbon fiber, J. Mater. Res. Technol. 4 (2015) 283–296. https://doi.org/10.1016/j.jmrt.2015.03.004.

[10] J.W. Johnson, W. Potter, P.G. Rose, G. Scott, Stabilisation of polyacrylonitrile by oxidative transformation, Br. Polym. J. 4 (1972) 527–540. https://doi.org/10.1002/pi.4980040606.

[11] Z. Bashir, A critical review of the stabilisation of polyacrylonitrile, Carbon. 29 (1991) 1081–1090. https://doi.org/10.1016/0008-6223(91)90024-D.

[12] R.B. Mathur, O.P. Bahl, J. Mittal, A new approach to thermal stabilisation of PAN fibres, Carbon. 30 (1992) 657–663. https://doi.org/10.1016/0008-6223(92)90185-Y.

[13] B. Saha, G.C. Schatz, Carbonization in Polyacrylonitrile (PAN) Based Carbon Fibers Studied by ReaxFF Molecular Dynamics Simulations, J. Phys. Chem. B. 116 (2012) 4684–4692. https://doi.org/10.1021/jp300581b.

[14] L.E. Feher, M.K. Thumm, Microwave innovation for industrial composite fabrication-the HEPHAISTOS technology, IEEE Trans. Plasma Sci. 32 (2004) 73–79. https://doi.org/10.1109/TPS.2004.823983.

[15] M. Bhattacharya, T. Basak, A review on the susceptor assisted microwave processing of materials, Energy. 97 (2016) 306–338. https://doi.org/10.1016/j.energy.2015.11.034.

[16] National Research Council, Division on Engineering and Physical Sciences, National Materials Advisory Board, Commission on Engineering and Technical Systems, Committee on Microwave Processing of Materials: An Emerging Industrial Technology, Microwave Processing of Materials, National Academies Press, Washington, D.C., UNITED STATES, 1994. http://ebookcentral.proquest.com/lib/univlime-ebooks/detail.action?docID=3376372 (accessed July 26, 2021).

[17] E.T. Thostenson, T.-W. Chou, Microwave processing: fundamentals and applications, Compos. Part Appl. Sci. Manuf. 30 (1999) 1055–1071. https://doi.org/10.1016/S1359-835X(99)00020-2.
[18] Y.C. Kim, C.H. Kim, D.K. Kim, Effect of microwave heating on densification and α→ β phase transformation of silicon nitride, J. Eur. Ceram. Soc. 17 (1997) 1625–1630.
[19] S.A. Nightingale, H.K. Worner, D.P. Dunne, Microstructural Development during the Microwave Sintering of Yttria—Zirconia Ceramics, J. Am. Ceram. Soc. 80 (1997) 394–400. https://doi.org/10.1111/j.1151-2916.1997.tb02843.x.
[20] B. Ravi, P. Ramesh, K. Rao, Microwave assisted preparation and sintering of Al 2 O 3, ZrO 2 and their composites from metalorganics, J. Mater. Chem. 7 (1997) 2043–2048.
[21] C. Zhao, J. Vleugels, C. Groffils, P.J. Luypaert, O. Van Der Biest, Hybrid sintering with a tubular susceptor in a cylindrical single-mode microwave furnace, Acta Mater. 48 (2000) 3795–3801. https://doi.org/10.1016/S1359-6454(00)00160-9.
[22] A. Goldstein, R. Ruginets, Y. Geffen, Microwave sintering of amorphous silica powders, J. Mater. Sci. Lett. 16 (1997) 310–312.
[23] H.-K. Lee, K.-M. Kim, M.-K. Park, W.-H. Kang, Microwave-assisted sintering of amorphous powders, J. Korean Ceram. Soc. 48 (2011) 14–19.
[24] B. Soesatyo, A. Blicblau, E. Siores, Effect of rapid curing doped epoxy adhesive between two polycarbonate substrates on the bond tensile strength, J. Mater. Process. Technol. 89 (1999) 451–456.
[25] P.K. Bajpai, I. Singh, J. Madaan, Joining of natural fiber reinforced composites using microwave energy: Experimental and finite element study, Mater. Des. 35 (2012) 596–602.
[26] R.M. Anklekar, D.K. Agrawal, R. Roy, Microwave sintering and mechanical properties of PM copper steel, Powder Metall. 44 (2001) 355–362.
[27] R.D. Kotecha, S.M.L. Nai, M. Gupta, Development of Al and Al/Cu (composite/alloy) formulations with enhanced properties through microwave power variations during hybrid sintering, J. Phys. Appl. Phys. 41 (2008) 175401.
[28] B. Nanthakumar, C.A. Pickles, S. Kelebek, Microwave pretreatment of a double refractory gold ore, Miner. Eng. 20 (2007) 1109–1119.
[29] S.C. Fong, C.Y. Wang, T.H. Chang, T.S. Chin, Crystallization of amorphous Si film by microwave annealing with SiC susceptors, Appl. Phys. Lett. 94 (2009) 102104.
[30] S.C. Fong, H.W. Chao, T.H. Chang, H.J. Leu, I.S. Tsai, S.Y. Cheng, C.Y. Wang, T.S. Chin, Microwave-crystallization of amorphous silicon film using carbon-overcoat as susceptor, Thin Solid Films. 519 (2011) 4196–4200. https://doi.org/10.1016/j.tsf.2011.02.017.
[31] C. Ellison, M.S. McKeown, S. Trabelsi, D. Boldor, Dielectric Properties of Biomass/Biochar Mixtures at Microwave Frequencies, Energies. 10 (2017) 502. https://doi.org/10.3390/en10040502.
[32] A. Shindo, Report 317, Osaka Ind. Res. Inst. (1961).
[33] J. Johnson, L.N. Phillips, W. Watt, The production of carbon fibers, Br. Pat. 1 (1965) 874.
[34] Polyacrylonitrile, Wikipedia. (2021). https://en.wikipedia.org/w/index.php?title=Polyacrylonitrile&oldid=1041049973 (accessed September 21, 2021).
[35] D.A. Baker, T.G. Rials, Recent advances in low-cost carbon fiber manufacture from lignin, J. Appl. Polym. Sci. 130 (2013) 713–728. https://doi.org/10.1002/app.39273.

[36] E. Frank, L.M. Steudle, D. Ingildeev, J.M. Spörl, M.R. Buchmeiser, Carbon Fibers: Precursor Systems, Processing, Structure, and Properties, Angew. Chem. Int. Ed. 53 (2014) 5262–5298. https://doi.org/10.1002/anie.201306129.
[37] A.G. Dumanlı, A.H. Windle, Carbon fibres from cellulosic precursors: a review, J. Mater. Sci. 47 (2012) 4236–4250. https://doi.org/10.1007/s10853-011-6081-8.
[38] M. Culebras, A. Beaucamp, Y. Wang, M.M. Clauss, E. Frank, M.N. Collins, Biobased Structurally Compatible Polymer Blends Based on Lignin and Thermoplastic Elastomer Polyurethane as Carbon Fiber Precursors, ACS Sustain. Chem. Eng. 6 (2018) 8816–8825. https://doi.org/10.1021/acssuschemeng.8b01170.
[39] E. Frank, F. Hermanutz, M.R. Buchmeiser, Carbon Fibers: Precursors, Manufacturing, and Properties, Macromol. Mater. Eng. 297 (2012) 493–501. https://doi.org/10.1002/mame.201100406.
[40] R. Katahira, T.J. Elder, G.T. Beckham, Chapter 1. A Brief Introduction to Lignin Structure, in: G.T. Beckham (Ed.), Energy Environ. Ser., Royal Society of Chemistry, Cambridge, 2018: pp. 1–20. https://doi.org/10.1039/9781788010351-00001.
[41] J. Ralph, K. Lundquist, G. Brunow, F. Lu, H. Kim, P.F. Schatz, J.M. Marita, R.D. Hatfield, S.A. Ralph, J.H. Christensen, W. Boerjan, Lignins: Natural polymers from oxidative coupling of 4-hydroxyphenyl- propanoids, Phytochem. Rev. 3 (2004) 29–60. https://doi.org/10.1023/B:PHYT.0000047809.65444.a4.
[42] W. Boerjan, J. Ralph, M. Baucher, Lignin biosynthesis, Annu. Rev. Plant Biol. 54 (2003) 519–546.
[43] J.S. Lupoi, S. Singh, R. Parthasarathi, B.A. Simmons, R.J. Henry, Recent innovations in analytical methods for the qualitative and quantitative assessment of lignin, Renew. Sustain. Energy Rev. 49 (2015) 871–906. https://doi.org/10.1016/j.rser.2015.04.091.
[44] C.W. Dence, The Determination of Lignin, in: Methods Lignin Chem., Springer, Berlin, Heidelberg, 1992: pp. 33–61. https://doi.org/10.1007/978-3-642-74065-7_3.
[45] J.B. Sluiter, R.O. Ruiz, C.J. Scarlata, A.D. Sluiter, D.W. Templeton, Compositional Analysis of Lignocellulosic Feedstocks. 1. Review and Description of Methods, J. Agric. Food Chem. 58 (2010) 9043–9053. https://doi.org/10.1021/jf1008023.
[46] A.J. Ragauskas, G.T. Beckham, M.J. Biddy, R. Chandra, F. Chen, M.F. Davis, B.H. Davison, R.A. Dixon, P. Gilna, M. Keller, P. Langan, A.K. Naskar, J.N. Saddler, T.J. Tschaplinski, G.A. Tuskan, C.E. Wyman, Lignin Valorization: Improving Lignin Processing in the Biorefinery, Science. 344 (2014) 1246843–1246843. https://doi.org/10.1126/science.1246843.
[47] S. Constant, H.L. J. Wienk, A. E. Frissen, P. de Peinder, R. Boelens, D.S. van Es, R.J. H. Grisel, B. M. Weckhuysen, W.J. J. Huijgen, R.J. A. Gosselink, P.C. A. Bruijnincx, New insights into the structure and composition of technical lignins: a comparative characterisation study, Green Chem. 18 (2016) 2651–2665. https://doi.org/10.1039/C5GC03043A.
[48] R. Rinaldi, R. Jastrzebski, M.T. Clough, J. Ralph, M. Kennema, P.C.A. Bruijnincx, B.M. Weckhuysen, Paving the Way for Lignin Valorisation: Recent Advances in Bioengineering, Biorefining and Catalysis, Angew. Chem. Int. Ed. 55 (2016) 8164–8215. https://doi.org/10.1002/anie.201510351.
[49] M.N. Collins, M. Nechifor, F. Tanasă, M. Zănoagă, A. McLoughlin, M.A. Stróżyk, M. Culebras, C.-A. Teacă, Valorization of lignin in polymer and composite systems for advanced engineering applications – A review, Int. J. Biol. Macromol. 131 (2019) 828–849. https://doi.org/10.1016/j.ijbiomac.2019.03.069.

[50] Q. Li, W.K. Serem, W. Dai, Y. Yue, M.T. Naik, S. Xie, P. Karki, L. Liu, H.-J. Sue, H. Liang, F. Zhou, J.S. Yuan, Molecular weight and uniformity define the mechanical performance of lignin-based carbon fiber, J. Mater. Chem. A. 5 (2017) 12740–12746. https://doi.org/10.1039/c7ta01187c.
[51] M. Culebras, H. Geaney, A. Beaucamp, P. Upadhyaya, E. Dalton, K.M. Ryan, M.N. Collins, Bio-derived Carbon Nanofibres from Lignin as High-Performance Li-Ion Anode Materials, ChemSusChem. (2019). https://doi.org/10.1002/cssc.201901562.
[52] S.Y. Park, J.-Y. Kim, H.J. Youn, J.W. Choi, Fractionation of lignin macromolecules by sequential organic solvents systems and their characterization for further valuable applications, Int. J. Biol. Macromol. 106 (2018) 793–802. https://doi.org/10.1016/j.ijbiomac.2017.08.069.
[53] V.K. Thakur, M.K. Thakur, Recent advances in green hydrogels from lignin: a review, Int. J. Biol. Macromol. 72 (2015) 834–847. https://doi.org/10.1016/j.ijbiomac.2014.09.044.
[54] Q. Yin, W. Yang, C. Sun, M. Di, PREPARATION AND PROPERTIES OF LIGNIN-EPOXY RESIN COMPOSITE, BioResources. 7 (2012). https://doi.org/10.15376/biores.7.4.5737-5748.
[55] H.R. Mansouri, P. Navarrete, A. Pizzi, S. Tapin-Lingua, B. Benjelloun-Mlayah, H. Pasch, S. Rigolet, Synthetic-resin-free wood panel adhesives from mixed low molecular mass lignin and tannin, Eur. J. Wood Wood Prod. 69 (2010) 221–229. https://doi.org/10.1007/s00107-010-0423-0.
[56] J.L. Espinoza-Acosta, P.I. Torres-Chávez, B. Ramírez-Wong, C.M. López-Saiz, B. Montaño-Leyva, Antioxidant, Antimicrobial, and Antimutagenic Properties of Technical Lignins and Their Applications, BioResources. 11 (2016). https://doi.org/10.15376/biores.11.2.
[57] M. Culebras, M.J. Sanchis, A. Beaucamp, M. Carsí, B.K. Kandola, A.R. Horrocks, G. Panzetti, C. Birkinshaw, M.N. Collins, Understanding the thermal and dielectric response of organosolv and modified kraft lignin as a carbon fibre precursor, Green Chem. 20 (2018) 4461–4472. https://doi.org/10.1039/C8GC01577E.
[58] W. Qu, J. Yang, X. Sun, X. Bai, H. Jin, M. Zhang, Towards producing high-quality lignin-based carbon fibers: A review of crucial factors affecting lignin properties and conversion techniques, Int. J. Biol. Macromol. 189 (2021) 768–784. https://doi.org/10.1016/j.ijbiomac.2021.08.187.
[59] Y. Imura, R.M.C. Hogan, M. Jaffe, 10 - Dry spinning of synthetic polymer fibers, in: D. Zhang (Ed.), Adv. Filam. Yarn Spinn. Text. Polym., Woodhead Publishing, 2014: pp. 187–202. https://doi.org/10.1533/9780857099174.2.187.
[60] M.G. Dunham, D.D. Edie, Model of stabilization for pan-based carbon fiber precursor bundles, Carbon. 30 (1992) 435–450. https://doi.org/10.1016/0008-6223(92)90042-U.
[61] D.A. Grove, A.S. Abhiraman, A mathematical model of solid-state thermo-oxidative stabilization of acrylic fibers, Carbon. 30 (1992) 451–457. https://doi.org/10.1016/0008-6223(92)90043-V.
[62] S. Nunna, M. Maghe, S.M. Fakhrhoseini, B. Polisetti, M. Naebe, A Pathway to Reduce Energy Consumption in the Thermal Stabilization Process of Carbon Fiber Production, Energies. 11 (2018) 1145. https://doi.org/10.3390/en11051145.
[63] H. Khayyam, R.N. Jazar, S. Nunna, G. Golkarnarenji, K. Badii, S.M. Fakhrhoseini, S. Kumar, M. Naebe, PAN precursor fabrication, applications and thermal stabilization process in carbon fiber production: Experimental and mathematical modelling, Prog. Mater. Sci. 107 (2020) 100575. https://doi.org/10.1016/j.pmatsci.2019.100575.

[64] H. Khayyam, M. Naebe, A. Bab-Hadiashar, F. Jamshidi, Q. Li, S. Atkiss, D. Buckmaster, B. Fox, Stochastic optimization models for energy management in carbonization process of carbon fiber production, Appl. Energy. 158 (2015) 643–655. https://doi.org/10.1016/j.apenergy.2015.08.008.
[65] G. Golkarnarenji, M. Naebe, K. Badii, A.S. Milani, A. Jamali, A. Bab-Hadiashar, R.N. Jazar, H. Khayyam, Multi-Objective Optimization of Manufacturing Process in Carbon Fiber Industry Using Artificial Intelligence Techniques, IEEE Access. 7 (2019) 67576–67588. https://doi.org/10.1109/ACCESS.2019.2914697.
[66] G. Golkarnarenji, M. Naebe, K. Badii, A.S. Milani, R.N. Jazar, H. Khayyam, Production of Low Cost Carbon-Fiber through Energy Optimization of Stabilization Process, Materials. 11 (2018) 385. https://doi.org/10.3390/ma11030385.
[67] N. Shirolkar, P. Patwardhan, A. Rahman, A. Spear, S. Kumar, Investigating the efficacy of machine learning tools in modeling the continuous stabilization and carbonization process and predicting carbon fiber properties, Carbon. 174 (2021) 605–616. https://doi.org/10.1016/j.carbon.2020.12.044.
[68] J. Dietrich, P. Hirt, H. Herlinger, Electron-beam-induced cyclisation to obtain C-fibre precursors from polyacrylonitrile homopolymers, Eur. Polym. J. 32 (1996) 617–623. https://doi.org/10.1016/0014-3057(95)00185-9.
[69] P. Miao, D. Wu, K. Zeng, G. Xu, C. Zhao, G. Yang, Influence of electron beam pre-irradiation on the thermal behaviors of polyacrylonitrile, Polym. Degrad. Stab. 95 (2010) 1665–1671. https://doi.org/10.1016/j.polymdegradstab.2010.05.028.
[70] H. Yuan, Y. Wang, P. Liu, H. Yu, B. Ge, Y. Mei, Effect of electron beam irradiation on polyacrylonitrile precursor fibers and stabilization process, J. Appl. Polym. Sci. 122 (2011) 90–96. https://doi.org/10.1002/app.33908.
[71] D.K. Seo, J.P. Jeun, H.B. Kim, P.H. Kang, Preparation and characterization of the carbon nanofiber mat produced from electrospun PAN/lignin precursors by electron beam irradiation, Rev Adv Mater Sci. 28 (2011) 31–34.
[72] H. Yu, H. Yuan, Y. Wang, Z. Wei, G. Xia, Effect of different doses of electron beam irradiation on the structure of PAN precursor fibers and resultant stabilized fibers, J. Wuhan Univ. Technol.-Mater Sci Ed. 28 (2013) 574–579.
[73] S. Park, S.H. Yoo, H.R. Kang, S.M. Jo, H.-I. Joh, S. Lee, Comprehensive stabilization mechanism of electron-beam irradiated polyacrylonitrile fibers to shorten the conventional thermal treatment, Sci. Rep. 6 (2016) 27330. https://doi.org/10.1038/srep27330.
[74] S.H. Yoo, S. Park, Y. Park, D. Lee, H.-I. Joh, I. Shin, S. Lee, Facile method to fabricate carbon fibers from textile-grade polyacrylonitrile fibers based on electron-beam irradiation and its effect on the subsequent thermal stabilization process, Carbon. 118 (2017) 106–113. https://doi.org/10.1016/j.carbon.2017.03.039.
[75] W. Zhang, M. Wang, W. Zhang, W. Liu, C. Yang, R. Shen, G. Wu, Significantly reduced pre-oxidation period of PAN fibers by continuous electron beam irradiation: Optimization by monitoring radical variation, Polym. Degrad. Stab. 158 (2018) 72–82. https://doi.org/10.1016/j.polymdegradstab.2018.10.027.
[76] U. Gohs, R. Böhm, H. Brünig, D. Fischer, L. Häussler, M. Kirsten, M. Malanin, M.-T. Müller, C. Cherif, D.S.J. Wolz, H. Jäger, Electron beam treatment of polyacrylonitrile copolymer above the glass transition temperature in air and nitrogen atmosphere, Radiat. Phys. Chem. 156 (2019) 22–30. https://doi.org/10.1016/j.radphyschem.2018.10.012.
[77] B.M. Tarakanov, Effect of γ-radiation on the structure and thermal properties of polyacrylonitrile fibres, Fibre Chem. 27 (1996) 150–154.

[78] W. Zhao, Y. Yamamoto, S. Tagawa, Regulation of the Thermal Reactions of Polyacrylonitrile by γ-Irradiation, Chem. Mater. 11 (1999) 1030–1034. https://doi.org/10.1021/cm9806836.
[79] W. Liu, M. Wang, Z. Xing, Y. Qi, G. Wu, Radiation-induced crosslinking of polyacrylonitrile fibers and the subsequent regulative effect on the preoxidation process, Radiat. Phys. Chem. 81 (2012) 622–627. https://doi.org/10.1016/j.radphyschem.2012.02.029.
[80] W. Liu, M. Wang, Z. Xing, G. Wu, Radiation oxidation and subsequent thermal curing of polyacrylonitrile fiber, Radiat. Phys. Chem. 94 (2014) 9–13. https://doi.org/10.1016/j.radphyschem.2013.06.015.
[81] W. Zhao, Y. Lu, J. Wang, Q. Chen, L. Zhou, J. Jiang, L. Chen, Improving crosslinking of stabilized polyacrylonitrile fibers and mechanical properties of carbon fibers by irradiating with γ-ray, Polym. Degrad. Stab. 133 (2016) 16–26. https://doi.org/10.1016/j.polymdegradstab.2016.07.018.
[82] W. Zhao, Y. Lu, L. Zhou, J. Jiang, J. Wang, Q. Chen, F. Tian, Effects on the oriented structure and mechanical properties of carbon fibers by pre-irradiating polyacrylonitrile fibers with γ ray, J. Mater. Sci. 51 (2016) 7073–7084. https://doi.org/10.1007/s10853-016-9875-x.
[83] L. Zhou, Y. Lu, W. Zhao, C. Yang, J. Jiang, Effects of gamma ray irradiation on poly(acrylonitrile-co-methyl acrylate) fibers, Polym. Degrad. Stab. 128 (2016) 149–157. https://doi.org/10.1016/j.polymdegradstab.2015.12.015.
[84] A.K. Naskar, R.A. Walker, S. Proulx, D.D. Edie, A.A. Ogale, UV assisted stabilization routes for carbon fiber precursors produced from melt-processible polyacrylonitrile terpolymer, Carbon. 43 (2005) 1065–1072. https://doi.org/10.1016/j.carbon.2004.11.047.
[85] H. Yuan, Y. Wang, H. Yu, Z. Wei, B. Ge, Y. Mei, Effect of UV irradiation on PAN precursor fibers and stabilization process, J. Wuhan Univ. Technol.-Mater Sci Ed. 26 (2011) 449–454. https://doi.org/10.1007/s11595-011-0247-8.
[86] H. Xu, Y. Sun, X. Chen, Microstructure characterization of PAN preoxidation fibers prepared with radio frequency plasma, Chin. Sci. Bull. 51 (2006) 1255–1260. https://doi.org/10.1007/s11434-006-1255-5.
[87] S.-W. Lee, H.-Y. Lee, S.-Y. Jang, S. Jo, H.-S. Lee, W.-H. Choe, S. Lee, Efficient preparation of carbon fibers using plasma assisted stabilization, Carbon. 55 (2013) 361–365. https://doi.org/10.1016/j.carbon.2012.10.062.
[88] S.-Y. Kim, S. Lee, S. Park, S.M. Jo, H.-S. Lee, H.-I. Joh, Continuous and rapid stabilization of polyacrylonitrile fiber bundles assisted by atmospheric pressure plasma for fabricating large-tow carbon fibers, Carbon. 94 (2015) 412–416. https://doi.org/10.1016/j.carbon.2015.07.012.
[89] S. Park, H.-S. Kil, D. Choi, S.-K. Song, S. Lee, Rapid stabilization of polyacrylonitrile fibers achieved by plasma-assisted thermal treatment on electron-beam irradiated fibers, J. Ind. Eng. Chem. 69 (2019) 449–454. https://doi.org/10.1016/j.jiec.2018.10.008.
[90] T.H.H. Elagib, E.A.M. Hassan, B. Liu, K. Han, M. Yu, Evaluation of composite PAN fibers incorporated with carbon nanotubes and titania and their performance during the microwave-induced pre-oxidation, Carbon Lett. 30 (2020) 235–245. https://doi.org/10.1007/s42823-019-00092-2.
[91] G. Zhao, J. Liu, L. Xu, S. Guo, Comparative study of conventional and microwave heating of polyacrylonitrile-based fibres, J. Polym. Eng. 41 (2021) 175–183. https://doi.org/10.1515/polyeng-2020-0167.
[92] C. Wang, H. Liu, L. Song, J. Tan, W. Yang, L. Cheng, Temperature evolution, atomistic hot-spot effects and thermal runaway during microwave heating of polyacrylonitrile: A ReaxFF molecular dynamics simulation, Nano Sel. (2021).

[93] T.L. White, F.L. Paulauskas, T.S. Bigelow, United States Patent: 8679592 - System to continuously produce carbon fiber via microwave assisted plasma processing, 8679592, 2014. https://patft.uspto.gov/netacgi/nph-Parser?Sect1=PTO1&Sect2=HITOFF&d=PALL&p=1&u=%2Fnetahtml%2FPTO%2Fsrchnum.htm&r=1&f=G&l=50&s1=8679592.PN.&OS=PN/8679592&RS=PN/8679592 (accessed July 23, 2021).
[94] S.Y. Kim, S.-Y. Kim, J. Choi, S. Lee, S.M. Jo, J. Joo, H.-S. Lee, Two step microwave plasma carbonization including low plasma power pre-carbonization for polyacrylonitrile based carbon fiber, Polymer. 69 (2015) 123–128. https://doi.org/10.1016/j.polymer.2015.05.040.
[95] S.-Y. Kim, S.Y. Kim, S. Lee, S. Jo, Y.-H. Im, H.-S. Lee, Microwave plasma carbonization for the fabrication of polyacrylonitrile-based carbon fiber, Polymer. 56 (2015) 590–595. https://doi.org/10.1016/j.polymer.2014.11.034.
[96] R.E. Norris, Jr, M.C. Kaufman, A.K. Naskar, F.L. Paulauskas, K.D. Yarborough, Development and Commercialization of Alternative Carbon Fiber Precursors and Conversion Technologies, 2014. https://doi.org/10.2172/1158746.
[97] S. Jin, C. Guo, Y. Lu, R. Zhang, Z. Wang, M. Jin, Comparison of microwave and conventional heating methods in carbonization of polyacrylonitrile-based stabilized fibers at different temperature measured by an in-situ process temperature control ring, Polym. Degrad. Stab. 140 (2017) 32–41. https://doi.org/10.1016/j.polymdegradstab.2017.04.002.
[98] J.H. Cho, M. Jang, I. Lee, J.W. Lee, S. Kim, K.H. Kim, Precusor fiber for preparing carbon fiber, preparation method for producing the same and preparation method of carbon fiber, KR20180110643A, 2018. https://patents.google.com/patent/KR20180110643A/en (accessed October 9, 2021).
[99] S.S. Lam, E. Azwar, W. Peng, Y.F. Tsang, N.L. Ma, Z. Liu, Y.-K. Park, E.E. Kwon, Cleaner conversion of bamboo into carbon fibre with favourable physicochemical and capacitive properties via microwave pyrolysis combining with solvent extraction and chemical impregnation, J. Clean. Prod. 236 (2019) 117692. https://doi.org/10.1016/j.jclepro.2019.117692.
[100] N.H. Williams, Curing Epoxy Resin Impregnates Pipe at 2450 Megahertz, J. Microw. Power. 2 (1967) 123–127.
[101] W.I. Lee, G.S. Springer, Microwave Curing of Composites, J. Compos. Mater. 18 (1984) 387–409. https://doi.org/10.1177/002199838401800405.
[102] E.T. Thostenson, T.-W. Chou, Microwave and conventional curing of thick-section thermoset composite laminates: Experiment and simulation, Polym. Compos. 22 (2001) 197–212. https://doi.org/10.1002/pc.10531.
[103] C. Nightingale, R.J. Day, Flexural and interlaminar shear strength properties of carbon fibre/epoxy composites cured thermally and with microwave radiation, Compos. Part Appl. Sci. Manuf. 33 (2002) 1021–1030. https://doi.org/10.1016/S1359-835X(02)00031-3.
[104] M. Kwak, P. Robinson, A. Bismarck, R. Wise, U. Middlesbrough, Curing of composite materials using the recently developed Hephaistos Microwave, 18th Int. Conf. Compos. Mater. (2011) 1–6.
[105] M. Kwak, P. Robinson, A. Bismarck, R. Wise, Microwave curing of carbon–epoxy composites: Penetration depth and material characterisation, Compos. Part Appl. Sci. Manuf. 75 (2015) 18–27. https://doi.org/10.1016/j.compositesa.2015.04.007.
[106] N. Li, Y. Li, X. Hang, J. Gao, Analysis and optimization of temperature distribution in carbon fiber reinforced composite materials during microwave

curing process, J. Mater. Process. Technol. 214 (2014) 544–550. https://doi.org/10.1016/j.jmatprotec.2013.10.012.
[107] N. Li, Y. Li, J. Jelonnek, G. Link, J. Gao, A new process control method for microwave curing of carbon fibre reinforced composites in aerospace applications, Compos. Part B Eng. 122 (2017) 61–70. https://doi.org/10.1016/j.compositesb.2017.04.009.
[108] X. Xu, X. Wang, Q. Cai, X. Wang, R. Wei, S. Du, Improvement of the Compressive Strength of Carbon Fiber/Epoxy Composites via Microwave Curing, J. Mater. Sci. Technol. 32 (2016) 226–232. https://doi.org/10.1016/j.jmst.2015.10.006.
[109] J. Zhang, Y. Duan, B. Wang, X. Zhang, Interfacial enhancement for carbon fibre reinforced electron beam cured polymer composite by microwave irradiation, Polymer. 192 (2020) 122327. https://doi.org/10.1016/j.polymer.2020.122327.
[110] C.O. Mgbemena, D. Li, M.-F. Lin, P.D. Liddel, K.B. Katnam, V.K. Thakur, H.Y. Nezhad, Accelerated microwave curing of fibre-reinforced thermoset polymer composites for structural applications: A review of scientific challenges, Compos. Part Appl. Sci. Manuf. 115 (2018) 88–103. https://doi.org/10.1016/j.compositesa.2018.09.012.
[111] J. Galos, Microwave processing of carbon fibre polymer composites: a review, Polym. Polym. Compos. 29 (2021) 151–162. https://doi.org/10.1177/0967391120903894.
[112] Z. Li, P. Wang, A. Haigh, C. Soutis, A. Gibson, Review of microwave techniques used in the manufacture and fault detection of aircraft composites, Aeronaut. J. 125 (2021) 151–179. https://doi.org/10.1017/aer.2020.91.
[113] O. Zabihi, M. Ahmadi, C. Liu, R. Mahmoodi, Q. Li, M. Naebe, Development of a low cost and green microwave assisted approach towards the circular carbon fibre composites, Compos. Part B Eng. 184 (2020) 107750. https://doi.org/10.1016/j.compositesb.2020.107750.
[114] S. Karuppannan Gopalraj, T. Kärki, A review on the recycling of waste carbon fibre/glass fibre-reinforced composites: fibre recovery, properties and life-cycle analysis, SN Appl. Sci. 2 (2020) 433. https://doi.org/10.1007/s42452-020-2195-4.
[115] J. Zhang, V.S. Chevali, H. Wang, C.-H. Wang, Current status of carbon fibre and carbon fibre composites recycling, Compos. Part B Eng. 193 (2020) 108053. https://doi.org/10.1016/j.compositesb.2020.108053.
[116] A. Wadhawan, D. Garrett, J.M. Pérez, Nanoparticle-assisted microwave absorption by single-wall carbon nanotubes, Appl. Phys. Lett. 83 (2003) 2683–2685.
[117] P.-C. Ma, N.A. Siddiqui, G. Marom, J.-K. Kim, Dispersion and functionalization of carbon nanotubes for polymer-based nanocomposites: A review, Compos. Part Appl. Sci. Manuf. 41 (2010) 1345–1367. https://doi.org/10.1016/j.compositesa.2010.07.003.
[118] F. Wen, F. Zhang, Z. Liu, Investigation on microwave absorption properties for multiwalled carbon nanotubes/Fe/Co/Ni nanopowders as lightweight absorbers, J. Phys. Chem. C. 115 (2011) 14025–14030.
[119] L. Wang, B. Wen, X. Bai, C. Liu, H. Yang, NiCo alloy/carbon nanorods decorated with carbon nanotubes for microwave absorption, ACS Appl. Nano Mater. 2 (2019) 7827–7838.
[120] E.T. Thostenson, W.Z. Li, D.Z. Wang, Z.F. Ren, T.W. Chou, Carbon nanotube/carbon fiber hybrid multiscale composites, J. Appl. Phys. 91 (2002) 6034–6037. https://doi.org/10.1063/1.1466880.
[121] R.B. Mathur, S. Chatterjee, B.P. Singh, Growth of carbon nanotubes on carbon fibre substrates to produce hybrid/phenolic composites with improved mechanical

properties, Compos. Sci. Technol. 68 (2008) 1608–1615. https://doi.org/10.1016/j.compscitech.2008.02.020.
[122] K. Naito, J.-M. Yang, Y. Tanaka, Y. Kagawa, Tensile properties of carbon nanotubes grown on ultrahigh strength polyacrylonitrile-based and ultrahigh modulus pitch-based carbon fibers, Appl. Phys. Lett. 92 (2008) 231912. https://doi.org/10.1063/1.2944258.
[123] T.R. Pozegic, I. Hamerton, J.V. Anguita, W. Tang, P. Ballocchi, P. Jenkins, S.R.P. Silva, Low temperature growth of carbon nanotubes on carbon fibre to create a highly networked fuzzy fibre reinforced composite with superior electrical conductivity, Carbon. 74 (2014) 319–328. https://doi.org/10.1016/j.carbon.2014.03.038.
[124] E. Detsri, S.T. Dubas, Layer-by-layer deposition of cationic and anionic carbon nanotubes into thin films with improved electrical properties, Colloids Surf. Physicochem. Eng. Asp. 444 (2014) 89–94. https://doi.org/10.1016/j.colsurfa.2013.12.040.
[125] A. Pavinatto, L.A. Mercante, C.S. Leandro, L.H.C. Mattoso, D.S. Correa, Layer-by-Layer assembled films of chitosan and multi-walled carbon nanotubes for the electrochemical detection of 17α-ethinylestradiol, J. Electroanal. Chem. 755 (2015) 215–220. https://doi.org/10.1016/j.jelechem.2015.08.002.
[126] L. Xi, D. Zhang, F. Wang, Z. Huang, T. Ni, Layer-by-layer assembly of poly(p-aminobenzene sulfonic acid)/quaternary amine functionalized carbon nanotube/p-aminobenzene sulfonic acid composite film on glassy carbon electrode for the determination of ascorbic acid, J. Electroanal. Chem. 767 (2016) 91–99. https://doi.org/10.1016/j.jelechem.2016.01.015.
[127] M. Culebras, C. Cho, M. Krecker, R. Smith, Y. Song, C.M. Gómez, A. Cantarero, J.C. Grunlan, High Thermoelectric Power Factor Organic Thin Films through Combination of Nanotube Multilayer Assembly and Electrochemical Polymerization, ACS Appl. Mater. Interfaces. 9 (2017) 6306–6313. https://doi.org/10.1021/acsami.6b15327.
[128] F. Qin, C. Brosseau, A Review and Analysis of Microwave Absorption in Polymer Composites Filled with Carbonaceous Particles, J. Appl. Phys. 111 (2012) 061301–24. https://doi.org/10.1063/1.3688435.
[129] F.S. Baker, N.C. Gallego, D.A. Baker, Low cost carbon fiber from renewable resources, EERE US Dept Energy Proj. ID Lm03baker. (2010).
[130] A. Beaucamp, Y. Wang, M. Culebras, M.N. Collins, Carbon fibres from renewable resources: the role of the lignin molecular structure in its blendability with biobased poly(ethylene terephthalate), Green Chem. 21 (2019) 5063–5072. https://doi.org/10.1039/C9GC02041A.
[131] M. Zieglowski, S. Trosien, J. Rohrer, S. Mehlhase, S. Weber, K. Bartels, G. Siegert, T. Trellenkamp, K. Albe, M. Biesalski, Reactivity of Isocyanate-Functionalized Lignins: A Key Factor for the Preparation of Lignin-Based Polyurethanes, Front. Chem. 7 (2019) 562. https://doi.org/10.3389/fchem.2019.00562.
[132] E. Delebecq, J.-P. Pascault, B. Boutevin, F. Ganachaud, On the Versatility of Urethane/Urea Bonds: Reversibility, Blocked Isocyanate, and Non-isocyanate Polyurethane, Chem. Rev. 113 (2013) 80–118. https://doi.org/10.1021/cr300195n.
[133] C.A. Balanis, Advanced engineering electromagnetics, John Wiley & Sons, 1999.
[134] M. Gupta, E.W.W. Leong, Microwaves and Metals, John Wiley & Sons, 2008.
[135] Y. Sekii, T. Hayashi, Measurements of Reflectance and Thermal Emissivity of a Black Surface Created by Electrostatic Flocking with Carbon-Fiber Piles, IEEE

Trans. Dielectr. Electr. Insul. 16 (2009) 649–654. https://doi.org/10.1109/TDEI.2009.5128501.
[136] F. Wang, L. Cheng, Q. Zhang, L. Zhang, Effects of heat treatment and coatings on the infrared emissivity properties of carbon fibers, J. Mater. Res. 29 (2014) 1162–1167. https://doi.org/10.1557/jmr.2014.106.
[137] F. Tuinstra, J.L. Koenig, Raman Spectrum of Graphite, J. Chem. Phys. 53 (1970) 1126–1130. https://doi.org/10.1063/1.1674108.
[138] L.G. Cançado, K. Takai, T. Enoki, M. Endo, Y.A. Kim, H. Mizusaki, A. Jorio, L.N. Coelho, R. Magalhães-Paniago, M.A. Pimenta, General equation for the determination of the crystallite size La of nanographite by Raman spectroscopy, Appl. Phys. Lett. 88 (2006) 163106. https://doi.org/10.1063/1.2196057.
[139] L.J. van der Pauw, A method of measuring the resistivity and Hall coefficient on lamellae of arbitrary shape, Philips Tech. Rev. 20 (1958) 220–224.
[140] R. Asmatulu, Highly Hydrophilic Electrospun Polyacrylonitrile/ Polyvinypyrrolidone Nanofibers Incorporated with Gentamicin as Filter Medium for Dam Water and Wastewater Treatment, J. Membr. Sep. Technol. 5 (2016) 38–56. https://doi.org/10.6000/1929-6037.2016.05.02.1.
[141] N.G. Sahoo, S. Rana, J.W. Cho, L. Li, S.H. Chan, Polymer nanocomposites based on functionalized carbon nanotubes, Prog. Polym. Sci. 35 (2010) 837–867. https://doi.org/10.1016/j.progpolymsci.2010.03.002.
[142] C. Cho, B. Stevens, J.-H. Hsu, R. Bureau, D.A. Hagen, O. Regev, C. Yu, J.C. Grunlan, Completely Organic Multilayer Thin Film with Thermoelectric Power Factor Rivaling Inorganic Tellurides, Adv. Mater. 27 (2015) 2996–3001. https://doi.org/10.1002/adma.201405738.
[143] C. Cho, Y. Song, J.-H. Hsu, C. Yu, D.L. Stevens, J.C. Grunlan, Organic thermoelectric thin films with large p-type and n-type power factor, J. Mater. Sci. 56 (2021) 4291–4304. https://doi.org/10.1007/s10853-020-05520-7.
[144] X. Liu, X. Quan, L. Bo, S. Chen, Y. Zhao, M. Chang, Temperature measurement of GAC and decomposition of PCP loaded on GAC and GAC-supported copper catalyst in microwave irradiation, Appl. Catal. Gen. 264 (2004) 53–58. https://doi.org/10.1016/j.apcata.2003.12.026.
[145] T.J. Xue, M.A. McKinney, C.A. Wilkie, The thermal degradation of polyacrylonitrile, Polym. Degrad. Stab. 58 (1997) 193–202. https://doi.org/10.1016/S0141-3910(97)00048-7.
[146] M.K. Jain, A.S. Abhiraman, Conversion of acrylonitrile-based precursor fibres to carbon fibres, J. Mater. Sci. 22 (1987) 278–300. https://doi.org/10.1007/BF01160584.
[147] R.H. Knibbs, The use of polarized light microscopy in examining the structure of carbon fibres*, J. Microsc. 94 (1971) 273–281. https://doi.org/10.1111/j.1365-2818.1971.tb02377.x.
[148] L.A. Feldman, Creep of Carbon Yarns and Composites at High Temperatures., AEROSPACE CORP EL SEGUNDO CA LAB OPERATIONS, 1988. https://apps.dtic.mil/sti/citations/ADA310443 (accessed September 28, 2021).
[149] W. Li, D. Long, J. Miyawaki, W. Qiao, L. Ling, I. Mochida, S.-H. Yoon, Structural features of polyacrylonitrile-based carbon fibers, J. Mater. Sci. 47 (2012) 919–928. https://doi.org/10.1007/s10853-011-5872-2.
[150] W. Chen, X. Liu, R.L. He, T. Lin, Q.F. Zeng, X.G. Wang, Activated carbon powders from wool fibers, Powder Technol. 234 (2013) 76–83. https://doi.org/10.1016/j.powtec.2012.09.026.
[151] C. Pascual-González, M. Iragi, A. Fernández, J. Fernández-Blázquez, L. Aretxabaleta, C. s Lopes, An approach to analyse the factors behind the

micromechanical response of 3D-printed composites, Compos. Part B Eng. 186 (2020) 107820. https://doi.org/10.1016/j.compositesb.2020.107820.
[152] T.-H. Ko, Raman spectrum of modified PAN-based carbon fibers during graphitization, J. Appl. Polym. Sci. 59 (1996) 577–580. https://doi.org/10.1002/(SICI)1097-4628(19960124)59:4<577::AID-APP2>3.0.CO;2-Q.
[153] N. Melanitis, P.L. Tetlow, C. Galiotis, Characterization of PAN-based carbon fibres with laser Raman spectroscopy, J. Mater. Sci. 31 (1996) 851–860. https://doi.org/10.1007/BF00352882.
[154] D.B. Schuepfer, F. Badaczewski, J.M. Guerra-Castro, D.M. Hofmann, C. Heiliger, B. Smarsly, P.J. Klar, Assessing the structural properties of graphitic and non-graphitic carbons by Raman spectroscopy, Carbon. 161 (2020) 359–372. https://doi.org/10.1016/j.carbon.2019.12.094.
[155] I. Brodin, M. Ernstsson, G. Gellerstedt, E. Sjöholm, Oxidative stabilisation of kraft lignin for carbon fibre production, 66 (2012) 141–147. https://doi.org/10.1515/HF.2011.133.
[156] I. Norberg, Y. Nordström, R. Drougge, G. Gellerstedt, E. Sjöholm, A new method for stabilizing softwood kraft lignin fibers for carbon fiber production, J. Appl. Polym. Sci. 128 (2013) 3824–3830. https://doi.org/10.1002/app.38588.
[157] Y.-G. Lü, D. Wu, Q.-F. Zha, L. Liü, C.-L. Yang, Skin-core structure in mesophase pitch-based carbon fibers: causes and prevention, Carbon. 36 (1998) 1719–1724. https://doi.org/10.1016/S0008-6223(97)00172-3.
[158] A.L. Compere, W.L. Griffth, C.F. Leitten Jr, J.M. Pickel, Evaluation of lignin from alkaline-pulped hardwood black liquor, ORNL. 118 (2005) 6–97.
[159] J. Luo, J. Genco, B.J.W. Cole, R.C. Fort, LIGNIN RECOVERED FROM THE NEAR-NEUTRAL HEMICELLULOSE EXTRACTION PROCESS AS A PRECURSOR FOR CARBON FIBER, BioResources. 6 (2011) 4566–4593.
[160] W. Fang, S. Yang, X.-L. Wang, T.-Q. Yuan, R.-C. Sun, Manufacture and application of lignin-based carbon fibers (LCFs) and lignin-based carbon nanofibers (LCNFs), Green Chem. 19 (2017) 1794–1827. https://doi.org/10.1039/C6GC03206K.
[161] J. Lin, B. Ding, J. Yu, Direct Fabrication of Highly Nanoporous Polystyrene Fibers via Electrospinning, ACS Appl. Mater. Interfaces. 2 (2010) 521–528. https://doi.org/10.1021/am900736h.
[162] W. Liu, G. Zhao, EFFECT OF TEMPERATURE AND TIME ON MICROSTRUCTURE AND SURFACE FUNCTIONAL GROUPS OF ACTIVATED CARBON FIBERS PREPARED FROM LIQUEFIED WOOD, BioResources. 7 (2012) 5552–5567.
[163] U. Gaur, S. Lau, B.B. Wunderlich, B. Wunderlich, Heat Capacity and Other Thermodynamic Properties of Linear Macromolecules VI. Acrylic Polymers, J. Phys. Chem. Ref. Data. 11 (1982) 1065–1089. https://doi.org/10.1063/1.555671.
[164] J. Guo, X. Wang, L. Zhang, T. Wang, Transient thermal characterization of micro/submicroscale polyacrylonitrile wires, Appl. Phys. A. 89 (2007) 153–156. https://doi.org/10.1007/s00339-007-4201-8.
[165] SciFinder^{n} Substance Detail, (n.d.). https://scifinder-n.cas.org/searchDetail/substance/6158a2643ee6ab3de1ffc383/substanceDetails (accessed October 2, 2021).
[166] S. Ozbek, D.H. Isaac, Strain-induced density changes in PAN-based carbon fibres, Carbon. 38 (2000) 2007–2016. https://doi.org/10.1016/S0008-6223(00)00060-9.

[167] Y.-R. Rhim, D. Zhang, D.H. Fairbrother, K.A. Wepasnick, K.J. Livi, R.J. Bodnar, D.C. Nagle, Changes in electrical and microstructural properties of microcrystalline cellulose as function of carbonization temperature, Carbon. 48 (2010) 1012–1024. https://doi.org/10.1016/j.carbon.2009.11.020.
[168] Y.-R. Rhim, D. Zhang, M. Rooney, D.C. Nagle, D.H. Fairbrother, C. Herman, D.G. Drewry, Changes in the thermophysical properties of microcrystalline cellulose as function of carbonization temperature, Carbon. 48 (2010) 31–40. https://doi.org/10.1016/j.carbon.2009.07.048.
[169] F. Hermansson, M. Janssen, M. Svanström, Prospective study of lignin-based and recycled carbon fibers in composites through meta-analysis of life cycle assessments, J. Clean. Prod. 223 (2019) 946–956. https://doi.org/10.1016/j.jclepro.2019.03.022.
[170] G. Wernet, C. Bauer, B. Steubing, J. Reinhard, E. Moreno-Ruiz, B. Weidema, The ecoinvent database version 3 (part I): overview and methodology, Int. J. Life Cycle Assess. 21 (2016) 1218–1230. https://doi.org/10.1007/s11367-016-1087-8.
[171] J. Moncada, I. Vural Gursel, W.J.J. Huijgen, J.W. Dijkstra, A. Ramírez, Techno-economic and ex-ante environmental assessment of C6 sugars production from spruce and corn. Comparison of organosolv and wet milling technologies, J. Clean. Prod. 170 (2018) 610–624. https://doi.org/10.1016/j.jclepro.2017.09.195.
[172] A. Fridrihsone-Girone, Preliminary Life Cycle Inventory of Rapeseed Oil Polyols for Polyurethane Production, J. Renew. Mater. 3 (2015) 28–33. https://doi.org/10.7569/JRM.2014.634136.
[173] S. Das, Life cycle assessment of carbon fiber-reinforced polymer composites, Int. J. Life Cycle Assess. 16 (2011) 268–282. https://doi.org/10.1007/s11367-011-0264-z.
[174] S. Fazio, D. Pennington, Polyacrylonitrile fibres (PAN); from acrylonitrile and methacrylate; production mix, at plant; PAN without additives (Location: EU-27), (2005). http://data.europa.eu/89h/jrc-eplca-db00901a-338f-11dd-bd11-0800200c9a66 (accessed October 8, 2021).
[175] M. Culebras, M. Pishnamazi, G.M. Walker, M.N. Collins, Facile Tailoring of Structures for Controlled Release of Paracetamol from Sustainable Lignin Derived Platforms, Molecules. 26 (2021) 1593. https://doi.org/10.3390/molecules26061593.
[176] A. Beaucamp, M. Culebras, M.N. Collins, Sustainable mesoporous carbon nanostructures derived from lignin for early detection of glucose, Green Chem. 23 (2021) 5696–5705. https://doi.org/10.1039/D1GC02062E.